Driven nonequilibrium systems modeled with Markov processes

by

Pelerine Tsobgni Nyawo

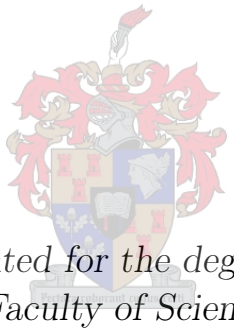

Dissertation presented for the degree of Doctorate of philosophy in the Faculty of Sciences at Stellenbosch University

Supervisors:

Prof. Hugo Touchette
Prof. Michael Kastner

December 2017

Declaration

By submitting this dissertation electronically, I declare that the entirety of the work contained therein is my own, original work, that I am the sole author thereof (save to the extent explicitly otherwise stated), that reproduction and publication thereof by Stellenbosch University will not infringe any third party rights and that I have not previously in its entirety or in part submitted it for obtaining any qualification.

Abstract

Driven nonequilibrium systems modeled with Markov processes

Pelerine Tsobgni Nyawo

Department of Physics,
University of Stellenbosch,
South Africa

Dissertation: PhD

July 2017

We study in this thesis the fluctuations of time-integrated functionals of Markov processes, which represent physical observables that can be measured in time for noisy systems driven in nonequilibrium steady states. The goal of the thesis is to illustrate how techniques from the theory of large deviations can be used to obtain the probability distribution of these observables in the long-time limit through the knowledge of an important function, called the rate function. We also illustrate in this thesis a recent theory of driven processes that aims to describe how fluctuations of observables are created in time by means of an effective process with modified forces or potentials. This is done by studying two simple models of nonequilibrium processes based on the Langevin equation. The first is a periodic diffusion that has current fluctuations, whereas the second is the simple drifted Brownian motion for which we study the occupation fluctuations. For these two models, we calculate analytically and numerically the rate function, as well as the associated driven process. The results for the periodic diffusion show, on the one hand, that there is a Gaussian to non-Gaussian crossover in the current fluctuations, which can easily be interpreted from the form of the driven process. On the other hand, the Brownian model provides one of the simplest examples of a dynamical phase transition, that is, a phase transition in the fluctuations of observables. Other connections with fluctuation relations, Josephson junctions, and the geometric Brownian motion are discussed.

Uittreksel

Modellering van nie-ewewig stelsels as Markov prosesse

Pelerine Tsobgni Nyawo

Fisika Departement,
Universiteit van Stellenbosch,
Suid Afrika

Proefskrif: PhD

Julie 2017

Ons bestudeer in hierdie tesis die fluktuasies van tyd-geïntegreerde funksionele van Markov prosesse, wat fisiese waarneembares wat in tyd gemeet kan word verteenwoordig vir stelses met geraas en wat gedryf word tot nie-ewewig bestendige state. Die doel van hierdie tesis is om te illustreer hoe tegnieke van die teorie van groot fluktuasies gebruik kan word om die waarskynlikheidsverspreiding van hierdie waarneembares in die lang-tyd limiet te bepaal deur kennis van 'n belangrike funksie, die sogenaamde koers funksie, te gebruik. Ons illustreer ook in hierdie tesis 'n onlangse teorie van gedrewe prosesse wat daarop gemik is om te beskryf hoe fluktuasies van waarneembares geskep word in tyd deur middel van 'n effektiewe proses met gewysigde kragte of potensiale. Hierdie word gedoen deur twee eenvoudige nie-ewewig prosesse wat op die Langevin-vergelyking gebaseer is te bestudeer. Die eerste proses is a periodieke diffusie wat stroom fluktuasies bevat, terwyl die tweede proses 'n eevoudige Browniese beweging met drif is waarvoor ons die besettings fluktuasies bestudeer. Vir hierdie twee modelle bereken ons analities en numeries die koers funksie asook die geassosieerde gedrewe proses. Die resultate vir die periodieke diffusie wys, aan die een kant, dat daar 'n oorkruising vanaf Gaussiese tot nie-Gaussiese stroom fluktuasies bestaan, wat maklik vanuit die vorm van die gedrewe proses geïnterpreteer kan word. Aan die ander kant verskaf die Browniese model die eenvoudigste voorbeeld van 'n dinamiese fase oorgang, dit wil sê, 'n oorgang in die fluktuasies van waarneembares. Ander verbindinge met fluktuasieverhoudinge, Josephson-kruisings en die geometriese Browniese beweging word bespreek.

Publications

The material presented in chapter 3 and part of chapter 4 has been published in

- P. Tsobgni Nyawo, H. Touchette, Large deviations of the current for driven periodic diffusions, Phys. Rev. E 94, 032101, 2016.
- P. Tsobgni Nyawo, H. Touchette, A minimal model of dynamical phase transition, Europhys. Lett. 116, 50009, 2016.

Other parts of chapter 4 are being prepared for submission.

Acknowledgements

I would like to express my sincere gratitude to Prof. Hugo Touchette, my supervisor, for proposing this research project for my thesis, and for his guidance during the PhD. I learnt many things from him; his advice and his broad perspective always encouraged me to go ahead in my research work. I owe him an enormous debt of gratitude for the knowledge received during the training.

During my studies, I was funded by a DAAD Scholarship, by the National Institute for Theoretical Physics (NITheP) and by the Physics Department, which provided support to attend conferences and writing the thesis. I am grateful to these institutions for the financial support. I am also grateful to Mrs. René Kotze and Mrs. Christine Ruperti at the Physics Department for administrative support and Mr. Botha Tinus for his assistance.

I am thankful to Dr. Florian Angeletti for fruitful discussions at the beginning of the second part of my project, which helped me have a deeper understanding of my topics.

My sincere appreciation to the examiners of the thesis, in particular Prof. Michael Kastner who acted as co-supervisor and Dr. Rosemary J. Harris. Her attention and her careful reading of the thesis allowed me to improve my work significantly.

Thank you to the Stellenbosch Writing Lab, especially Venita Januarie, for helping me during the writing part of my thesis.

I am thankful to my fellow postgraduate students, especially Johan Du Buisson, for his help with translating the abstract in Afrikaans. Thank you also to Christel Kimene, Stanard Pachong, Florence Azote, Philipp Uhrich and Ishmael Takyi for the good moments we spent together. Many thanks also to the Stellenbosch International Fellowship family (SIF) especially the worship group, for amazing moments through songs. Thank you to Jolly Jogger group in particular, papa Ulli, and all my friends for supporting me, especially Abiodun, Sylvie, Anicia and Wilfried.

Finally, a big thank you to my close family, in particular to my lovely husband Tala Joseph and our two children, Loic Tsobgni and Maxime Fongue.

Dedications

I dedicate my thesis to all whom have contributed into making me who I am today, especially my parents, my husband and our two boys.

Contents

List of Figures

Chapter 1

Introduction

We study in this thesis the fluctuations of Markov processes modeling the dynamics of equilibrium and nonequilibrium systems driven by external forces and noise. The use of Markov processes for modeling noisy systems has a long history in physics dating back at least to Einstein who studied Brownian motion as a model of particles diffusing in gases and liquids [1–3]. Since then, Markov processes have become a model of choice for studying various other types of systems such as

- Populations of bacteria or other cells as modeled by birth-death or branching processes [1, 4].
- Polymers in solution as modeled by random walks and Markov chains in general [5].
- The decay of radioactive material following Poisson-type processes [1].
- The transport of energy or particles through ion channels or between reservoirs, modeled by Markov jump processes, including Markov interacting particle models such as the zero-range process and the exclusion process [6].
- Brownian and colloidal particles and molecular motors controlled by external forces and perturbed by thermal noise [2, 3, 7–9]. In this case, the models are based on Langevin-type (diffusion) equations and the Fokker-Planck equation.

Other examples related to statistical physics can be found in [1, 3].

In all of these systems the goal is usually to describe the state X_t of the system and its statistics in time, as characterized by its distribution $P(x,t) = P(X_t = x)$. From this distribution, we can find, for example, the mean $\langle X_t \rangle$ at a fixed time t or as $t \to \infty$. We can also compute the moments such as $\langle X_t^k \rangle$,

and the correlation function $\langle X(t)X(t')\rangle$ for $t \neq t'$, which is related to diffusion and transport coefficients [1, 10]. The methods used to study these quantities are based on the Master equation or the Fokker-Planck equation, depending on whether the system considered has discrete or continuous degrees of freedom [2].

In this thesis, we do not focus on the state X_t, as such, but on time-integrated functionals or observables A_T that depend on the whole trajectory of X_t over the time interval $[0, T]$. There has been a lot of interest in these quantities recently, especially in connection with the field of stochastic thermodynamics [7, 9], which tries to develop the thermodynamics of small systems perturbed by noise. Examples of such quantities include

- Thermodynamic energy-like quantities such as the work, the heat exchanged with an environment and the entropy production of nonequilibrium processes [7].
- The activity corresponding to the number of jumps that a process experiences in the time interval $[0, T]$, and particle currents appearing in interacting particle systems [11, 12].
- The fraction of time that a system spends in some region Δ of its state space [12].

The statistical properties of these quantities are determined, similarly to the state X_t, by the probability distribution $P(A_T = a)$. This distribution is not given by a Master equation or the Fokker-Planck equation. Moreover, in general, it is difficult to find this distribution exactly for a fixed T. In many cases, however, it is possible to use techniques from the theory of large deviations [13, 14] to approximate $P(A_T = a)$ as follows:

$$P(A_T = a) \approx e^{-TI(a)}, \tag{1.0.1}$$

in the long-time limit $T \to \infty$.

This approximation or scaling of $P(A_T = a)$ is very general and gives through the function $I(a)$, called the rate function, a lot of information about the small fluctuations of A_T around its typical value corresponding to the zero of $I(a)$, which are generally Gaussian, and the large fluctuations of A_T away from this typical value, which are generally not Gaussian. For this reason, the rate function, and large deviation theory in general, have come to play an important role recently in statistical physics, especially in connection with nonequilibrium systems [11, 13, 15, 16].

In this context, we should note many works related to interacting particle systems, such as the zero-range and exclusion processes, which have played

an important role for modeling the transport of energy and particles under nonequilibrium conditions. For these, the rate function has been studied for the density and for the current, and gives information about the stationary value of these observables, as well as their fluctuations. The rate function in this case can be obtained by a matrix ansatz [6] or from the so-called additivity principle, and also gives information about phase transitions in these models [6, 15, 17, 18].

Rate functions have also been studied in the context of diffusions, especially, as mentioned, for Langevin-type systems modeling manipulated Brownian particles, colloids and Brownian motors [7]. In this case, quantities or observables of interest are energy-like quantities such as the work, heat, or the entropy production, which is related to the nonequilibrium nature of a stochastic process, i.e., the fact that the detailed balance property of the dynamics is broken because of non-conservative forces and the presence of currents. For the entropy production, it is interesting to note that the rate function is found to satisfy a general symmetry, known as the fluctuation relation or fluctuation theorem, which is believed to hold for general nonequilibrium systems (see [13, 19, 20]).

The goal of this thesis is to continue these studies by investigating the large deviations of observables of nonequilibrium processes modeled by Langevin equations and by illustrating a recent theory of driven processes that tries to explain how fluctuations or large deviations of these observables are dynamically created in time by means of an effective process that includes additional potentials or forces compared to the original process [12, 21, 22].

Some applications of this theory have been presented recently in [12, 21, 23]. In this thesis, we present two more applications related to the current of a periodic diffusion, which has been extensively used in the past to model noisy systems that diffuse in potentials [10], and to the occupation of Brownian motion. For these two models, we calculate using various methods the rate function characterizing the fluctuations of the observables considered, and also construct, more importantly, the driven process that explains how the fluctuations are created in terms of a modified process. For the ring model, we will see that this effective process modifies the potential in a non-linear and non-local way so as to produce currents that are far from the typical current. In the case of the Brownian motion, we will see that a potential is created to allow this process to spend more or less time in certain regions of the state space. For the Brownian motion, we will also see that the fluctuations of the occupation are characterized by a phase transition referred to as a dynamical phase transition.

These models and results should serve in the future as a reference that shows how the theory of driven processes can be applied in practice to study the large deviations of more physical processes and especially diffusions. The

results related to the Brownian motion are also important, as they provide the simplest model in which a dynamical phase transition arises with a single large deviation limit, corresponding here to the long-time limit.

This thesis is divided as follows. In Chap. 2 we expose the basic concepts of the theory of Markov processes and the theory of large deviations needed in the thesis. In Chap. 3, we then apply these theories to study the current fluctuations of a one-dimensional, periodic diffusion, obtaining for this model the current rate function and the underlying driven process. In Chap. 4 we use the same formalism but now apply it to the occupation fluctuations of the standard and drifted Brownian motion. We conclude by proposing possible extensions and problems for the future.

Chapter 2

Elements of large deviation theory

We present in this chapter the large deviation methods that will be used in the rest of the thesis to study the fluctuations of observables of Markov processes. We begin by defining the large deviation approximation mentioned in the introduction, which is known as the large deviation principle and which defines the rate function. We then present the main result, called the Gärtner-Ellis Theorem, that will be used to obtain the rate function. We give examples of applications of this result for simple sums of random variables and then explain how it can be used for Markov diffusions. For this part we follow [13, 14, 24, 25]. We end the chapter by explaining, following [12, 21], how the driven process is constructed from certain large deviation elements and by explaining its meaning or interpretation as a modified process that gives an effective description of fluctuations.

2.1 Large deviation principle

We consider in this thesis a random variable S_n indexed by n, which can be, for example, a sample mean

$$S_n = \frac{1}{n}\sum_{i=1}^{n} X_i, \tag{2.1.1}$$

or more generally any functional of the form

$$S_n = \frac{1}{n}\sum_{i=1}^{n} f(X_i) + \frac{1}{n}\sum_{i=1}^{n-1} g(X_i, X_{i+1}), \tag{2.1.2}$$

where f and g are arbitrary functions. In both cases, $X_1, \ldots, X_n$ could be a sequence of independent and identically distributed (iid) random variables, representing for example the outcomes of n measurements or experiments, or the states of a Markov process evolving in discrete time. For a Markov process

X_t that evolves continuously in time, we will consider instead functionals such as

$$S_T = \frac{1}{T}\int_0^T f(X_t)dt + \frac{1}{T}\sum_{t:\Delta X_t \neq 0} g(X_{t^-}, X_{t^+}), \tag{2.1.3}$$

where the sum is replaced by an integral up to a time T and the sum over g is now over all times where the process jumps. X_{t^-} represents the state before a jump and X_{t^+} the state after a jump.

In all cases, we are interested to find the probability density function (pdf) of S_n (or S_T) written as $P(S_n = s)$. This pdf is generally difficult to obtain exactly but can be approximated when n is very large as

$$P(S_n = s) = e^{-nI(s)+o(n)}, \tag{2.1.4}$$

where $o(n)$ is any correction term that is sub-linear in n and so smaller than n. This means that the dominant order of the pdf is the decaying exponential so that

$$P(S_n = s) \approx e^{-nI(s)}, \tag{2.1.5}$$

where $I(s)$ is the rate function that controls the rate at which the pdf decays to zero for $n \to \infty$.

In this thesis, we will focus on this approximation and calculate the rate function $I(s)$ which can be obtained by the limit

$$I(s) = \lim_{n\to\infty} -\frac{1}{n}\ln P(S_n = s). \tag{2.1.6}$$

Whenever this limit exists, we say that S_n or $P(S_n = s)$ satisfies a large deviation principle (LDP) with the rate function $I(s)$ [13, 14, 25]. This scaling of probabilities is the subject of large deviation theory and implies that the fluctuations of S_n are exponentially rare to be observed in the large n limit.

Example 2.1.1 (Gaussian sample mean). Consider a sample mean in Eq. (2.1.1) assuming that the X_i's are iid Gaussian random variables with density

$$P(X_i = x) = \frac{1}{\sqrt{2\pi\sigma^2}}\exp\left[-\frac{(x-\mu)^2}{2\sigma^2}\right]. \tag{2.1.7}$$

The pdf of the sample mean in this case is also a Gaussian given by

$$P(S_n = s) = \sqrt{\frac{n}{2\pi\sigma^2}}\exp\left[-\frac{n(x-\mu)^2}{2\sigma^2}\right]. \tag{2.1.8}$$

It is clear from this result that the dominant term in n in the pdf is

$$P(S_n = s) \approx e^{-nI(s)} \tag{2.1.9}$$

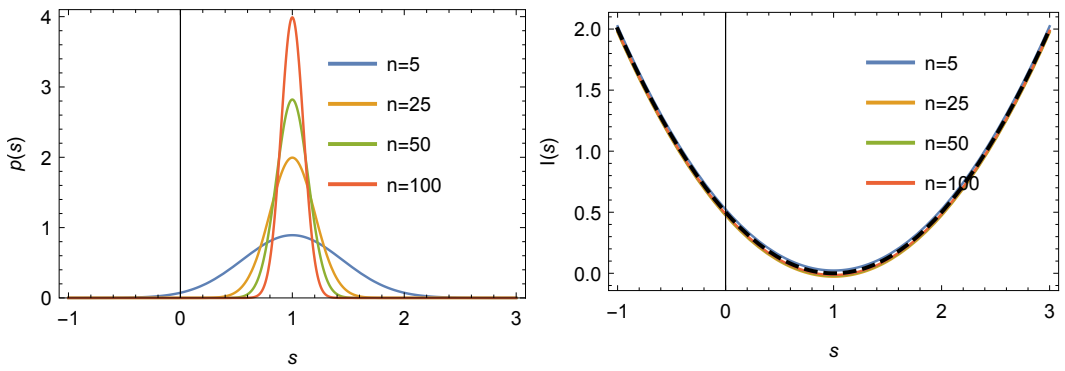

Figure 2.1: *Left: Probability density* $p(s) = P(S_n = s)$ *of the Gaussian sample mean* S_n *for* $\mu = \sigma = 1$ *and for different values of* n*. Right: Rate function* $I(s)$ *extracted from* $P(S_n = s)$ *for the same values of* n *and parameters. The black dashed line is the analytical rate function.*

with

$$I(s) = \frac{(s-\mu)^2}{2\sigma^2}. \tag{2.1.10}$$

The same result follows from the large deviation limit (2.1.6).

The behaviour of the exact expression of $P(S_n = s)$ as n grows is shown in Fig. 2.1 (left) for $\mu = 1$ and $\sigma = 1$. We notice how $P(S_n = s)$ concentrates around its mean $\mu = 1$ as $n \to \infty$, which means that $P(S_n = s) \to \delta(s - \mu)$. This follows from the shape of $I(s)$ shown in Fig. 2.1 (right), which is such that $I(s) > 0$ for $s \neq \mu$. Therefore, $P(S_n = s)$ decays exponentially to zero as $n \to \infty$ for all s except at $s = \mu$, where it concentrates.

Example 2.1.2 (Bernoulli sample mean). Suppose now that the X_i's in S_n Eq. (2.1.1) are Bernoulli random variables taking values in the set $\{0, 1\}$ with probability $P(X_i = 0) = 1 - \alpha$ and $P(X_i = 1) = \alpha$. In this case S_n is now a discrete variable taking values in the set $\left\{0, \frac{1}{n}, \frac{2}{n}, \ldots, \frac{n-1}{n}, 1\right\}$ with a distribution corresponding to the binomial distribution:

$$P(S_n = s) = \frac{n!}{ns!\,(1-s)n!}\alpha^{ns}(1-\alpha)^{(1-s)n}. \tag{2.1.11}$$

Using Stirling's approximation, $n! \approx n^n e^{-n}$, we can extract from this distribution a dominant contribution having the form

$$P(S_n = s) \approx e^{-nI(s)} \tag{2.1.12}$$

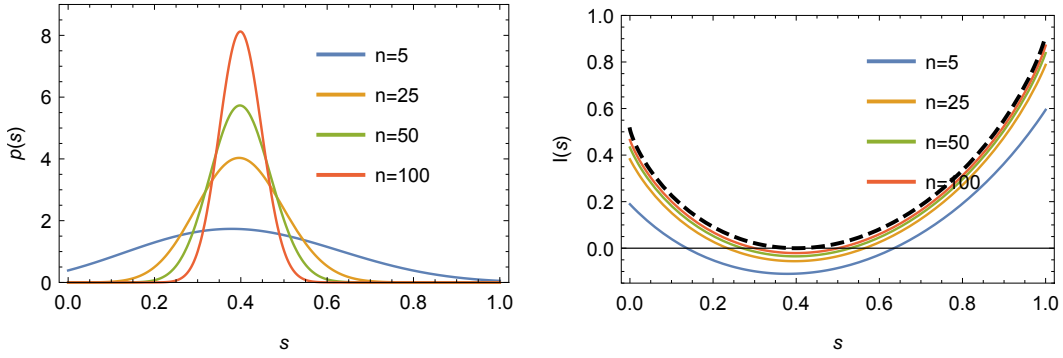

Figure 2.2: *Left: Effective probability density of the Bernoulli sample mean S_n for $\alpha = 0.4$ and for increasing values of n. We notice the concentration of the density for increasing values of n. Right: Rate function $I(s)$. The black dashed line is the analytical rate function.*

with the rate function

$$I(s) = s \ln \frac{s}{\alpha} + (1-s) \ln \frac{1-s}{1-\alpha}, \quad s \in [0,1]\,. \tag{2.1.13}$$

Since the values of S_n become dense in $[0,1]$, we show in Fig. 2.2 (left) the distribution of S_n divided by the spacing $\Delta = \frac{1}{n}$ of its values in order to get an effective pdf for S_n which concentrates as $n \to \infty$. This concentration is related again to the rate function, which has a single minimum and zero located at $s = \alpha$, as shown in Fig. 2.2 (right).

2.2 Gärtner-Ellis Theorem

Large deviation principles and their rate functions are very difficult to obtain directly from the distribution of S_n. In some cases, they can be obtained numerically. Another important result that can be used to derive rate functions is the Gärtner-Ellis Theorem, which is based on the calculation of the following function:

$$\lambda(k) = \lim_{n\to\infty} \frac{1}{n} \ln \left\langle e^{nkS_n} \right\rangle, \tag{2.2.1}$$

known as the scaled cumulant generating function (SCGF). The Gärtner-Ellis Theorem [13, 14, 25] says that, if $\lambda(k)$ exists and is differentiable, then

1. S_n has a large deviation principle.

2. Its rate function $I(s)$ is given by the Legendre-Fenchel transform of $\lambda(k)$ as
$$I(s) = \sup_{k\in\mathbb{R}} \{ks - \lambda(k)\}, \tag{2.2.2}$$
where sup stands for the supremum.

In most cases considered, $\lambda(k)$ is strictly convex, which implies that the Legendre-Fenchel transform above reduces to the Legendre transform given by

$$I(s) = k(s)s - \lambda(k(s)), \tag{2.2.3}$$

where $k(s)$ is the unique solution of

$$\lambda'(k) = s. \tag{2.2.4}$$

As an application, let us consider again a sample mean S_n of iid random variables as in Eq. (2.1.1). In this case, the SCGF is

$$\lambda(k) = \lim_{n\to\infty} \frac{1}{n} \ln \left\langle \prod_{i=1}^{n} e^{kX_i} \right\rangle. \tag{2.2.5}$$

Since the X_i's are iid, this can be written as

$$\lambda(k) = \lim_{n\to\infty} \frac{1}{n} \ln \left\langle e^{kX_i} \right\rangle^n, \tag{2.2.6}$$

which gives the result

$$\lambda(k) = \ln \left\langle e^{kX_i} \right\rangle. \tag{2.2.7}$$

Example 2.2.1 (Gaussian sample mean). In the case of a sample mean of iid Gaussian random variables, the SCGF is obtained as

$$\lambda(k) = \mu k + \frac{1}{2}\sigma^2 k^2. \tag{2.2.8}$$

This function is everywhere differentiable; hence the rate function is, by Legendre transform,

$$I(s) = \frac{(s-\mu)^2}{2\sigma^2}, \quad s \in \mathbb{R}, \tag{2.2.9}$$

which is the same rate function that we obtained previously in Example 2.1.1.

Example 2.2.2 (Bernoulli sample means). For the Bernoulli sample mean, we have

$$\lambda(k) = \ln \sum_{i=0,1} p_i e^{ki} = \ln(\alpha e^k + 1 - \alpha). \tag{2.2.10}$$

Applying the Legendre transform to this $\lambda(k)$, as given by (2.2.3), yields

$$I(s) = s \ln \frac{s}{\alpha} + (1-s) \ln \frac{1-s}{1-\alpha}, \quad s \in [0,1], \tag{2.2.11}$$

which is also the result obtained before in Example 2.1.2.

2.3 Properties of large deviation functions

We now state a number of properties of the SCGF and rate function in the case where the latter is obtained from the Gärtner-Ellis Theorem. The properties listed hold for an arbitrary random variable S_n, including iid sample means.

2.3.1 General properties

- Normalization: $\lambda(0) = 0$. This follows directly from the definition (2.2.1) of the SCGF:

$$\lambda(0) = \lim_{n\to\infty} \frac{1}{n} \ln\langle e^{n0S_n}\rangle = \lim_{n\to\infty} \frac{1}{n} \ln\langle 1\rangle = 0, \tag{2.3.1}$$

  since $\langle 1\rangle = 1$.

- Mean:

$$\lambda'(0) = \lim_{n\to\infty} \langle S_n\rangle. \tag{2.3.2}$$

  This also follows directly by taking the derivative of the SCGF.

- Convexity: $\lambda(k)$ is always convex as a function of k. This follows from Hölder's inequality; see Sec. 3.5 of [13].

- Variance:

$$\lambda''(0) = \lim_{n\to\infty} n\left(\langle S_n^2\rangle - \langle S_n\rangle^2\right). \tag{2.3.3}$$

  This follows directly by taking the second derivation of $\lambda(k)$. In the iid case,

$$\lambda''(0) = \langle X^2\rangle - \langle X\rangle^2. \tag{2.3.4}$$

- Inverse transform [13, 14]:

$$\lambda(k) = \sup_{s\in\mathbb{R}} \{ks - I(s)\}. \tag{2.3.5}$$

  This always holds because $\lambda(k)$ is always convex.

2.3.2 Duality

We have seen when calculating the rate function of the Gaussian and Bernoulli sample means that the Legendre transform involved in the Gärtner-Ellis Theorem reduces to the standard Legendre transform

$$I(s) = k(s)s - \lambda(k(s)), \tag{2.3.6}$$

where $k(s)$ is the unique solution of $\lambda'(k) = s$. This transformation and its inverse, Eq. (2.3.5), imply a duality relation between k and the slopes of $I(s)$

and between s and the slopes of $\lambda(k)$. This is expressed in mathematical form as

$$I'(s) = k(s) \tag{2.3.7}$$

or equivalently as

$$\lambda'(k) = s(k), \tag{2.3.8}$$

where $s(k)$ is the inverse function of $k(s)$ [13]. This duality is useful in practice to plot rate functions because we can then write the Legendre transform in parametric form as

$$I(s(k)) = k\lambda'(k) - \lambda(k). \tag{2.3.9}$$

Physically, the duality is also the analogue of the relation between free energy and entropy in thermodynamics. In particular, Eq. (2.3.7) can be seen as the analogue of the formula of thermodynamics expressing the temperature (here k) as the derivative of the entropy (here $I(s)$); see [13] for more details.

2.3.3 Law of Large Numbers and Central Limit Theorem

We have seen in Figs. 2.1 and 2.2 that $P(S_n = s)$ decreases exponentially with n around the concentration point $s = \mu$, corresponding to the mean value of S_n. This mean value is the the most probable value of S_n, since it is the minimum and the zero of $I(s)$ and so the only point where $P(S_n = s)$ does not decay exponentially. This means that

$$\lim_{n\to\infty} P(|S_n - \mu| > \epsilon) \to 0, \tag{2.3.10}$$

as $n \to \infty$ for all $\epsilon > 0$, so that S_n converges in probability to its mean. This result is known as the Law of Large Numbers and can be expressed less rigorously as

$$\lim_{n\to\infty} P(S_n = s) \to \delta(s - \mu) \tag{2.3.11}$$

as noted before.

In many cases, including the examples of sample means considered before, the rate function is locally quadratic around its minimum and zero located at $s = \mu$, so that

$$I(s) = \frac{1}{2} I''(\mu)(s - \mu)^2 + \cdots. \tag{2.3.12}$$

This implies that

$$P(S_n = s) \approx e^{-n\frac{1}{2}I''(\mu)(s-\mu)^2} \tag{2.3.13}$$

so that S_n has Gaussian fluctuations around its mean, in accordance with the Central Limit Theorem.

2.4 Markov chains and jump processes

Up to now we have derived rate functions analytically for sample means of iid random variables. We now consider the case where random variables are correlated according to a Markov chain or a Markov jump process. The case of Markov diffusions is explained in the next section.

2.4.1 Markov chains

A Markov chain is a sequence $X_1, X_2, \ldots, X_n$ of random variables in which X_{i+1} depends on X_i so that the joint pdf

$$p(x_1, x_2, \ldots, x_n) = P(X_1 = x_1, X_2 = x_2, \ldots, X_n = x_n) \tag{2.4.1}$$

factorizes as

$$p(x_1, x_2, \ldots, x_n) = p(x_1)\Pi(x_2|x_1)\ldots\Pi(x_n|x_{n-1}), \tag{2.4.2}$$

where $p(x_1)$ is the initial pdf of X_1 and $\Pi(x_{i+1}|x_i)$ is the conditional or transition probability density of X_{i+1} given X_i, which encodes the correlations between the random variables [4]. As a conditional probability, $\Pi(y|x)$ is such that

$$\sum_y \Pi(y|x) = 1, \tag{2.4.3}$$

for all x. In matrix terms this means that the columns of Π all sum to one. For simplicity, we consider here the case of a homogeneous Markov chain for which $\Pi(x_{i+1}|x_i)$ does not depend on time.

As before, we are interested in studying the fluctuations of observables of the process. To be general, we consider an observable of the form

$$S_n = \frac{1}{n}\sum_{i=1}^{n} f(X_i) + \frac{1}{n}\sum_{i=1}^{n-1} g(X_i, X_{i+1}), \tag{2.4.4}$$

where f and g are arbitrary functions. Because the sequence $X_1, X_2, \ldots, X_n$ defining S_n is now a Markov chain, the SCGF does not have the simple form of Eq. (2.2.7) that we had for iid sample means. Instead, in the Markov case it can be proved using the Perron-Frobenius Theorem (see [13] and Appendix A) that

$$\lambda(k) = \ln \zeta_{\max}(\Pi_k), \tag{2.4.5}$$

where $\zeta_{\max}$ is the dominant eigenvalue of a certain positive matrix Π_k, called the tilted matrix, which is a deformation or perturbation of Π [13, 14, 25]. For the general observable shown in Eq. (2.4.4), the tilted matrix is given by

$$\Pi_k(y|x) = \Pi(y|x)e^{kf(y)+kg(x,y)}. \tag{2.4.6}$$

To find the rate function of S_n we must therefore construct this matrix and find its dominant eigenvalue. From there, we can obtain the rate function $I(s)$ using the Gärtner-Ellis Theorem. We present next some examples.

Example 2.4.1 (Activity fluctuations in discrete time). Let us consider a Markov chain with two states, 0 and 1, with the transition matrix between these states given by

$$\Pi = \begin{pmatrix} 1-\alpha & \beta \\ \alpha & 1-\beta \end{pmatrix}. \tag{2.4.7}$$

For this process, we are interested in the number of jumps from 0 to 1 or 1 to 0, which can be expressed as

$$S_n = \frac{1}{n}\sum_{i}^{n} g(X_i, X_{i+1}) \tag{2.4.8}$$

with $g(x,y) = 1 - \delta_{x,y}$. In this case, the tilted matrix is given by

$$\Pi_k = \begin{pmatrix} 1-\alpha & \beta e^k \\ \alpha e^k & 1-\beta \end{pmatrix}. \tag{2.4.9}$$

By finding the dominant eigenvalue of this matrix, we get the SCGF as

$$\lambda(k) = -\ln 2 + \ln\left(2 - \alpha - \beta + \sqrt{\alpha^2 - 2\alpha\beta + 4e^{2k}\alpha\beta + \beta^2}\right). \tag{2.4.10}$$

This is differentiable for all k, so that taking the Legendre transform gives

$$\begin{aligned} I(s) \;=\; & \frac{1}{2}s\ln\left[m\left(2a^2 - s(\alpha^2 - 4 + \alpha(4-6\beta) + \beta(4+\beta)) + w(2-b)\right)\right] \\ & - \ln\left[-2(-2+b) + \sqrt{l\left(4a^2 + 2s^2(b-2)^2 + 2s(-2a^2 + (2-b)w\right)}\right] \\ & - \frac{3}{2}s\ln 2 + \ln 4, \end{aligned} \tag{2.4.11}$$

where $a = \alpha - \beta$, $b = \alpha + \beta$,

$$\begin{aligned} l &= \frac{1}{(s-1)^2}, \\ m &= \frac{ls}{\alpha\beta}, \\ w &= \sqrt{a^2(4-4s) + s^2(b-2)^2}. \end{aligned} \tag{2.4.12}$$

This result is shown in Fig. 2.3. For the symmetric case $\alpha = \beta$, the previous equation becomes

$$I(s) = s\ln\frac{s}{\alpha} + (1-s)\ln\frac{1-s}{1-\alpha}, \tag{2.4.13}$$

which is the rate function obtained for the Bernoulli iid sample mean with parameter α.

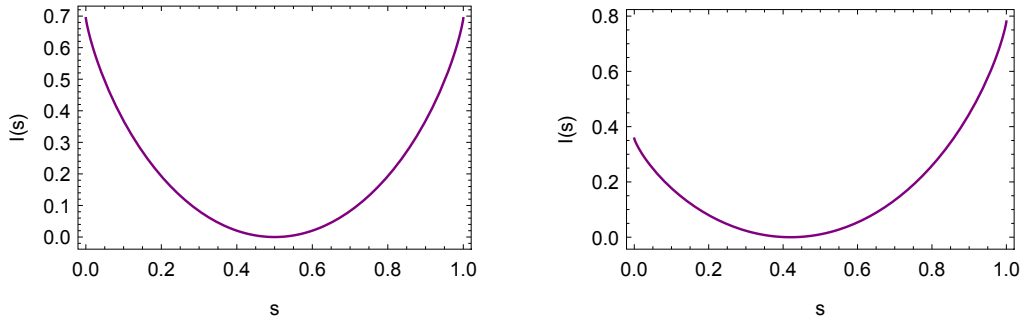

Figure 2.3: *Left: Rate function for the two-state symmetric Markov chain with* $\alpha = 0.5$ *and* $\beta = 0.5$. *Right: Rate function for two-state Markov chain with* $\alpha = 0.3$ *and* $\beta = 0.7$.

2.4.2 Jump processes

A jump process X_t is a Markov chain evolving in continuous time t. It is described not by a transition probability, but by transition rates W_{ji} obtained by the limit

$$W_{ji} = \lim_{\Delta t \to 0} \frac{\Pi_{\Delta t}(j|i)}{\Delta t}, \tag{2.4.14}$$

where $\Pi_{\Delta t}(j|i)$ is the probability that the process makes the jump to $X_{t+\Delta t} = j$ from $X_t = i$. Thus W_{ji} gives the probability per unit time for jumps from i to j. Mathematically, the transition rates define what is called the generator G such that

$$\Pi_t = e^{Gt}. \tag{2.4.15}$$

The explicit expression of G is

$$G_{ji} = W_{ji} - r_i \delta_{ij}, \tag{2.4.16}$$

where r_i is the escape rate from i defined as

$$r_i = \sum_{j \neq i} W_{ji}. \tag{2.4.17}$$

This implies that

$$\sum_j G_{ji} = 0 \tag{2.4.18}$$

for all i, so that in matrix terms the columns of G sum to zero. This property is needed for Π_t to be a stochastic matrix, that is, to have its columns summing to one.

Let us now consider an observable S_T of this process. Similarly to the case of Markov chains, we can consider two parts in this observable: a part that

involves a function of X_t that is integrated in time, and a part that depends on the jumps of X_t from one state to another. In general, we can thus write

$$S_T = \frac{1}{T}\int_0^T f(X_t)dt + \frac{1}{T}\sum_{t:\Delta X_t \neq 0} g(X_{t^-}, X_{t^+}), \tag{2.4.19}$$

where f is an arbitrary function of X_t and g is a function of the state X_{t^-} before a jump and the state X_{t^+} after a jump, so that the sum involving g is over all times t where there is a jump $\Delta X_t \neq 0$.

As before, we need to find the SCGF $\lambda(k)$ for this observable. Similarly to Markov chains [11, 14], it can be shown that $\lambda(k)$ is given by a dominant eigenvalue $\zeta_{\max}(G_k)$ of a tilted generator having the form

$$(G_k)_{ji} = G_{ji}e^{kg(i,j)} + (kf(i) - r_i)\delta_{ij}. \tag{2.4.20}$$

Thus

$$\lambda(k) = \zeta_{\max}(G_k). \tag{2.4.21}$$

There is no logarithm here compared to Eq. (2.4.5) because we consider G_k not Π_k. The next example shows how this is applied in practice.

Example 2.4.2 (Occupation of a two-state jump process). Let us consider a Markov jump process with state $X_t \in \{0, 1\}$ and generator

$$G = \begin{pmatrix} -\alpha & \beta \\ \alpha & -\beta \end{pmatrix}. \tag{2.4.22}$$

For this process, consider the observable

$$S_T = \frac{1}{T}\int_0^T \delta_{X_t,0}dt, \tag{2.4.23}$$

which represents the fraction of time that X_t spends in the state 0 over a period of time T. The tilted generator for this process is obtained from Eq. (2.4.20) as

$$G_k = \begin{pmatrix} k-\alpha & \beta \\ \alpha & -\beta \end{pmatrix},$$

since $g = 0$ and $f(i) = \delta_{i,0}$. The SCGF, corresponding to the dominant eigenvalue of the latter matrix, is

$$\lambda(k) = \ln 2 + \ln\left(k - \alpha - \beta + \sqrt{4k\beta + (\alpha + \beta - k)^2}\right). \tag{2.4.24}$$

The rate function obtained from the Legendre transform of this SCGF is

$$I(s) = s(\alpha - \beta) + \beta - \frac{1}{2}\left(\frac{q}{s(1-s)} + \sqrt{\frac{\alpha\beta}{s(1-s)}}\right), \tag{2.4.25}$$

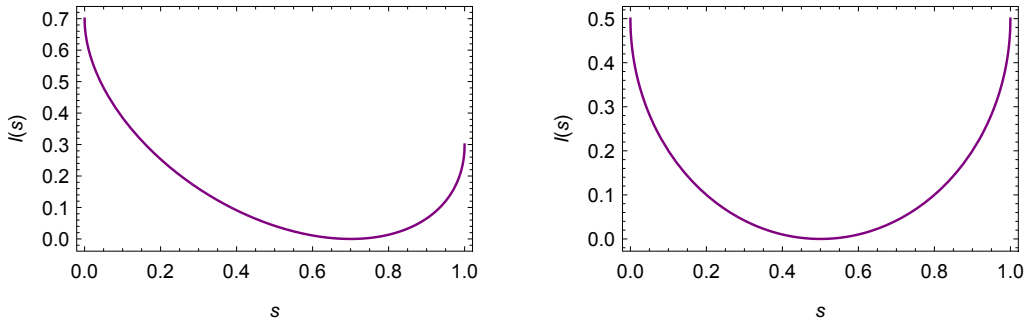

Figure 2.4: *Left: Rate function $I(s)$ for the fraction of time the two-state jump process spends in the state $x = 0$ for the parameters $\alpha = 0.3$, $\beta = 0.7$. Right: Same rate function for $\alpha = \beta = 0.5$.*

where

$$q = \sqrt{(1-2s)^2(s-1)s\alpha\beta}, \tag{2.4.26}$$

as shown in Fig. 2.4 for different values of α and β. This figure shows that $s \in [0, 1]$ and the rate function $I(s)$ is steep at $s = 0$ and $s = 1$. This implies, by duality, that the SCGF $\lambda(k)$ has asymptotic slopes equal to 0 and 1 as $k \to -\infty$ and $k \to +\infty$ respectively.

2.5 Markov diffusion processes

All the models that we will study in the next chapters are Markov diffusions defined by the following stochastic differential equation (SDE):

$$dX_t = F(X_t)dt + \sigma dW_t, \tag{2.5.1}$$

where F is a function of X_t called the drift, σ is the noise intensity and W_t is a Brownian motion. For simplicity, we consider the one-dimensional case where $X_t \in \mathbb{R}$ and $W_t \in \mathbb{R}$ is a one-dimensional Brownian motion.

Following the previous sections, we explain how to obtain the pdf of the process and how to obtain large deviations of observables of this process that depend on X_t and its increments.

2.5.1 Time-dependent and stationary probability density

The evolution of the time-dependent pdf $p(x, t) = P(X_t = x)$ of X_t is given by the Fokker-Planck equation [10]

$$\frac{\partial}{\partial t}p(x,t) = -\frac{\partial}{\partial x}F(x)p(x,t) + \frac{\sigma^2}{2}\frac{\partial^2}{\partial x^2}p(x,t), \tag{2.5.2}$$

which can be written in operator form as

$$\frac{\partial}{\partial t}p(x,t) = L^{\dagger}p(x,t), \tag{2.5.3}$$

where

$$L^{\dagger} = -\frac{\partial}{\partial x}F(x) + \frac{\sigma^2}{2}\frac{\partial^2}{\partial x^2}, \tag{2.5.4}$$

is the Fokker-Planck operator. The dual L of this linear differential operator, which has the form

$$L = F(x)\frac{\partial}{\partial x} + \frac{\sigma^2}{2}\frac{\partial^2}{\partial x^2}, \tag{2.5.5}$$

determines the evolution of expectations (i.e, average values) of functions of X_t according to [3]

$$\frac{\partial}{\partial t}\langle f(X_t)\rangle = \langle (Lf)(X_t)\rangle. \tag{2.5.6}$$

Assuming that X_t is ergodic, it has a unique invariant pdf which satisfies the equation

$$L^{\dagger}p_s(x) = 0, \tag{2.5.7}$$

which is also the stationary pdf as

$$\lim_{t\to\infty} p(x,t) = p_s(x). \tag{2.5.8}$$

The stationary pdf can be obtained easily in one-dimension and, in general, for $X_t \in \mathbb{R}^d$ when the drift $F(x)$ is the gradient of a scalar potential function, that is,

$$F(x) = -\nabla U(x). \tag{2.5.9}$$

In this case, we have

$$p_s(x) = e^{-\phi(x)}, \tag{2.5.10}$$

where

$$\phi(x) = \frac{2U(x)}{\sigma^2} + c \tag{2.5.11}$$

is the quasi-potential, and c is a normalization constant. This stationary pdf is known as the Gibbs distribution.

2.5.2 Large deviations

The stationary pdf $p_s(x)$ provides information about the fluctuation of the state X_t in the long-time limit. Following the previous sections, we will be interested here to study the fluctuations not of this state but of observables of the trajectories of the process, defined in general as

$$S_T = \frac{1}{T}\int_0^T f(X_t)dt + \frac{1}{T}\int_0^T g(X_t)\circ dX_t, \tag{2.5.12}$$

where $f(x)$ and $g(x)$ are real functions of the state. The integral involving f was already considered for jump processes. The integral involving g is the diffusion equivalent of the jump term that we had for jump processes and Markov chains. It now involves not the jumps of X_t (a Markov diffusion has no jump), but the increments dX_t of this process multiplied by $g(X_t)$ according to the Stratonovich product denoted by $\circ$ [3].

The form of f and g depends on the applications considered. In Chap. 3, we will consider the integrated current of a particle moving on a ring, obtained by choosing $f = 0$ and $g = 1$. In Chap. 4, we will consider instead the fraction of time that a Brownian particle spends in some interval Δ over the time interval $[0, T]$. In this case, we have $f(x) = \mathbb{1}_\Delta(x)$ and $g = 0$ where $\mathbb{1}_\Delta(x)$ is the indicator function equal to 1 if $x \in \Delta$ and 0 otherwise.

As before, we study the large deviations of S_T by calculating its SCGF

$$\lambda(k) = \lim_{T\to\infty} \frac{1}{T} \ln\langle e^{TkS_T}\rangle. \tag{2.5.13}$$

Similarly to Markov chains and Markov jump processes, it can be proved that $\lambda(k)$ is given by the dominant eigenvalue of a tilted generator L_k, which in this case is a deformation of the differential operator L shown in Eq. (2.5.5). Specifically, for the observable S_T defined in Eq. (2.5.12), the tilted generator has the form

$$L_k = F(x)\left(\frac{\partial}{\partial x} + kg\right) + \frac{\sigma^2}{2}\left(\frac{\partial}{\partial x} + kg\right)\left(\frac{\partial}{\partial x} + kg\right) + kf. \tag{2.5.14}$$

Thus

$$\lambda(k) = \zeta_{\max}(L_k). \tag{2.5.15}$$

This is proved in Appendix B using the Feynman-Kac formula.

In order to find the dominant eigenvalue of L_k, we need to solve the spectral equation

$$L_k r_k(x) = \lambda(k) r_k(x), \tag{2.5.16}$$

where $\lambda(k)$ is the dominant (real) eigenvalue of L_k and $r_k(x)$ is the corresponding eigenfunction which is positive by the Perron-Frobenius Theorem. The method used to solve this spectral problem depends on the system considered and the form of L. For our purpose we can distinguish the following cases:

- If L is Hermitian ($L = L^\dagger$), $f \neq 0$ and $g = 0$, then L_k is also Hermitian since

  $$L_k = L + kf. \tag{2.5.17}$$

  In this case, we have essentially a quantum problem that can be solved using quantum mechanical techniques.

- If L is non-Hermitian ($L \neq L^\dagger$) but its spectrum is real, then X_t is a reversible or equilibrium process having a gradient drift $F = -\nabla U$ (assuming that σ is constant). In this case we can transform L into a Hermitian operator H from the knowledge of the stationary pdf $p_s(x)$. This transformation, called a symmetrization, can also be applied to L_k when $f \neq 0$ and $g = 0$, as will be illustrated in the next section.
- If L is non-Hermitian ($L \neq L^\dagger$) and its spectrum is not real, then X_t is known to be a non-reversible and nonequilibrium process for which L cannot be symmetrized [10]. This also applies if L_k is non-Hermitian, for example, if F is non-gradient, as will be studied in Chap. 3.

It is useful to note for what follows that $r_k(x)$ must be a constant when $k \to 0$ since $L_{k=0} = L$ and Eq. (2.5.6) gives 0 when the test function f is a contant. By normalization, we can choose this constant to be 1. Thus $r_{k=0}(x) = 1$.

2.5.3 Symmetrization

Let us consider a d-dimensional diffusion $X_t \in \mathbb{R}^d$ given by the SDE (2.5.1) with gradient drift $F = -\nabla U$ and $W_t \in \mathbb{R}^d$. In this case, it is known that the spectrum of L is real even though this generator, as given in (2.5.5), is not Hermitian, so that X_t represents a reversible or equilibrium process. As a result, L must be conjugated in a unitary way to a Hermitian operator, constructed explicitly by the transformation

$$H = p_s^{\frac{1}{2}} L p_s^{-\frac{1}{2}}, \tag{2.5.18}$$

where P_s is the Gibbs stationary distribution pdf of X_t. This transformation is called a symmetrization. Replacing the expression of P_s given by Eq. (2.5.10) and the expression of the operator L given by Eq. (2.5.5) into the previous relation yields

$$H\psi = e^{-\frac{U}{\sigma^2}}(F \cdot \nabla + \frac{\sigma^2}{2}\Delta)e^{\frac{U}{\sigma^2}}\psi, \tag{2.5.19}$$

for the action of H on a function ψ, where $\Delta = \nabla^2$ is the Laplacian. Replacing $F = -\nabla U$ into this expression and expanding gives

$$\begin{aligned} H\psi &= e^{-\frac{U}{\sigma^2}}\Big[-\frac{(\nabla U)^2}{\sigma^2}\psi - \nabla U \nabla\psi \\ &\quad + \frac{\sigma^2}{2}\left(\frac{(\nabla U)^2}{\sigma^4}\psi + 2\frac{\nabla U}{\sigma^2}\nabla\psi + \psi\frac{\Delta U}{\sigma^2} + \Delta\psi\right)\Big]e^{\frac{U}{\sigma^2}}. \end{aligned} \tag{2.5.20}$$

Simplifying the latter expression then leads to

$$H\psi = \frac{\sigma^2}{2}\Delta\psi - \frac{(\nabla U)^2}{2\sigma^2}\psi + \frac{\Delta U}{2}\psi, \tag{2.5.21}$$

which can be rewritten as

$$H\psi = \left(\frac{\sigma^2}{2}\Delta - V\right)\psi, \tag{2.5.22}$$

where

$$V = \frac{(\nabla U)^2}{2\sigma^2} - \frac{\Delta U}{2} \tag{2.5.23}$$

is an "effective" Schrödinger potential for the Schrödinger "Hamiltonian" H which is obviously self-adjoint.

This symmetrization can also be applied to L_k if $g = 0$. In this case, we simply have $L_k = L + kf$ so that

$$H_k = H + kf = \frac{\sigma^2}{2}\Delta - V_k, \tag{2.5.24}$$

where

$$V_k = V - kf = \frac{(\nabla U)^2}{2\sigma^2} - \frac{\Delta U}{2} - kf. \tag{2.5.25}$$

Moreover, it is easy to see that the eigenfunctions of H_k defined by

$$H_k\psi_k(x) = \lambda(k)\psi_k(x), \tag{2.5.26}$$

are such that

$$\psi_k(x) = e^{-\phi(x)/2}r_k(x), \tag{2.5.27}$$

where $r_k(x)$ is, as before, the dominant eigenfunction of L_k with dominant eigenvalue $\lambda(k)$.

Example 2.5.1 (Ornstein-Uhlenbeck process with linear observable). The one-dimensional Ornstein-Uhlenbeck process is defined as

$$dX_t = -\gamma X_t dt + \sigma dW_t, \tag{2.5.28}$$

where the force $F(x) = -\gamma x$ derives from the potential $U(x) = \frac{\gamma x^2}{2}$, so that the quasi-potential is $\phi = \frac{\gamma x^2}{\sigma^2}$. Let us consider the observable defined as

$$S_T = \frac{1}{T}\int_0^T X_t dt. \tag{2.5.29}$$

The tilted generator associated with this observable is obtained by replacing $g = 0$ and $f = x$ into Eq. (2.5.14), which gives

$$L_k = -\gamma x\frac{\partial}{\partial x} + \frac{\sigma^2}{2}\frac{\partial^2}{\partial x^2} + kx. \tag{2.5.30}$$

This tilted generator is not Hermitian, but since X_t is gradient, it can be symmetrized, leading to

$$H_k = \frac{\sigma^2}{2}\Delta - V_k, \tag{2.5.31}$$

where

$$V_k(x) = \frac{\gamma^2 x^2}{2\sigma^2} - \frac{\gamma}{2} - kx. \tag{2.5.32}$$

The SCGF is thus found by solving the equation

$$\frac{\sigma^2}{2}\frac{\partial^2}{\partial x^2}\psi_n(x) - \left(\zeta_n + \frac{\gamma^2 x^2}{2\sigma^2} - \frac{\gamma}{2} - kx\right)\psi_n(x) = 0, \tag{2.5.33}$$

where ζ_n are the eigenvalues. This can be rewritten as

$$\frac{\partial^2}{\partial y^2}\psi_n(y) + (\epsilon_n - y^2)\psi_n(y) = 0, \tag{2.5.34}$$

where

$$\epsilon_n = -\frac{2\zeta_n}{\gamma} + \frac{\sigma^2 k^2}{\gamma^3} + 1 \tag{2.5.35}$$

and

$$y = \frac{\sqrt{\gamma}}{\sigma}\left(x - \frac{\sigma^2 k}{\gamma^2}\right). \tag{2.5.36}$$

We recognize in this equation the Schrödinger equation for the quantum harmonic oscillator with quantized energies given by

$$\epsilon_n = 2n + 1, \tag{2.5.37}$$

which give rise to

$$\zeta_n = \frac{\sigma^2 k^2}{2\gamma^2} - \frac{n\gamma}{2}, n = 0, 1, \ldots \tag{2.5.38}$$

The maximum eigenvalue of L_k corresponds to the minimum Schrödinger eigenvalue of H_k, $\zeta_0 = \frac{\sigma^2 k^2}{2\gamma^2}$, so that the SCGF is

$$\lambda(k) = \frac{\sigma^2 k^2}{2\gamma^2}. \tag{2.5.39}$$

The SCGF is differentiable and quadratic in k; hence the rate function obtained from the Legendre transform of $\lambda(k)$ is also quadratic:

$$I(s) = \frac{\gamma^2 s^2}{2\sigma^2}. \tag{2.5.40}$$

This result is shown in Fig. 2.5, where the curve is quadratic around its mean $s^\star = 0$ and possesses parabolic branches far from the mean. In this case the fluctuations are Gaussian.

Example 2.5.2 (Ornstein-Uhlenbeck process with quadratic observable). We consider the same Ornstein-Uhlenbeck process X_t as before but now with the observable

$$S_T = \frac{1}{T}\int_0^T X_t^2 dt. \tag{2.5.41}$$

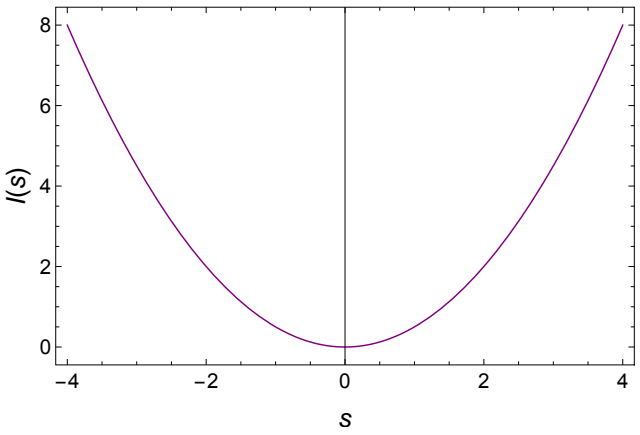

Figure 2.5: *Rate function $I(s)$ of the area per unit time of the Ornstein-Uhlenbeck process for $\gamma = 1$ and $\sigma = 1$.*

The calculation leading to the SCGF is similar to the previous example, with the difference only in the effective potential written as

$$V_k(x) = \frac{\gamma^2 x^2}{2\sigma^2} - \frac{\gamma}{2} - kx^2. \tag{2.5.42}$$

In this case, the Schrödinger equation is

$$\frac{\partial^2}{\partial^2}\psi_n(y) + (\epsilon_n - y^2)\psi_n(y) = 0, \tag{2.5.43}$$

which is again the equation of the quantum harmonic oscillator with energy

$$\epsilon_n = \frac{2}{\sqrt{\gamma^2 - 2\sigma^2 k}}\left(-\zeta_n + \frac{\gamma}{2}\right), \tag{2.5.44}$$

obtained by using the rescaled length $y = x\sqrt{\alpha}$ and $\alpha = \frac{\sqrt{\gamma^2 - 2\sigma^2 k}}{\sigma^2}$.

The energy of the harmonic oscillator is quantized, according to

$$\epsilon_n = 2n + 1, \tag{2.5.45}$$

so that for $n = 0$

$$\lambda(k) = \frac{\gamma}{2} - \frac{1}{2}\sqrt{\gamma^2 - 2\sigma^2 k} \tag{2.5.46}$$

for $k < \frac{\gamma^2}{2\sigma^2}$. Since $\lambda(k)$ is differentiable, the rate function is obtained from the Legendre transform. The result is

$$I(s) = \frac{\gamma^2 s}{2\sigma^2} - \frac{\gamma}{2} + \frac{\sigma^2}{8s} \tag{2.5.47}$$

for $s \geq 0$. This result is shown in Fig. 2.6. We notice that when $s \to \infty$ the curve is linear with the slope $\gamma^2/2\sigma^2$, and when $s \to 0$, the curve diverges as $1/s$. In this case, the fluctuations of S_T are Gaussian around its mean but non-Gaussian far from its mean.

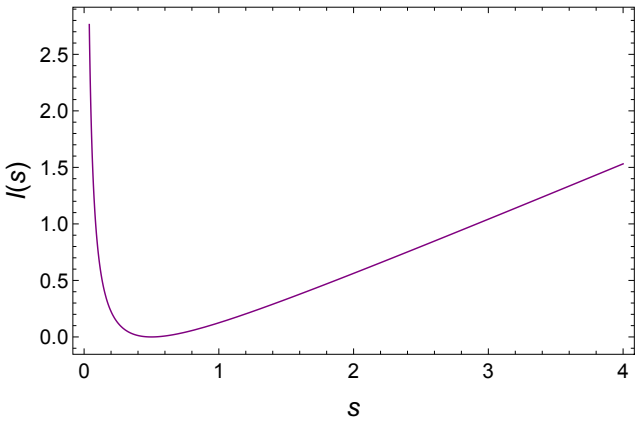

Figure 2.6: *Rate function $I(s)$ of the quadratic integral of the Ornstein-Uhlenbeck process for $\sigma = 1$ and $\gamma = 1$.*

2.6 Driven process

We have obtained in the previous sections the large deviation functions describing the fluctuations of time-integrated observables S_n or S_T of Markov processes. In this section we study a process that describes how these fluctuations are created in terms of an effective process, called the driven process.

This driven process was studied by Jack and Sollich [26] and more recently by Chetrite and Touchette [12, 21, 22]. For a diffusion process described by the general SDE (2.5.1), the driven process is constructed from the dominant eigenfunction $r_k(x)$ entering in the spectral problem (2.5.16). Given this eigenfunction, the effective process is the new diffusion $\hat{X}_t$ given by the SDE

$$d\hat{X}_t = F_k(\hat{X}_t)dt + \sigma dW_t, \tag{2.6.1}$$

where

$$F_k(x) = F(x) + D(kg + \nabla \ln r_k) \tag{2.6.2}$$

and $D = \sigma\sigma^T$.

It is shown in [12, 21] that this process corresponds in the long-time limit to the original process X_t conditioned on reaching the fluctuation $S_T = s$ if we choose the parameter k such that

$$\lambda'(k) = s \tag{2.6.3}$$

or equivalently

$$I'(s) = k \tag{2.6.4}$$

if $I(s)$ is convex. This is similar to choosing the temperature of the canonical ensemble in such a way that the microcanonical ensemble with fixed energy is equivalent to the canonical ensemble with fixed temperature. Here, the

process X_t conditioned on $S_T = s$ represents a microcanonical ensemble of trajectories whereas the process $\hat{X}_t$ defined by (2.6.1) is a canonical ensemble of trajectories [21].

More simply, the effective process can be seen as the process that makes a fluctuation $S_T = s$, which is atypical for X_t, typical for $\hat{X}_t$. In other words, paths of X_t leading to atypical values of S_T, having a low probability to be observed become typical for $\hat{X}_t$ and thus have a high probability to be observed. This can be seen from the relation

$$\langle S_T \rangle_k = \lambda'(k) = s, \tag{2.6.5}$$

which shows that the average value of S_T in the driven process with parameter k is the fluctuation S_T in the original process if k is chosen as in Eq. (2.6.3). In this sense, $\hat{X}_t$ can be seen as the process that creates such fluctuations. For a proof of this relation, see [12, 21]. The following example, also taken from [12], illustrates these results.

Example 2.6.1 (Ornstein-Uhlenbeck process with linear observable). We revisit the example about the Ornstein-Uhlenbeck process with a linear observable

$$S_T = \frac{1}{T}\int_0^T X_t dt. \tag{2.6.6}$$

The eigenvalue equation associated with this observable is the analogue of the quantum harmonic oscillator, as already mentioned in Example 2.5.1. The quantum eigenfunction $\psi_k(x)$ of the ground state is

$$\psi_k(x) = Ne^{-\frac{y^2}{2}} = Ne^{-\frac{\gamma}{2\sigma^2}\left(x-\frac{\sigma^2 k}{\gamma^2}\right)^2}, \tag{2.6.7}$$

where N is a normalization constant. Therefore the dominant eigenfunction $r_k(x)$ of L_k is given from Eq. (2.5.27) as

$$r_k(x) = e^{\frac{kx}{\gamma} - \frac{\sigma^2 k^2}{2\gamma^3}}. \tag{2.6.8}$$

From this, we find the modified force or drift $F_k(x)$ from Eq. (2.6.2) as

$$F_k(x) = -\gamma x + \frac{\sigma^2 k}{\gamma}. \tag{2.6.9}$$

Using the known expression of the SCGF $\lambda(k)$ for this problem, as given in Eq. (2.5.39), we solve for

$$\lambda'(k) = \frac{\sigma^2 k}{\gamma^2} = s \tag{2.6.10}$$

to find

$$k(s) = \frac{\gamma^2 s}{\sigma^2}, \tag{2.6.11}$$

so that

$$F_{k(s)}(x) = -\gamma x + \gamma s. \tag{2.6.12}$$

This is the modified drift of the new diffusion $\hat{X}_t$ that creates the fluctuation $S_T = s$. We notice that the change in the original force is just a shift of the original force according to the value of s considered. In this case, conditioning X_t on $S_T = s$ only adds a constant drift to the original process.

Example 2.6.2 (Ornstein-Uhlenbeck process with quadratic observable). Repeating the same calculation for the Ornstein-Uhlenbeck process but with the quadratic observable S_T of Eq. (2.5.41) gives

$$\psi_k(x) = Ne^{-\frac{x^2}{2\sigma^2}\sqrt{\gamma^2-2\sigma^2 k}} \tag{2.6.13}$$

and

$$r_k(x) = e^{\frac{x^2}{2\sigma^2}\left(\gamma-\sqrt{\gamma^2-2\sigma^2 k}\right)}. \tag{2.6.14}$$

In this case, the modified force is obtained as

$$F_k(x) = -x\sqrt{\gamma^2 - 2\sigma^2 k}, \tag{2.6.15}$$

for $k \geq \gamma^2/2\sigma^2$. Using the known expression of $\lambda(k)$ in Eq. (2.5.46), we then obtain

$$F_{k(s)}(x) = -\frac{\sigma^2}{2s}x. \tag{2.6.16}$$

In this case, the modified force has a slope that does not depend anymore on γ but only on σ and s: the conditioning keeps the original force linear, but changes its friction, which increases or decreases the value of the variance S_T.

Chapter 3

Current large deviations for driven periodic diffusions

We begin in this chapter our study of large deviations by considering the current fluctuations of a diffusion on the circle, which models the overdamped motion of a Brownian particle driven in a nonequilibrium state by a constant force, a potential, and a noise source. We first define the model and analyze its stationary distribution and mean current for various parameters. Then we proceed to calculate the rate function of the time-integrated current, which characterizes its fluctuations in the long-time limit, and the driven process that explains how these fluctuations arise. We will see from these results that there is a strong crossover, for some parameters, between Gaussian and non-Gaussian fluctuations, which is clearly explained by the form of the driven process.

3.1 Model

The model that we consider is defined by the following SDE:

$$d\theta_t = (\gamma + V_0 \sin\theta_t)dt + \sigma dW_t, \tag{3.1.1}$$

where

- $\theta_t \in [0, 2\pi)$ is the angular position of the particle at time t.
- $V_0 \sin\theta$ is the force deriving from the periodic potential $U(\theta) = V_0 \cos\theta$ so that $f(\theta) = -U'(\theta)$.
- $V_0 > 0$ is the potential amplitude.
- $\gamma > 0$ is a constant drive or torque.
- W_t is a one-dimensional Brownian motion.

- $\sigma > 0$ is the noise amplitude.

Physically, this equation can be thought of as representing the overdamped motion of a particle of mass $m = 1$ moving on the ring of unit radius subjected to two forces: the force $f(\theta) = V_0 \sin\theta$ deriving from the periodic potential, and the constant torque γ. This diffusion represents one of the simplest nonequilibrium systems violating detailed balance when a torque is applied ($\gamma \neq 0$) and has played, as such, an important role in the development of recent results about nonequilibrium theory [8, 27–29]. It is also used as a model of Josephson junctions subjected to thermal noise [10, 30, 31] as explained in Appendix D, Brownian ratchets [27, 32], and manipulated Brownian particles [33–35], among other systems, and is thus an ideal experimental testbed for the physics of nonequilibrium systems.

In the next sections, we first describe the dynamics of this model without noise ($\sigma = 0$) and then describe its stationary distribution in the presence of noise with and without torque. This is useful for understanding the mean velocity of the particle which we will complement by studying the large deviations of the current far away from its mean.

3.1.1 Deterministic motion

Without noise, the SDE (3.1.1) becomes an ordinary differential equation (ODE) corresponding to

$$\dot{\theta}_t = F(\theta_t), \tag{3.1.2}$$

where

$$F(\theta) = V_0 \sin\theta + \gamma \tag{3.1.3}$$

is the total force. The long-time behaviour of this dynamics is determined by its fixed points $\theta^\star$ which are the values of θ such that $F(\theta^\star) = 0$. They are thus obtained by solving the equation

$$\sin\theta^\star = -\frac{\gamma}{V_0}. \tag{3.1.4}$$

This equation has two solutions for $0 \leq \gamma < V_0$, one solution for $\gamma = V_0$, and no solution for $\gamma > V_0$. The stability of these solutions is determined by the sign of the derivative of $F(\theta^\star)$ which has the form

$$F'(\theta^\star) = V_0 \cos(\theta^\star) \tag{3.1.5}$$

The amplitude V_0 is positive by assumption. Thus, when $0 \leq \gamma < V_0$, the fixed point $\theta^\star$ with $\cos\theta^\star < 0$ corresponds to a stable fixed point while the fixed point $\theta^\star$ with $\cos\theta^\star > 0$ corresponds to an unstable fixed point.

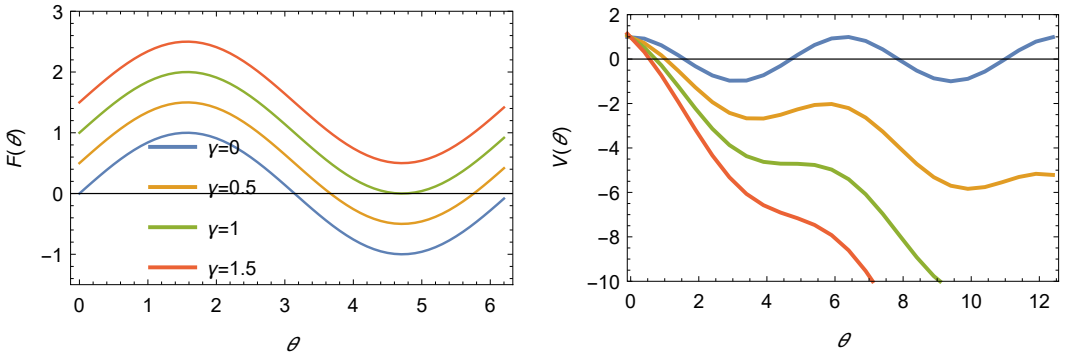

Figure 3.1: *Left: Force $F(\theta)$ given by Eq. (3.1.3). Right: Associated potential $V(\theta)$ given by Eq. (3.1.7).*

The existence and stability of fixed points can also be determined by defining a potential associated with the total force $F(\theta)$ as

$$F(\theta) = -V'(\theta) \tag{3.1.6}$$

or equivalently

$$V(\theta) = -\int_0^\theta F(\alpha)d\alpha. \tag{3.1.7}$$

This potential is plotted in Fig. 3.1 for different values of γ and is compared with $F(\theta)$. From this figure, we notice the following cases:

- $\gamma = 0$: In this case, θ_t has a stable fixed point $\theta^\star = \pi$ corresponding to the minimum of $V(\theta)$, to which any initial condition is attracted as $t \to \infty$. The other fixed point at $\theta^\star = 0$ is unstable and corresponds to the maximum of $V(\theta)$.

- $0 < \gamma < V_0$: In this case, the stable and unstable fixed points move away from π and 0, respectively, but still correspond to the minimum and maximum of $V(\theta)$, respectively. Moreover, they get closer and closer as $\gamma \to V_0$.

- $\gamma = V_0$: In this case, there is only one fixed point at $\theta^\star = \frac{3\pi}{2}$, which is a marginally stable point. It is a critical point of $V(\theta)$ which is neither a maximum nor a minimum.

- $\gamma > V_0$: In this case, there is no longer a fixed point. The dynamics of θ_t started from any initial condition θ_0 will freely rotate with a velocity given by the ODE (3.1.2).

It follows from these observations that, if $\gamma < V_0$, then there is a fixed point which attracts permanently the particle as $t \to \infty$. In this case, it is impossible for the particle to flow around the circle. We called this the locked state. On the other hand, if $\gamma > V_0$ there are no longer fixed points. The particle is no longer trapped and rotates, in what we call the running state. The running state has in general a space-dependent velocity given by $F(\theta)$. In the case $V_0 = 0$, $F(\theta) = \gamma$, so the particle rotates at constant velocity equal to the torque.

3.1.2 Stationary distribution

The time-dependent probability density $p(\theta, t) = P(\theta_t = \theta)$ evolves according to the Fokker-Planck equation

$$\frac{\partial}{\partial t}p(\theta,t) = -\frac{\partial}{\partial \theta}F(\theta,t)p(\theta,t) + \frac{\sigma^2}{2}\frac{\partial^2}{\partial \theta^2}p(\theta,t), \tag{3.1.8}$$

as mentioned already in Chap. 2, where $F(\theta)$ is, as before, the total force or drift of the SDE (3.1.1). This equation can be rewritten as

$$\frac{\partial}{\partial t}p(\theta,t) + \frac{\partial}{\partial \theta}J(\theta,t) = 0, \tag{3.1.9}$$

where

$$J(\theta,t) = F(\theta)p(\theta,t) - \frac{\sigma^2}{2}\frac{\partial}{\partial \theta}p(\theta,t) \tag{3.1.10}$$

is the Fokker-Planck probability current. Assuming that the diffusion θ_t is ergodic, it has a unique stationary density, $p_s(\theta)$, satisfying

$$\frac{\partial}{\partial t}p_s(\theta,t) = 0 \tag{3.1.11}$$

or, equivalently,

$$\frac{\partial}{\partial \theta}J(\theta,t) = 0. \tag{3.1.12}$$

For the periodic diffusion that we consider, $p_s(\theta)$ exists for all $V_0 \geq 0$, $\gamma \geq 0$, $\sigma > 0$, and strongly depends on whether $\gamma = 0$ or $\gamma \neq 0$. For $\gamma = 0$, the total force $F(\theta)$ is gradient which leads to the stationary distribution

$$p_s(\theta) = ce^{-\frac{2U(\theta)}{\sigma^2}}, \tag{3.1.13}$$

where c is the constant determined by normalizing $p_s(\theta)$. This Gibbs distribution applies to equilibrium processes, which is the case here since $J(\theta, t) = 0$. For $\gamma \neq 0$, the total force $F(\theta)$ is no longer the gradient of a periodic potential, so that $p_s(\theta)$ is not the Gibbs distribution. In this case, there is a constant current

$$J(\theta,t) = c_1, \tag{3.1.14}$$

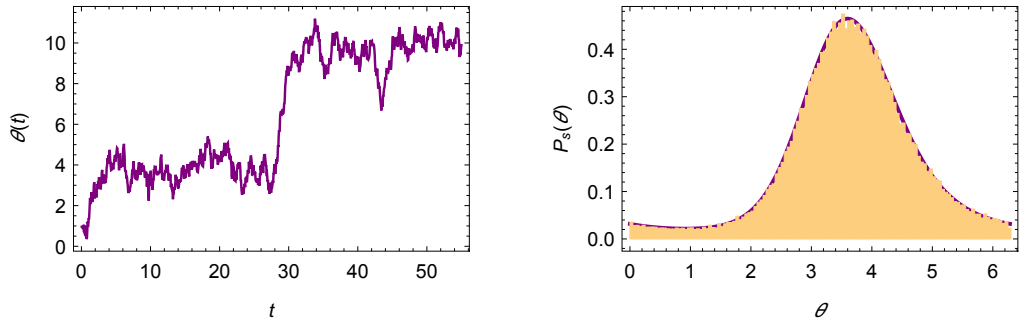

Figure 3.2: *Left: Sample trajectory of the ring model for* $\gamma = 0.5$, $\sigma = 1$ *and* $V_0 = 1$ *showing the (real) angle jumping around the locked state at* $\theta^\star = 7\pi/6$. *Right: Corresponding stationary distribution. The yellow bins represent the pdf histogram of* 10^5 *trajectories for the same parameters after a time* $t = 10$ *for a step time* $dt = 0.02$. *The solid curve is the analytical stationary solution.*

which can be used to obtain the stationary distribution from the Fokker-Planck equation by imposing the periodic boundary condition

$$p_s(\theta) = p_s(\theta + 2\pi n) \tag{3.1.15}$$

and the normalization condition, as shown in [10]. The end result is

$$p_s(\theta) = ce^{-\frac{2V(\theta)}{\sigma^2}} \left(1 - l\int_0^\theta e^{\frac{2V(\theta')}{\sigma^2}} d\theta'\right), \tag{3.1.16}$$

where $V(\theta)$ is the non-periodic potential defined in Eq. (3.1.7),

$$l = \frac{(1 - e^{-\frac{4\pi\gamma}{\sigma^2}})}{w} \tag{3.1.17}$$

and

$$w = \int_0^{2\pi} e^{\frac{2V(\theta)}{\sigma^2}} d\theta. \tag{3.1.18}$$

The normalization constant c is

$$c = \frac{1}{\int_0^{2\pi} p_s(\theta) d\theta} \tag{3.1.19}$$

and the stationary current c_1 in Eq. (3.1.14) is

$$c_1 = \frac{c\sigma^2}{2w}(1 - e^{-\frac{4\pi\gamma}{\sigma^2}}). \tag{3.1.20}$$

These results are illustrated in Fig. 3.2 and 3.3 and are compared with histograms obtained numerically by sampling trajectories of the SDE with $N = 10^5$ and $dt = 0.02$ up to the final time $t = 10$. A few cases are worth noting:

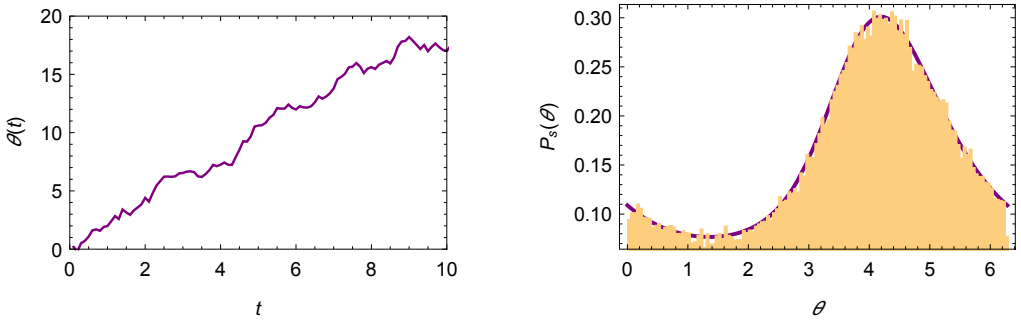

Figure 3.3: *Left: Trajectory of the ring model for* $\gamma = 1.5$, $\sigma = 1$ *and* $V_0 = 1$ *showing a running state. Right: Corresponding stationary distribution. The yellow bins represent the pdf histogram of* 10^5 *trajectories for the same parameters after a time* $t = 10$. *The solid curve is the analytical stationary solution.*

- $V_0 = 0, \gamma = 0$: In this case, the particle moves according to the Brownian motion, leading to the uniform stationary distribution

$$p_s(\theta) = \frac{1}{2\pi}, \tag{3.1.21}$$

for $\theta \in [0, 2\pi)$.

- $V_0 > 0, \gamma = 0$: In this case, the Gibbs stationary distribution $p_s(\theta)$, as given by Eq. (3.1.16), is peaked around the stable fixed point $\theta^\star = \pi$ corresponding to the minimum of the potential $U(\theta)$.

- $V_0 > 0$, $\gamma < V_0$: In this case, $p_s(\theta)$ is also peaked around the stable fixed point $\theta^\star$ which now corresponds to the minimum of $V(\theta)$, as shown in Fig. 3.2. This figure also shows that although the particle is attracted by the stable fixed point, the noise and γ can also force it to jump from one well of $V(\theta)$ to another, thus creating a current on the ring.

- $V_0 > 0$, $\gamma > V_0$: In this case, the torque γ is larger than the potential barrier of $V(\theta)$ and so the particle is free to rotate around the ring as shown in Fig. 3.3, with a positive average velocity $\langle \dot{\theta} \rangle$. The stationary distribution $p_s(\theta)$ is not uniform, as seen in this figure, because the velocity of the particle is not constant as a function of θ, as is the case for $V_0 = 0$.

3.1.3 Mean current

We have just seen that the particle has a positive mean velocity $\langle \dot{\theta} \rangle$ when $\gamma > V_0$. In this section we calculate this mean velocity $\langle \dot{\theta} \rangle$ by averaging the

velocity over one period τ of its motion [36]

$$\langle \dot{\theta} \rangle = \frac{1}{\tau} \int_0^\tau \dot{\theta}_t dt. \tag{3.1.22}$$

In the case without noise, $\sigma = 0$, this time average can be computed explicitly, as done in Appendix C, and gives

$$\langle \dot{\theta} \rangle = \sqrt{\gamma^2 - V_0^2} \tag{3.1.23}$$

for $|\gamma| > V_0$. For $|\gamma| \leq V_0$, the particle is attracted by the fixed point $\theta^\star$ (locked state) which means that $\langle \dot{\theta} \rangle = 0$. There is thus a bifurcation between the locked and the running states at $\gamma = V_0$.

For the case with noise, $\sigma > 0$, the average velocity can be calculated in the stationary regime from the so-called Stratonovich formula [10] as

$$\langle \dot{\theta} \rangle = \langle F(\theta) \rangle = \int_0^{2\pi} F(\theta) p_s(\theta) d\theta. \tag{3.1.24}$$

From Eq. (3.1.14), we obtain

$$F(\theta) p_s(\theta) = c_1 + \frac{\sigma^2}{2} \frac{\partial}{\partial \theta} p_s(\theta), \tag{3.1.25}$$

which yields from Eq. (3.1.24)

$$\langle \dot{\theta} \rangle = 2\pi c_1, \tag{3.1.26}$$

where c_1 is the stationary current shown in Eq. (3.1.20). Therefore,

$$\langle \dot{\theta} \rangle = \frac{\pi \sigma^2 \left(1 - e^{\frac{4\pi\gamma}{\sigma^2}}\right)}{1 - \left(1 - e^{-\frac{4\pi\gamma}{\sigma^2}}\right) \int_0^{2\pi} e^{-\frac{2V(\theta)}{\sigma^2}} \left(\int_0^\theta e^{\frac{2V(\theta')}{\sigma^2}} d\theta' \right) d\theta}, \tag{3.1.27}$$

This result, plotted in Fig. 3.4, confirms the result derived in [8, 27]. The dashed black curve in that figure shows the noiseless mean velocity, whereas the coloured curves show the mean velocity, which is proportional to the mean current, for different values of σ.

From this plot, we can see that when $\gamma > V_0$, there is no longer a fixed point and the particle gets into the running state, creating a current. For this case, the mean current is essentially equal to γ, in agreement with Eq. (3.1.23). When $\gamma = V_0$, the stable fixed point and the unstable fixed point collide and give rise to a bifurcation point (marginally stable point) corresponding to the point $\gamma = 1$ in Fig. 3.4.

With the presence of the noise, the bifurcation point is rounded and the particle rotates on the ring even for the case $\gamma < V_0$. However, then the mean current is essentially zero, whereas for $\gamma > V_0$ the mean current grows according to the intensity of the torque γ.

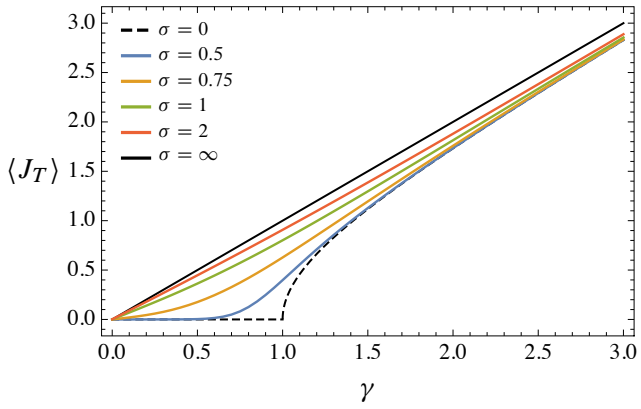

Figure 3.4: *Mean velocity $\langle\dot{\theta}\rangle$ which is proportional to the mean current $\langle J_T\rangle$ as a function of γ for $V_0 = 1$ and different values of σ. The dashed curve is the noiseless result whereas the coloured curves are the results with noise.*

3.2 Current fluctuations

We have seen in the previous section that the particle on the ring has a non-zero stationary mean velocity $\langle\dot{\theta}\rangle$ which is proportional to the stationary current. In this section we will study the fluctuations of the time-integrated current or velocity

$$J_T = \frac{1}{T}\int_0^T \dot{\theta}_t dt \tag{3.2.1}$$

around the mean using the large deviation results presented in Chap. 2.

Previous works [37, 38] have looked at the large deviations of this quantity, as well as the large deviations of the entropy production, which is linearly related to J_T [39–41]. Our goal in this section is to complete these studies by investigating the large deviation functions characterizing the fluctuations of J_T in all noise regimes. We also want to describe the diffusion conditionally on observing a current $J_T = j$ away from the mean current $\langle J_T\rangle$, by constructing the effective or driven process described before Sec. 2.6. This process is physically important for the reason explained in that section: it describes by means of a modified stochastic process how fluctuations of the current are created in time.

3.2.1 Definition of the current and LDP

The paths of pure diffusions are nowhere differentiable, as is well known, so the expression of the current shown in Eq. (3.2.1) is only a formal expression that should be rewritten as

$$J_T = \frac{1}{T}\int_0^T d\theta_t = \frac{2\pi N_T + (\theta_T - \theta_0)}{T}, \tag{3.2.2}$$

where N_T is the net number of turns done by the particle and θ_t is the angular position of the particle at time t taking values in $[0, 2\pi)$. Because the particle is moving in the periodic space, for any initial angle θ_0 chosen, the difference with the final angle θ_T may give zero. For that reason, we have to add the term $2\pi N_T$ such as to have a finite change in the angular position. This observable represents a fluctuating current. In the notations introduced in Chap. 2, it corresponds to the choice $f = 0$, $g = 1$.

Since θ_t is ergodic for $\sigma > 0$, then J_T satisfies an LDP in the long-time limit $T \to \infty$, expressed as

$$P(J_T = j) = e^{-TI(j)+o(T)}, \tag{3.2.3}$$

where, as before, $I(j)$ is the rate function characterizing the dominant exponential behaviour of the pdf and $o(T)$ represents any corrections in T that are smaller than linear in T. To find the rate function, we follow Sec. 2.5 by calculating the SCGF $\lambda(k)$ which corresponds to the dominant eigenvalue of the tilted generator

$$L_k = F(\theta)\left(\frac{d}{d\theta} + k\right) + \frac{\sigma^2}{2}\left(\frac{d}{d\theta} + k\right)^2. \tag{3.2.4}$$

Following the Gärtner-Ellis Theorem (see Sec. 2.2), if $\lambda(k)$ exists and is differentiable, then J_T has an LDP with rate function given by the Legendre transform

$$I(j) = k(j)j - \lambda(k(j)), \tag{3.2.5}$$

where $k(j)$ is the solution of $\lambda'(k) = j$.

In what follows, we will also construct the driven process associated with the fluctuation $J_T = j$ of the current, following Sec. 2.6. For the ring model, this process is the new diffusion

$$d\hat{\theta}_t = F_k(\hat{\theta}_t)dt + \sigma dW_t \tag{3.2.6}$$

with modified drift

$$F_k(\theta) = F(\theta) + \sigma^2\left(k + \frac{d}{d\theta}\ln r_k(\theta)\right), \tag{3.2.7}$$

where $r_k(\theta)$ is the dominant eigenfunction of L_k. To match the fluctuation $J_T = j$, k must be chosen as in Eq. (2.6.3) or Eq. (2.6.4).

It is difficult in general to find analytically the dominant eigenvalue $\lambda(k)$ of the non-Hermitian operator L_k and the associated driven process. We can find analytical solutions only in the case where $V_0 = 0$ as shown next. In all other cases, we must rely on numerical solutions.

3.2.2 Analytical solution for $\gamma \neq 0$ and $V_0 = 0$

In order to find the largest eigenvalue of the generator L_k, we need to find the spectrum of the eigenvalue equation defined by

$$L_k r_k(\theta) = \lambda(k) r_k(\theta), \tag{3.2.8}$$

where $\lambda(k)$ is the eigenvalue and $r_k(\theta)$ its corresponding eigenfunction. For our model with $\gamma \neq 0$ and $V_0 = 0$, this equation has the form

$$\frac{\sigma^2}{2}\frac{d^2}{d\theta^2} r_k(\theta) + (\gamma + \sigma^2 k)\frac{d}{d\theta} r_k(\theta) + \left(\frac{k^2\sigma^2}{2} + k\gamma\right) r_k(\theta) = \lambda(k) r_k(\theta). \tag{3.2.9}$$

This equation cannot be symmetrized for $\gamma \neq 0$, but can be solved by choosing the ansatz

$$r_k(\theta) = e^{s_k \theta}, \tag{3.2.10}$$

which yields, when substituted in Eq. (3.2.8),

$$\frac{\sigma^2}{2} s_k^2 + (\gamma + \sigma^2 k) s_k + \frac{k^2\sigma^2}{2} + k\gamma - \lambda(k) = 0. \tag{3.2.11}$$

The two solutions of s_k are

$$s_k = \frac{-(\gamma + \sigma^2 k) \pm i\sqrt{-2\sigma^2\lambda(k) - \gamma^2}}{\sigma^2}, \tag{3.2.12}$$

so that

$$r_k(\theta) = e^{-\frac{\gamma+\sigma^2 k}{\sigma^2}\theta}\left(A e^{i\frac{\sqrt{-2\sigma^2\lambda(k)-\gamma^2}}{\sigma^2}\theta} + B e^{-i\frac{\sqrt{-2\sigma^2\lambda(k)-\gamma^2}}{\sigma^2}\theta}\right). \tag{3.2.13}$$

This expression can be rewritten as

$$r_k(\theta) = e^{-\frac{\gamma+\sigma^2 k}{\sigma^2}\theta}\left(A e^{im\theta} + B e^{-im\theta}\right), \tag{3.2.14}$$

where

$$m = \frac{\sqrt{-2\sigma^2\lambda(k) - \gamma^2}}{\sigma^2} \tag{3.2.15}$$

and A and B are constants determined by the boundary and the normalization conditions.

From the periodic boundary condition, $r_k(0) = r_k(2\pi)$, we obtain

$$e^{(-\frac{\gamma+\sigma^2 k}{\sigma^2} \pm im)2\pi} = 1 \tag{3.2.16}$$

which yields

$$-\frac{\gamma + \sigma^2 k}{\sigma^2} \pm im = n. \tag{3.2.17}$$

The largest eigenvalue of the operator L_k corresponds to the minimum eigenvalue obtained for $n = 0$, so that

$$m = \pm i\frac{\gamma + \sigma^2 k}{\sigma^2}. \tag{3.2.18}$$

Replacing this result into Eq. (3.2.14) and imposing the normalization condition $\int_0^{2\pi} r_k(\theta) = 1$, we get $A = \frac{1}{2\pi}$ and $B = 0$. Thus, the eigenfunction is simply

$$r_k(\theta) = \frac{1}{2\pi}, \tag{3.2.19}$$

so that

$$\lambda(k) = k\gamma + \frac{\sigma^2 k^2}{2}, \tag{3.2.20}$$

which is differentiable. Thus, the rate function is obtained by the Legendre transform, Eq. (3.2.5), as

$$I(j) = \frac{(j-\gamma)^2}{2\sigma^2}. \tag{3.2.21}$$

Therefore, we see that the fluctuations of J_T in the absence of potential ($V_0 = 0$) are Gaussian around the value γ, which corresponds to the mean current $\langle J_T \rangle = \gamma$. From this result, we obtain the driven process by noting that $\lambda'(k) = j$ gives

$$k(j) = \frac{j-\gamma}{\sigma^2} \tag{3.2.22}$$

and thus

$$F_{k(j)}(\theta) = j. \tag{3.2.23}$$

In this case, we see that the driven process is simple: it has an added drift or torque that creates the fluctuation $J_T = j$ as a typical current. In particular, for $J_T = \langle J_T \rangle = \gamma$, we obtain $k(\gamma) = 0$ and so $F_{k=0}(\theta) = \gamma$, which is the original process. For $k \neq 0$, we have instead $\langle J_T \rangle_k = j(k) = \lambda'(k)$.

3.3 Numerical solution

This section is devoted to solving the eigenvalue equation (3.2.8), which determines the SCGF $\lambda(k)$ and the associated eigenfunction $r_k(x)$, using a Fourier-Bloch decomposition of that equation [40]. We explain the method next and then present its application for different values of V_0, γ and σ.

3.3.1 Fourier-Bloch method

The state θ_t is periodic and so is the force $F(\theta) = \gamma - U'(\theta)$ and $r_k(\theta)$. As a result, it makes sense to decompose $U'(\theta)$ and $r_k(\theta)$ in Fourier series as

$$r_k(\theta) = \sum_n c_n e^{in\theta}, \quad n \in \mathbb{Z} \tag{3.3.1}$$

$$U'(\theta) = \sum_l v_l e^{il\theta}, \quad l \in \mathbb{Z}. \tag{3.3.2}$$

Substituting these expressions into the eigenvalue equation Eq. (3.2.8) yields

$$\left(\gamma - \sum_l v_l e^{il\theta} + \sigma^2 k\right) \sum_n inc_n e^{in\theta} - \frac{\sigma^2}{2} \sum_n n^2 c_n e^{in\theta} + \frac{k^2\sigma^2}{2} \sum_n c_n e^{in\theta}$$
$$+ \left(\gamma - \sum_l v_l e^{il\theta}\right) k \sum_n c_n e^{in\theta} = \lambda(k) \sum_n c_n e^{in\theta}. \tag{3.3.3}$$

Expanding this equation and regrouping each term gives

$$\sum_n \left[\left(in(\gamma + \sigma^2 k) - \frac{\sigma^2 n^2}{2} + k\gamma + \frac{k^2\sigma^2}{2} - \lambda(k)\right) c_n - \sum_l (i(n-l) - k) v_l c_{n-l}\right] e^{in\theta} = 0, \tag{3.3.4}$$

which leads to the following recurrence relation for the coefficients c_n:

$$\left(in(\gamma + \sigma^2 k) - \frac{\sigma^2 n^2}{2} + k\gamma + \frac{k^2\sigma^2}{2} + (in + k)v_0 - \lambda(k)\right) c_n - \sum_{l \neq n} (i(n-l) - k) v_l c_{n-l} = 0. \tag{3.3.5}$$

For our model, $U'(\theta) = -V_0 \sin(\theta)$, so the Fourier coefficients are $v_{-1} = \frac{V_0}{2i}, v_0 = 0$ and $v_1 = -\frac{V_0}{2i}$. Consequently, the previous relation becomes

$$b_n^- c_{n-1} + (a_n - \lambda(k)) c_n + b_n^+ c_{n+1} = 0, \tag{3.3.6}$$

where

$$\begin{aligned} a_n &= in(\gamma + \sigma^2 k) - \frac{\sigma^2 n^2}{2} + k\gamma + \frac{k^2\sigma^2}{2}, \\ b_n^- &= \frac{V_0}{2}(n - 1 - ik), \\ b_n^+ &= \frac{V_0}{2}(-n - 1 + ik). \end{aligned} \tag{3.3.7}$$

This system of equations can be represented as an infinite tridiagonal matrix

$$\begin{pmatrix}
\ddots & \ddots & 0 & \dots & \dots & \dots & \dots & \dots & 0 \\
b_{-3}^- & a_{-3}-\lambda(k) & b_{-3}^+ & \ddots & \ddots & \ddots & \ddots & \ddots & \vdots \\
0 & b_{2}^- & a_{-2}-\lambda(k) & b_{2}^+ & \ddots & \ddots & \ddots & \ddots & \vdots \\
\vdots & \ddots & b_{-1}^- & a_{-1}-\lambda(k) & b_{-1}^+ & \ddots & \ddots & \ddots & \vdots \\
\vdots & \ddots & \ddots & b_{0}^- & a_{0}-\lambda(k) & b_{0}^+ & \ddots & \ddots & \vdots \\
\vdots & \ddots & \ddots & \ddots & b_{1}^- & a_{1}-\lambda(k) & b_{1}^+ & \ddots & \vdots \\
\vdots & \ddots & \ddots & \ddots & \ddots & b_{2}^- & a_{2}-\lambda(k) & b_{2}^+ & 0 \\
\vdots & \ddots & \ddots & \ddots & \ddots & \ddots & b_{3}^- & a_{3}-\lambda(k) & b_{3}^+ \\
0 & \dots & \dots & \dots & \dots & \dots & 0 & \ddots & \ddots
\end{pmatrix} \tag{3.3.8}$$

To determine the SCGF $\lambda(k)$, we truncate this tridiagonal system to a discrete range $n \in [-N, \dots, N]$ of modes and compute numerically the dominant eigenvalue of the corresponding $(2N+1) \times (2N+1)$ matrix, checking that the result converges for N large enough. In addition, we compute the dominant eigenfunction $r_k(\theta)$ which is a vector of size $2N+1$.

For example, truncation at $N = 2$ gives a 5×5 tridiagonal matrix corresponding to

$$\begin{pmatrix}
a_{-2}-\lambda(k) & b_{2}^+ & 0 & 0 & 0 \\
b_{-1}^- & a_{-1}-\lambda(k) & b_{-1}^+ & 0 & \\
0 & b_{0}^- & a_{0}-\lambda(k) & b_{0}^+ & 0 \\
0 & 0 & b_{1}^- & a_{1}-\lambda(k) & b_{1}^+
\end{pmatrix}, \tag{3.3.9}$$

while truncation at $N = 3$ gives a 7×7 tridiagonal matrix

$$\begin{pmatrix}
a_{-3}-\lambda(k) & b_{-3}^+ & 0 & 0 & 0 & 0 & 0 \\
b_{2}^- & a_{-2}-\lambda(k) & b_{2}^+ & 0 & 0 & 0 & 0 \\
0 & b_{-1}^- & a_{-1}-\lambda(k) & b_{-1}^+ & 0 & 0 & 0 \\
0 & 0 & b_{0}^- & a_{0}-\lambda(k) & b_{0}^+ & 0 & 0 \\
0 & 0 & 0 & b_{1}^- & a_{1}-\lambda(k) & b_{1}^+ & 0 \\
0 & 0 & 0 & 0 & b_{2}^- & a_{2}-\lambda(k) & b_{2}^+
\end{pmatrix}. \tag{3.3.10}$$

In these examples, the matrix coefficients are given as in Eq. (3.3.7) as

follows:

$$\begin{aligned}
b^-_{-2} &= \frac{V_0}{2}(-3-ik), \quad a_{-2} = -2i(\gamma+\sigma^2 k) - 2\sigma^2 + m_0, \quad b^+_{-2} = \frac{V_0}{2}(1+ik) \\
b^-_{-1} &= \frac{V_0}{2}(-2-ik), \quad a_{-1} = -i(\gamma+\sigma^2 k) - \frac{\sigma^2}{2} + m_0, \quad b^+_{-1} = \frac{V_0}{2}ik \\
b^-_{0} &= \frac{V_0}{2}(-1-ik), \quad a_{0} = m_0, \quad b^+_{0} = \frac{V_0}{2}(-1+ik) \\
b^-_{1} &= -\frac{V_0}{2}ik, \quad a_{1} = i(\gamma+\sigma^2 k) - \frac{\sigma^2}{2} + m_0, \quad b^+_{1} = \frac{V_0}{2}(-2+ik) \\
b^-_{2} &= \frac{V_0}{2}(1-ik), \quad a_{2} = 2i(\gamma+\sigma^2 k) - 2\sigma^2 + m_0, \quad b^+_{2} = \frac{V_0}{2}(-3+ik)
\end{aligned} \tag{3.3.11}$$

where $m_0 = k\gamma + \frac{k^2\sigma^2}{2}$.

We present the results of these calculations for various parameters V_0, γ and σ in the next sections. In all cases, the N used is between $N = 5$ and $N = 30$ modes depending mostly on the ratio σ/V_0. In general, the smaller σ/V_0 is, the larger N must be chosen.

3.3.1.1 $V_0 = 0$, $\gamma = 0$

The result of the Fourier-Bloch decomposition for these parameters is shown in Fig. 3.5. We can see that $\lambda(k)$ is a parabola, in agreement with the exact result of Eq. (3.2.20) with linear slope shown in the plot of $\lambda'(k)$. The rate function $I(j)$ is then also a parabola, following Eq. (3.2.21), centered at 0. As a result the current fluctuations are Gaussian around a zero mean current $\langle J_T \rangle = 0$, which arises because the system with $\gamma = 0$ is an equilibrium system satisfying detailed balance.

The bottom right plot in Fig. 3.5 shows that the effective force is constant everywhere, which means that the driven process is just a simple diffusion with a constant drift $F_k(\theta) = \sigma^2 k$, in agreement with what we found in Sec. 3.2.2. This result will be important for other cases: whenever the driven process has a constant torque, it is associated with Gaussian current fluctuations.

3.3.1.2 $V_0 = 0$, $\gamma > 0$

This case is similar to the previous case. All that changes is the value of $\lambda'(0)$ which determines the zero of $I(j)$ and thus the mean current $\langle J_T \rangle$, which in Fig. 3.6 is at $\gamma = 1$. We also see from this figure that the rate function (bottom left) is quadratic around the mean current $j = \gamma$, but is now asymmetric with respect to $j = 0$, in agreement with the exact result of Eq. (3.2.21). We will come to express this property later in terms of the fluctuation relation.

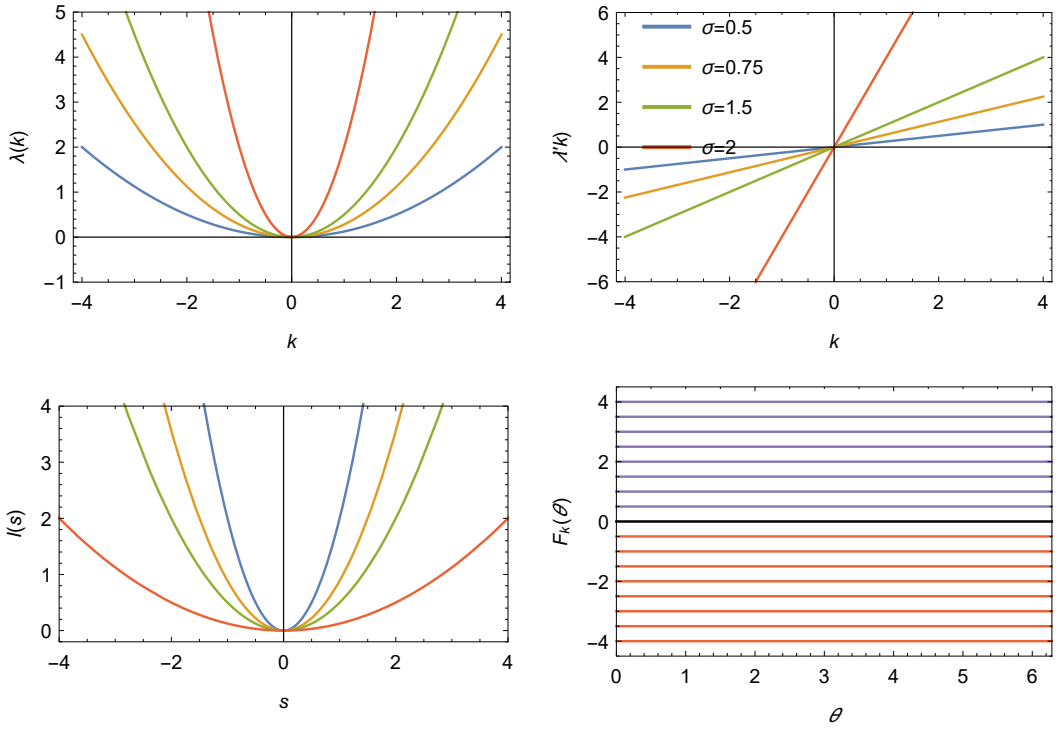

Figure 3.5: *Large deviation functions of the current for $V_0 = 0$, $\gamma = 0$ (free motion) and different noise amplitudes $\sigma \in \{0.5, 0.75, 1.5, 2\}$. Top left: SCGF $\lambda(k)$. Top right: Derivative of $\lambda(k)$. Bottom left: Rate function $I(j)$. Bottom right: Effective force $F_k(\theta)$ for $\sigma = 1$ and for different values of k taken in spacing of 0.5. The black line represents the unmodified force $F(\theta)$ obtained for $k = 0$, while the blue and red lines, obtained for $k > 0$ and $k < 0$, represent, respectively, positive and negative currents.*

The effective force (bottom right) is also seen to be constant in θ because $r_k(\theta)$ is also constant, as found before. In this case, again, we find

$$F_k(\theta) = \gamma + \sigma^2 k, \tag{3.3.12}$$

which is in agreement with Eq. (3.2.23).

3.3.1.3 $\gamma = 0$, $V_0 = 1$

We now consider in Fig. 3.7 the case where there is no torque but a potential. We observe that at high noise ($\sigma = 2$), $\lambda(k)$ is approximately parabolic, so that the rate function $I(j)$ is also parabolic. At low noise ($\sigma = 0.5$), these functions also have parabolic tails, but close to $k = 0$, $\lambda(k)$ now develops a flat plateau giving rise by Legendre transform to a corner in $I(j)$ at $j = 0$. If $I(j)$ had a real corner, we should have a discontinuous jump in the plot of $\lambda'(k)$ which is not the case. Zooming in the plot of $\lambda(k)$ shows in fact that the plateau of $\lambda(k)$ is not exactly flat, so that $I(j)$ is rounded at $j = 0$.

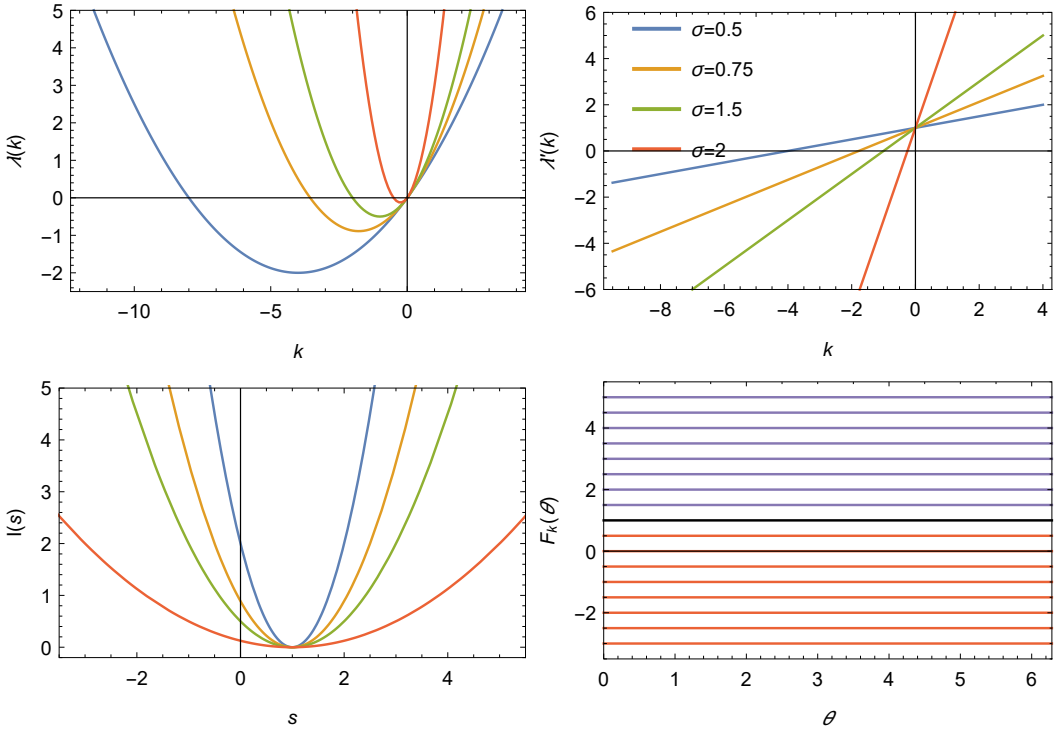

Figure 3.6: *Large deviation functions of the current for* $V_0 = 0$, $\gamma = 1$ *and for different values of* $\sigma \in \{0.5, 0.75, 1.5, 2\}$. *These parameters correspond to a running state without potential. Top left: SCGF* $\lambda(k)$. *Top right: Derivative of* $\lambda(k)$. *Bottom left: Rate function* $I(j)$. *Bottom right: Effective force* $F_k(\theta)$ *for* $\sigma = 1$ *and for different values of* k *taken in spacing of* 0.5. *The black line represents the unmodified force* $F(\theta)$ *obtained for* $k = 0$, *while the blue and red lines represent, respectively, positive and negative current fluctuations.*

These results show that, at high noise, current fluctuations are essentially Gaussian, whereas at low noise they are Gaussian for large current values but non-Gaussian for the small current values close to $J_T = 0$.

This difference between Gaussian and non-Gaussian fluctuations can be explained by looking at the effective force $F_k(\theta)$, shown in the bottom-right plot of Fig. 3.7. For small k, the periodic force is deformed in a nonlinear way around the fixed points (see green curves) in such a way as to create a small current fluctuation that is not Gaussian. For large $|k|$, however, meaning large current fluctuations in magnitude, $F_k(\theta)$ becomes a constant (see red or blue curves), as in the previous cases, and so leads to Gaussian current fluctuations.

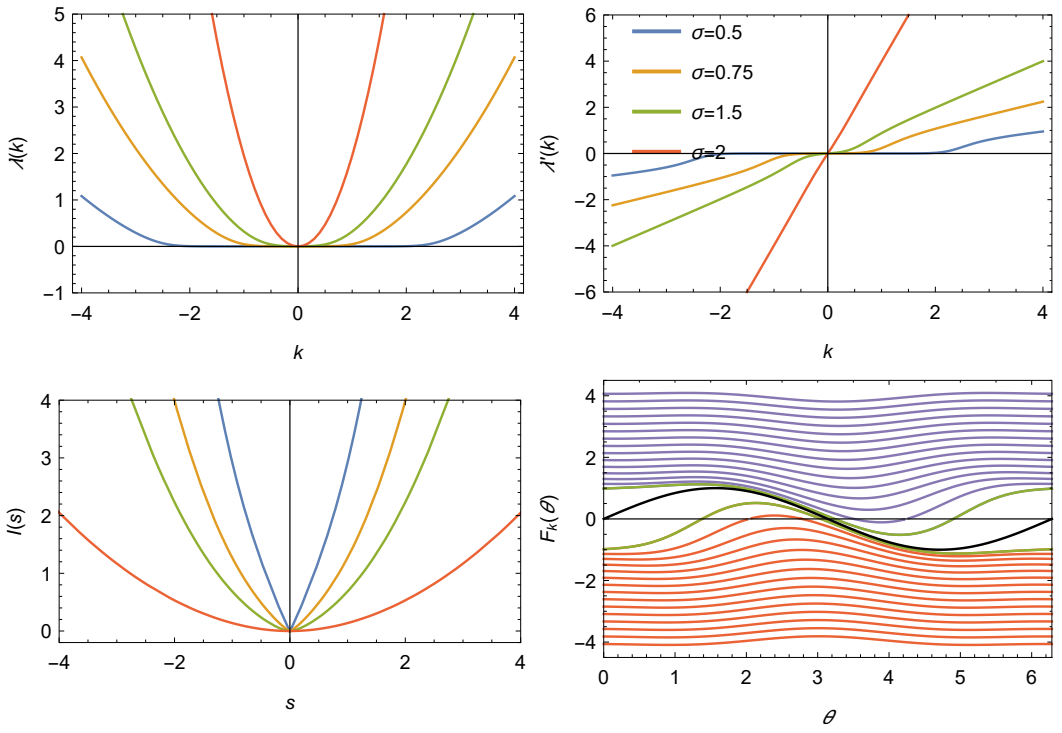

Figure 3.7: *Large deviation functions of the current for $V_0 = 1$, $\gamma = 0$ and for different values of $\sigma \in \{0.5, 0.75, 1.5, 2\}$. These parameters correspond to an equilibrium state with potential but no torque. Top left: SCGF $\lambda(k)$. Top right: Derivative of $\lambda(k)$. Bottom left: Rate function $I(j)$. Bottom right: Effective force $F_k(\theta)$ for $\sigma = 1$ and for different values of k taken in spacing of 0.5. The black line represents the unmodified force $F(\theta)$ obtained for $k = 0$, the green lines represent the small current values, while the blue and red lines represent, respectively, larger positive and smaller negative current fluctuations.*

3.3.1.4 $V_0 > 0$, $\gamma < V_0$

The current fluctuations discussed in the previous section are modified only slightly when adding a drive γ smaller than the critical value $\gamma = V_0$. The minimum of the rate function $I(j)$ is close to $j = 0$ but the rate function is now slightly tilted to the right because of γ, as can be seen in Fig. 3.8. The rounded corner of $I(j)$, associated with the quasi-flat plateau of $\lambda(k)$, is also there and becomes more pronounced for σ small. As for the effective force $F_k(\theta)$, it is only shifted above by γ compared to the case $\gamma = 0$ considered before.

3.3.1.5 $V_0 > 0$, $\gamma > V_0$

When $\gamma > V_0$, we know that the particle is free to rotate around the ring, which translates into a positive mean current $\langle J_T \rangle$, given by Eq. (3.1.27). The

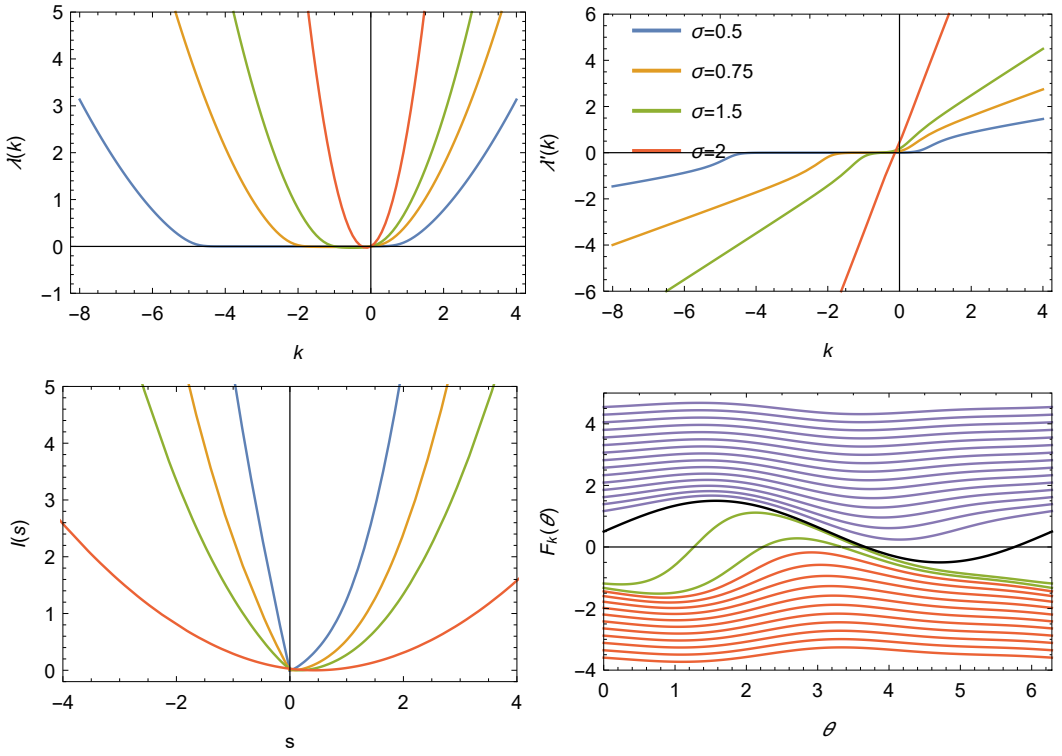

Figure 3.8: *Large deviation functions of the current for $V_0 = 1$, $\gamma = 0.5$ and for different values of $\sigma \in \{0.5, 0.75, 1.5, 2\}$. These parameters correspond to a locked state. Top left: SCGF $\lambda(k)$. Top right: Derivative of $\lambda(k)$. Bottom left: Rate function $I(j)$. Bottom right: Effective force $F_k(\theta)$ for $\sigma = 1$ and for different values of k taken in spacing of 0.5. The black line represents the unmodified force $F(\theta)$ obtained for $k = 0$, the green lines represent the small current values, while the blue and red lines represent, respectively, larger positive and smaller negative current fluctuations.*

plot of $I(j)$ in Fig. 3.9 shows that the large positive or large negative current fluctuations away from this mean are still Gaussian, since $\lambda'(k)$ is essentially linear for $k \to \pm\infty$. As before, the SCGF also has a quasi-plateau which gives rise to the same rounded corner of $I(j)$ at $j = 0$. Around this point, the current fluctuations are therefore non-Gaussian.

These fluctuations can be understood again by looking at the effective force $F_k(\theta)$ in the bottom-right plot of Fig. 3.9. For large values of k, $F_k(\theta)$ is nearly constant (see blue curves) and increases as $k \to \infty$, leading to Gaussian fluctuations above the mean. For small values of k, $F_k(\theta)$ is modified in a complicated way (see green curves) to create an attracting fixed point that reduces the current. Above or below a certain k, the force loses the fixed point and gradually decreases to become constant, thus creating negative current values that are approximately Gaussian.

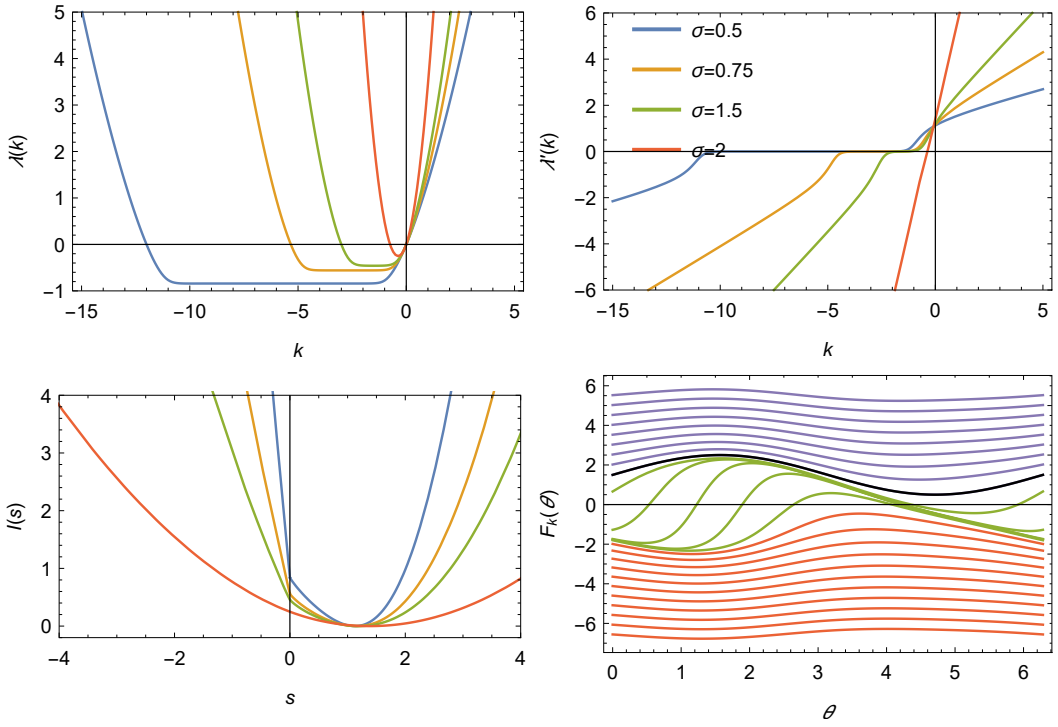

Figure 3.9: *Large deviation functions of the current for $V_0 = 1$, $\gamma = 1.5$ and for different values of $\sigma \in \{0.5, 0.75, 1.5, 2\}$. These parameters correspond to a running state. Top left: SCGF $\lambda(k)$. Top right: Derivative of $\lambda(k)$. Bottom left: Rate function $I(j)$. Bottom right: Effective force $F_k(\theta)$ for $\sigma = 1$ and for different values of k taken in spacing of 0.5. The black line represents the unmodified force $F(\theta)$, obtained for $k = 0$, the green lines represent the small current values, while the blue and red lines represent, respectively, larger positive and smaller negative currents.*

3.4 Entropy production and fluctuation relation

Our goal in this section is to relate the large deviations of the current J_T derived in the previous sections to the large deviations of another quantity, called the entropy production, which was studied before in [20, 39–41].

The entropy production Σ_T per unit time is an integrated random variable related to the nonequilibrium property of the process considered. For an overdamped diffusion such as the ring model, it is defined as

$$\Sigma_T = \frac{2}{T\sigma^2} \int_0^T F(\theta_t) \circ d\theta_t, \tag{3.4.1}$$

where $F(\theta)$ is as before the total drift entering in Eq. (3.1.1) and $\circ$ denotes the Stratonovich integral. Physically, Σ_T is up to a constant the work per unit

time:

$$W_T = \frac{1}{T}\int_0^T F(\theta_t) \circ d\theta_t \tag{3.4.2}$$

done by $F(\theta)$ over an interval of time $[0, T]$. Replacing $F(\theta)$ by its expression of Eq. (3.1.6) gives

$$\Sigma_T = \frac{2\gamma}{T\sigma^2}\int_0^T d\theta_t - \frac{2}{T\sigma^2}\int_0^T U'(\theta_t)d\theta_t, \tag{3.4.3}$$

so that

$$\Sigma_T = \frac{2\gamma}{\sigma^2}J_T - \frac{2}{T\sigma^2}\Delta U_T, \tag{3.4.4}$$

where J_T is the current fluctuation and

$$\Delta U_T = U(\theta_T) - U(\theta_0) \tag{3.4.5}$$

is the variation of potential energy over T. Because this potential energy is bounded on the ring, we can neglect this term in Σ_T as $T \to \infty$, so that

$$\Sigma_T = \frac{2\gamma}{\sigma^2}J_T. \tag{3.4.6}$$

Thus, the entropy production is linearly related to the current, as was also found in [37, 38, 42], which means that the large deviation functions of Σ_T are up to the constant $c = \frac{2\gamma}{\sigma^2}$ those of J_T.

This result is useful because it is known that the pdf of Σ_T always satisfies the relation

$$\frac{P(\Sigma_T = s)}{P(\Sigma_T = -s)} = e^{Ts}, \tag{3.4.7}$$

which implies, by applying the change of variables Eq. (3.4.6),

$$I(-j) = I(j) + cj \tag{3.4.8}$$

or equivalently,

$$\lambda(k) = \lambda(-k - c), \tag{3.4.9}$$

where $c = \frac{2\gamma}{\sigma^2}$. These symmetries for the large deviation functions are collectively referred to as fluctuation relations [20, 43–45] (see [19] for a review) and are connected for the entropy production to a general symmetry of its tilted generator; see Sec. 5 of [20]. For our model, this operator symmetry, which takes the form

$$L_k^\dagger = L_{-k-c}, \tag{3.4.10}$$

is not a priori satisfied, since J_T is only proportional to Σ_T in the limit $T \to \infty$ because of the potential boundary terms in (3.4.6). For $V_0 = 0$, however, J_T

is exactly proportional to Σ_T for all T, so the operator symmetry of (3.4.10) holds, as can be verified from the expression of L_k :

$$L_k^\dagger = -(\gamma + \sigma^2 k)\frac{d}{d\theta} + \frac{\sigma^2}{2}\frac{d^2}{d\theta^2} + \frac{k^2\sigma^2}{2} + k\gamma \tag{3.4.11}$$

and

$$L_{-k-c} = (\gamma - \sigma^2 k - \sigma^2 c)\frac{d}{d\theta} + \frac{\sigma^2}{2}\frac{d^2}{d\theta^2} + \frac{(k+c)^2\sigma^2}{2} + (k+c)\gamma. \tag{3.4.12}$$

Replacing $c = \frac{2\gamma}{\sigma^2}$ into the previous equation yields

$$L_{-k-c} = -(\gamma + \sigma^2 k)\frac{d}{d\theta} + \frac{\sigma^2}{2}\frac{d^2}{d\theta^2} + \frac{k^2\sigma^2}{2} + k\gamma, \tag{3.4.13}$$

which satisfies Eq. (3.4.10). In this case, the symmetry relation given by Eq. (3.4.9) holds not only for the dominant eigenvalue, but for the whole spectrum.

3.5 Rate function upper bounds

We close our study of the fluctuations of J_T for the ring model by deriving two useful upper bounds for its rate function $I(j)$. The first follows from a variational formula recently derived in [22] (see also [26, 37, 38]), which shows that the rate function is obtained by solving the constrained optimization

$$I(j) = \inf_{u:\langle u\rangle_u = j} K(u), \tag{3.5.1}$$

where

$$\langle u\rangle_u = \int_0^{2\pi} u(\theta)\rho_u^{inv}(\theta)d\theta \tag{3.5.2}$$

is the average current calculated with respect to the stationary pdf ρ_u^{inv} of a diffusion with total force u. Similar optimizations were considered in [37, 38, 42] as a way to study the large deviations of the ring model. They are difficult to solve in general, but can be expanded in Fourier-Bloch modes at the level of u to give what is essentially the eigenfunction $r_k(\theta)$ constructed in the previous section. In fact, it can be proved that the minimizer of the variational problem (3.5.1) is the effective drift F_k with $\langle F_k\rangle = j$ [22].

In some cases, approximate solutions can be found, for example, by considering constant drifts $u(\theta) = u$. Then $u = j$ and ρ_u^{inv} is constant, which yields

$$I_{aux}(j) = \frac{(j-\gamma)^2}{2\sigma^2} + \frac{V_0^2}{4\sigma^2}. \tag{3.5.3}$$

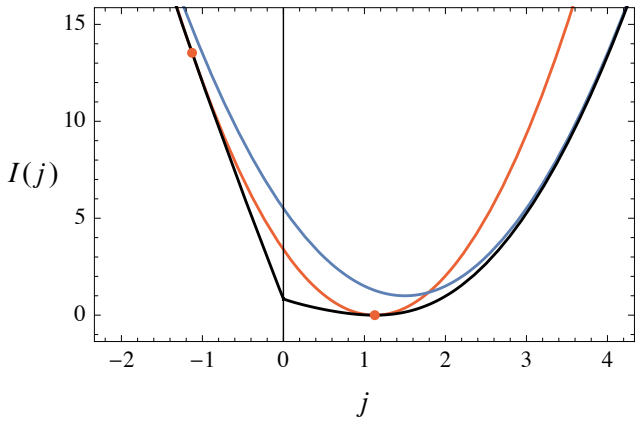

Figure 3.10: *Black curve: Rate function of the current for $V_0 = 1$, $\gamma = 1.5$, $\sigma = 0.5$. Blue curve: Driven upper bound. Red curve: Entropic upper bound.*

This rate function is the same as the one obtained in Eq. (3.2.21) if we set $V_0 = 0$. In other cases, the real minimizer of (3.5.1) is not constant, so that (3.5.3) is only an upper bound to the rate function:

$$I(j) \leq I_{aux}(j). \tag{3.5.4}$$

The second bound follows from a result recently derived for jump processes in [46] (see also [47]), which here takes the form

$$I(j) \leq I_{ent}(j) = \frac{(j - j^\star)^2}{4(j^\star)^2}\Sigma^\star, \tag{3.5.5}$$

where $\Sigma^\star = \frac{2\gamma}{\sigma^2}$ is the mean entropy production associated with the mean current $j^\star = \lambda'(0)$.

These two bounds are quadratic in j but limit the rate function in different ways, as can be seen in Fig. 3.10. The entropic bound (3.5.5) is tight at the mean current j^* as well as at $-j^*$, since it satisfies the fluctuation relation of Eq. (3.4.8), but departs from the true $I(j)$ in the tails. By contrast, the bound (3.5.4) obtained from the driven process approximation is tight in the tails but not around the mean by construction. It also gives a non-trivial bound for $\gamma = 0$. The two bounds are identical and in fact equal to $I(j)$ when $V_0 = 0$, since $I(j)$ is then exactly quadratic with $\langle J_T \rangle = \gamma$.

3.6 Conclusions

We have studied in this chapter a simple periodic diffusion used as a model of nonequilibrium system carrying a current. For this model, we have calculated the mean current $\langle J_T \rangle$, which shows a rounded bifurcation as a function of the

external drive γ in Eq. (3.1.23), as previously found in [8]. We extended these studies here by calculating the rate function $I(j)$ characterizing the fluctuations of the current J_T around this mean and have also derived the expression of the driven process that explains how these fluctuations are created.

The results obtained show a rich trade-off between modifying γ , V_0 and σ to reach low or high current fluctuations. The main results worth mentioning are as follows:

- For large noise ($\sigma \gg 1$), the current fluctuations are essentially Gaussian. They are exactly Gaussian for $V_0 = 0$.
- For $V_0 > 0$ and $\gamma > 0$, and low noise ($\sigma \ll 1$), $I(j)$ has a pronounced, rounded corner at $j = 0$, which shows a crossover in the current fluctuations from large Gaussian fluctuations to small non-Gaussian fluctuations.
- This crossover is similar to a dynamical phase transition [18, 48–52] but is not a real phase transition as the corner in $I(j)$ is rounded so that $I'(j)$ is continuous. The driven process also shows this transition as a crossover between a regime where the force is nearly constant, for large positive or negative currents, and a regime where the particle is trapped by a potential that changes non-linearly for small currents.

These results have been reported in a paper published in Physical Review E [53]. In that paper, we also report other results related to the low-noise limit $\sigma \to 0$, using the Freidlin-Wentzell theory [54, 55]. These results are not described here as they were developed in collaboration with my supervisor, and use techniques that go beyond this thesis.

Chapter 4

Occupation fluctuations for Brownian motion

We study in this chapter the fluctuations of the occupation of the pure and drifted Brownian motion in one dimension, which can be seen as a toy model of nonequilibrium systems when there is a drift. The motivation for considering this model is that, contrary to the ring model, it shows a real dynamical phase transition, which can be related to a localization/delocalization transition in the driven process. The rate function is obtained for this model by applying the symmetrization transform described in Chap. 2. An application of the model related to the conditioning of the geometric Brownian motion, which is often used as a model of stock prices in finance, is also presented.

4.1 Model and observable

The basic model that we consider is the drifted Brownian motion (BM) given by the SDE

$$dX_t = \mu dt + \sigma dW_t, \tag{4.1.1}$$

where $X_t \in \mathbb{R}$ is the state, $\mu \in \mathbb{R}$ is the drift, $\sigma > 0$ is the noise intensity, and W_t the simple Brownian motion. Physically, X_t may represent the position of a small particle evolving in a fluid moving at slow, constant velocity or in a static fluid with additional forces (created, e.g., by laser tweezers [56] or an AC trap [57]) that pull the particle at constant mean velocity. By analogy with electrical circuits perturbed by Nyquist noise [58], X_t can also represent the charge dissipated in a resistor upon the application of a ramped voltage.

Later, we will also study a variation of the model called the geometric Brownian motion (or gBM) satisfying

$$dS_t = \mu S_t dt + \sigma S_t dW_t. \tag{4.1.2}$$

This model, which is an exponential transformation of the drifted BM, is often used to describe the fluctuation of stock prices, as will be explained later.

For all these models, the observable that we are interested to study is the fraction of time that X_t (or S_t) spends in some interval $\Delta = [a, b]$ of $\mathbb{R}$. This observable can be written as

$$\rho_T = \frac{1}{T}\int_0^T \mathbb{1}_\Delta(X_t)dt, \tag{4.1.3}$$

where $\mathbb{1}_\Delta(x)$ is the indicator function equal to 1 if $X_t \in \Delta$ and 0 otherwise. This time-integrated quantity is such that $\rho_T = 0$ for paths of X_t that never enter $[a, b]$ and $\rho_T = 1$ for paths that always stay in that interval. In the notation of Chap. 2, this observable corresponds to the choice $f(x) = \mathbb{1}_\Delta(x)$ and $g = 0$.

Our goal in the next sections is to calculate the rate function $I(\rho)$ associated with the LDP

$$P(\rho_T = \rho) = e^{-TI(\rho)+o(T)} \tag{4.1.4}$$

of ρ_T in the long-time limit $T \to \infty$. The zero of $I(\rho)$, corresponding to the mean and typical value of ρ_T, is found here to be $\rho = 0$, since X_t is unlikely to stay in any finite interval for a long time, so that $\rho_T \to 0$ with probability 1 as $T \to \infty$ [23]. This is confirmed by noticing that the density of X_t, with or without drift, gets flatter as time increases, so that $\langle \mathbb{1}_\Delta(X_t)\rangle \to 0$. The rate function $I(\rho)$ thus characterizes unlikely fluctuations of the occupation around the typical value $\rho = 0$.

4.2 Pure Brownian motion

We study the fluctuations of ρ_T by considering the pure BM ($\mu = 0$) first. The drifted BM will be considered separately in another section. The calculation follows closely a previous study of the occupation fluctuations done for the Ornstein-Uhlenbeck process [23].

4.2.1 SCGF

To find the rate function $I(\rho)$, we follow the Gärtner-Ellis Theorem presented in Chap. 2 and calculate the SCGF $\lambda(k)$ of ρ_T. The tilted generator L_k in this case is given by

$$L_k = \frac{\sigma^2}{2}\frac{d^2}{dx^2} + k\mathbb{1}_\Delta(x), \tag{4.2.1}$$

where $\Delta = [a, b]$. This is a Hermitian operator so we do not need to symmetrize it. Moreover the spectral equation

$$L_k r_k(x) = \lambda(k) r_k(x) \tag{4.2.2}$$

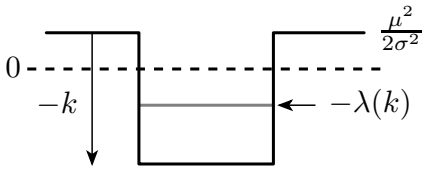

Figure 4.1: *Equivalent quantum well problem determining the SCGF $\lambda(k)$ of the occupation of Brownian motion.*

is equivalent to the Schrödinger equation

$$\frac{d^2 r_k(x)}{dx^2} + \frac{2}{\sigma^2}(k\mathbb{1}_\Delta(x) - \lambda(k))r_k(x) = 0, \tag{4.2.3}$$

representing a quantum particle in a finite well of depth $-k$ extending from a to b. As a result, $\lambda(k)$, the dominant eigenvalue of L_k, is just minus the ground state energy of that well, as illustrated in Fig. 4.1.

Since we know that the energy spectrum of the finite well does not depend on its position, but only on its width $b-a$, we can translate the interval $[a,b]$ around zero so as to solve the problem on $[-a,a]$ instead. The solution for this symmetric interval can then be translated to any asymmetric interval $[a,b]$. For $\Delta = [-a,a]$, the Schrödinger equation takes the form

$$\begin{cases} \frac{d^2}{dx^2} r_k(x) - \frac{2}{\sigma^2}\lambda_k r_k(x) = 0 & x < -a \\ \frac{d^2}{dx^2} r_k(x) + \frac{2}{\sigma^2}(k-\lambda_k) r_k(x) = 0 & -a \le x \le a \\ \frac{d^2}{dx^2} r_k(x) - \frac{2}{\sigma^2}\lambda_k r_k(x) = 0 & x > a. \end{cases} \tag{4.2.4}$$

The eigenfunctions of this system are written explicitly as

$$\begin{cases} r_k(x) = Ae^{K_1 x} + Ee^{-K_1 x} & x < -a \\ r_k(x) = B\cos K_2 x + C\sin K_2 x & -a \le x \le a \\ r_k(x) = De^{-K_1 x} + Fe^{K_1 x} & x > a, \end{cases} \tag{4.2.5}$$

where

$$K_1^2 = \frac{2}{\sigma^2}\lambda(k) \tag{4.2.6}$$

and

$$K_2^2 = \frac{2}{\sigma^2}(k - \lambda(k)). \tag{4.2.7}$$

To ensure that eigenfunctions are finite when $x \to \pm\infty$, we must set $E = F = 0$ to eliminate the physically unacceptable solutions that grow exponentially. The result for the first and third equations of the previous system are

$$\begin{cases} r_k(x) = Ae^{K_1 x} & x < -a \\ r_k(x) = De^{-K_1 x} & x > a. \end{cases} \tag{4.2.8}$$

Taking into account the symmetry of the problem, the bound state eigenfunction is either even or odd under space inversion. This means that the solutions of the system. (4.2.5) are either antisymmetric or symmetric. The solutions for the antisymmetric case are

$$r_k(x) = \begin{cases} r_k(x) = Ae^{K_1 x} & x < -a \\ r_k(x) = C \sin K_2 x & -a \leq x \leq a \\ r_k(x) = De^{-K_1 x} & x > a, \end{cases} \tag{4.2.9}$$

while those of the symmetric case are

$$r_k(x) = \begin{cases} r_k(x) = Ae^{K_1 x} & x < -a \\ r_k(x) = B \cos K_2 x & -a \leq x \leq a \\ r_k(x) = De^{-K_1 x} & x > a, \end{cases} \tag{4.2.10}$$

where A, B, C and D are constants that are fixed by imposing the continuity of $r_k(x)$ and its derivatives at $x = \pm a$, and by normalising it. The continuity conditions lead to the following equations:

$$K_2 \tan K_2 a = K_1, \quad \text{for the symmetric case} \tag{4.2.11}$$

$$K_2 \cot K_2 a = -K_1, \quad \text{for the antisymmetric case,} \tag{4.2.12}$$

for K_1, K_2 defined in Eq. (4.2.6) and Eq. (4.2.7), respectively.

These two transcendental equations cannot be solved analytically, but can easily be solved numerically. To this end, let us write $y^2 = K_2^2 a^2$ so that the previous equation can be rewritten in a simple form as

$$\sqrt{\frac{u^2}{y^2} - 1} = \begin{cases} \tan y & n = 1, 3, 5, \cdots \\ -\cot y & n = 2, 4, 6, \cdots, \end{cases} \tag{4.2.13}$$

where $u^2 = \frac{2ka^2}{\sigma^2}$. The SCGF $\lambda(k)$, which corresponds to the minimum eigenvalue with $n = 1$, leads us to keep only the even solution in the rest of our study. This solution can be rewritten as

$$|\cos y| = \frac{y}{u}, \tag{4.2.14}$$

where for every value of u we need to find the intersection of $\cos y$ with the straight line y/u. Denoting this solution by $y^\star(k)$, we thus obtain

$$\lambda(k) = k - \frac{\sigma^2 (y^\star(k))^2}{2a^2}, \tag{4.2.15}$$

from Eq. (4.2.7).

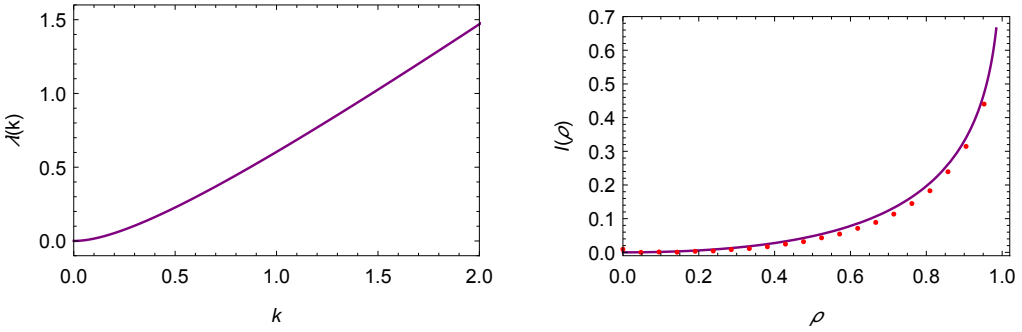

Figure 4.2: *Left: SCGF $\lambda(k)$ for the occupation of pure BM in the symmetric interval $\Delta = [-1, 1]$ for $\sigma = 1$. Right: Corresponding rate function $I(\rho)$. The red data points on the curve are the results of Monte Carlo simulations.*

This function is shown in the left plot of Fig. 4.2. We notice that it is convex and that $\lambda(0) = 0$, as expected. We also have $\lambda(k) > 0$ for $k > 0$, since the ground state energy of the particle in the well is always negative by taking the zero energy reference as in Fig. 4.1. For $k < 0$, the quantum well becomes a quantum wall or barrier for which there is no quantification of the energy and bound states. In this case, we can still consider that the minimum energy of the particle is 0 (no kinetic energy), so that $\lambda(k) = 0$ for $k < 0$.

To find the rate function $I(\rho)$, we can notice that $\lambda(k)$ is differentiable in k, since the ground state energy of the finite well is known to be analytic as a function of its depth. As a result, we can use the Gärtner-Ellis Theorem to find the rate function $I(\rho)$ as

$$I(\rho) = k(\rho)\rho - \lambda\left(k(\rho)\right), \tag{4.2.16}$$

where $k(\rho)$ is the solution of $\lambda'(k) = \rho$. This rate function is shown in the right plot of Fig. 4.2. It is defined for $\rho \in [0, 1]$, and the zero of $I(\rho)$ is at $\rho = 0$, as expected. For $\rho < 0$, $I = \infty$, and this is consistent by Legendre transform with the observation above that $\lambda(k) = 0$ for $k < 0$. The rate function is confirmed in the plot of Fig. 4.2 by Monte Carlo results obtained by simulating 10^7 trajectories for $\Delta t = 0.05$ and $T = 30$ and by then transforming to a rate function the histogram of the values of ρ_T obtained (see [24] for details). The numerical results agree very well with the analytical curve.

4.2.2 Asymptotic limit of the SCGF

We can see in Fig. 4.2 that the SCGF $\lambda(k)$ is asymptotically linear with slope 1 as $k \to \infty$. This can be found from the eigenvalue calculation by noting that the Eq. (4.2.14) for y approaches the equation $\cos y = 0$ for $k \to \infty$, which is

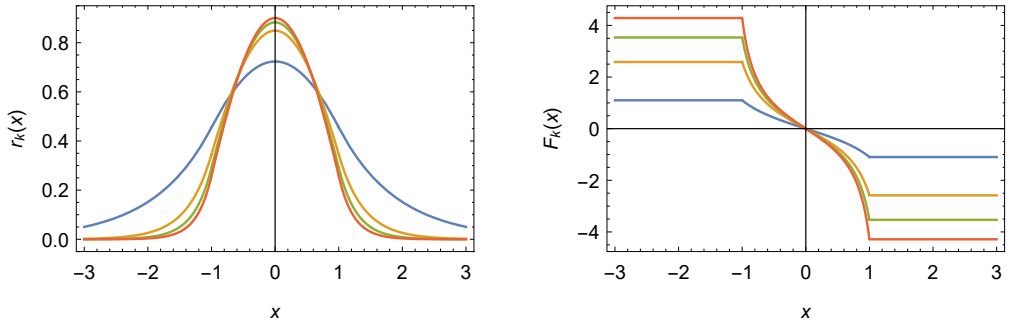

Figure 4.3: *Left: Dominant eigenfunction $r_k(x)$ for the pure BM with $\sigma = 1$ conditioned to stay in the interval $\Delta = [-1, 1]$. The different curves are for $\sigma = 1$ and $k = \{1, 3, 6, 9\}$ (from the blue to the red curve). Right: Corresponding effective force $F_k(x)$.*

solved by $y = \frac{\pi}{2}$ for $n = 1$. As a result, we obtain for the dominant eigenvalue

$$\lambda(k) = k - \frac{\sigma^2\pi^2}{8a^2}. \tag{4.2.17}$$

For the quantum well problem, this only confirms that the lowest energy of the infinite well is $\frac{\sigma^2\pi^2}{8a^2}$. Thus we see that $\lambda(k)$ becomes a straight line with slope 1, as shown in Fig. 4.2. The slope is asymptotically equal to 1 because $\rho = 1$ is the maximum value of ρ_T.

We can also note that the same equation for $k \to 0$ becomes $\tan y \approx y$, which implies $\cos y \approx 1$ and so $\frac{y}{u} = 1$. This gives

$$\frac{2a^2}{\sigma^2}(k - \lambda(k)) = \frac{2ka^2}{\sigma^2}, \tag{4.2.18}$$

so that $\lambda(k) = 0$ as expected. This merely shows that the ground state energy of the particle in the well goes to zero as the depth of the well vanishes.

4.2.3 Driven process

We now construct the driven process associated with the large deviations of the occupation fraction found in the previous section. To find the effective drift of the process, we need to find the bound state eigenfunctions of the Schrödinger equation for the symmetric case given in Eq. (4.2.10). The coefficients A, B, D are fixed again by requiring that $r_k(x)$ and its derivative are continuous at

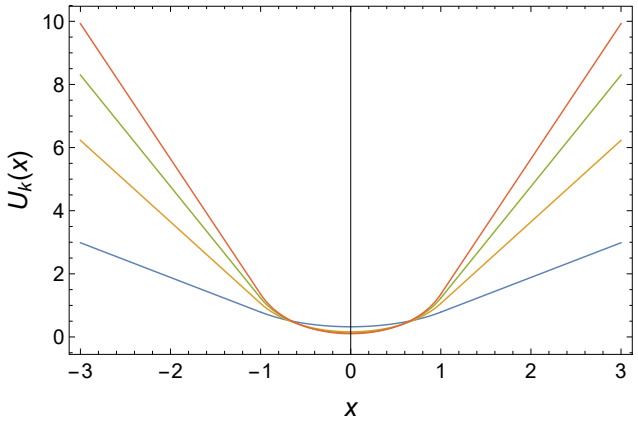

Figure 4.4: *Effective potential $U_k(x)$ for pure BM conditioned to stay in the interval $\Delta = [-1, 1]$ for $\sigma = 1$ and $k = \{1, 3, 6, 9\}$ (from the bottom to the top curve).*

$x = \pm a$, which leads to

$$r_k(x) = \begin{cases} r_k(x) = \sqrt{\frac{K_1}{K_1 a+1}} \cos(K_2 a) e^{K_1(x+a)} & x < -a \\ r_k(x) = \sqrt{\frac{K_1}{K_1 a+1}} \cos K_2 x & -a \leq x \leq a \\ r_k(x) = \sqrt{\frac{K_1}{K_1 a+1}} \cos(K_2 a) e^{-K_1(x-a)} & x > a, \end{cases} \tag{4.2.19}$$

where K_1 and K_2 are defined in Eq. (4.2.6) and Eq. (4.2.7) respectively. From this symmetric solution, we then find the effective drift $F_k(x)$ from the general result of Eq. (2.6.2) of Chap. 2 with $F(x) = 0$ and $g = 0$ as

$$F_k(x) = \sigma^2 \frac{d}{dx} \ln r_k(x). \tag{4.2.20}$$

Replacing Eq. (4.2.19) and the expressions of K_1 and K_2 into the previous relation yields

$$F_k(x) = \begin{cases} \sigma\sqrt{2\lambda(k)} & x < -a \\ -\sigma\sqrt{2(k-\lambda(k))} \tan\left(\frac{\sqrt{2(k-\lambda(k))}}{\sigma} x\right) & -a \leq x \leq a \\ -\sigma\sqrt{2\lambda(k)} & x > a. \end{cases} \tag{4.2.21}$$

Since this drift is defined for $x \in \mathbb{R}$, we can also associate it with an effective potential $U_k(x)$ such that

$$F_k(x) = -\frac{dU_k(x)}{dx}. \tag{4.2.22}$$

By comparing the previous equation with Eq. 4.2.20, we then have

$$U_k(x) = -\sigma^2 \ln r_k(x). \tag{4.2.23}$$

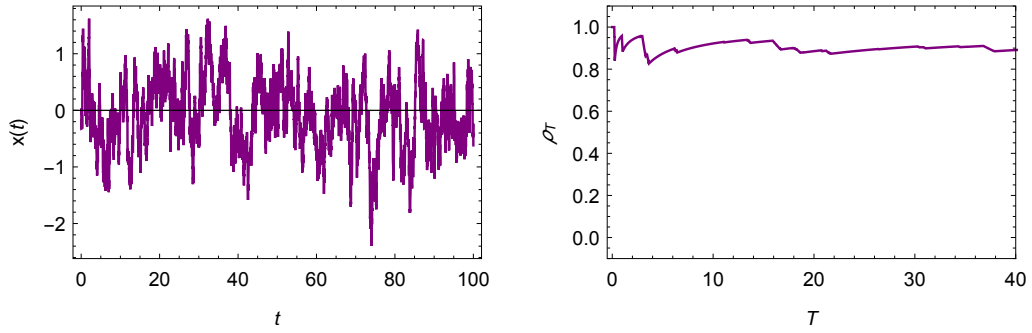

Figure 4.5: *Illustration of the driven process for the Brownian motion conditioned to stay in the interval* $\Delta = [-1, 1]$. *Left: Sample trajectory of the process* $\hat{X}_t$ *spending* 85% *of its time in that region. Right: Fraction of* ρ_T *spent in* Δ *as a function of the time* T.

These results are plotted in Fig. 4.3 and Fig. 4.4 for $a = 1$ and lead us to the following observations:

- Outside the occupation interval $\Delta = [-1, 1]$, $r_k(x)$ decays exponentially, which leads to a constant effective force and, equivalently, an effective potential $U_k(x)$ that grows linearly, as seen in Fig. 4.4.
- The decay of $r_k(x)$ goes like $\sigma\sqrt{2\lambda(k)}$, so the effective force grows as $k \to \infty$, matching the effective potential which becomes steep in that limit.
- Inside $\Delta = [-1, 1]$, $r_k(x)$ is a cosine leading to a tangent force and logarithmic cosine for the effective potential.
- There is a discontinuity in the derivative of $F_k(x)$ at $x = \pm 1$ due to the fact that there is a jump in the second derivative of $r_k(x)$ or $U_k(x)$. This arises because the Schrödinger well problem has a discontinuous potential.

We see from these results that the effect of $F_k(x)$ or $U_k(x)$ is to confine the particle so as to reach higher occupations in $\Delta = [-1, 1]$ according to the relation $\lambda'(k) = \rho$. This is illustrated in Fig. 4.5, which shows a simulation of the driven process $\hat{X}_t$ obtained with $F_k(x)$ and k chosen so that $\hat{X}_t$ spends 85% of its time in $\Delta = [-1, 1]$. As T grows, we see that ρ_T indeed converges approximately to 0.85. By repeating this simulation for different values k, we obtain different mean occupations, which we show in Fig. 4.6. Error bars for these results are also shown and were obtained by repeating the simulations 10 times for each value of k. The simulations confirm in the end the results for r_k, F_k and U_k.

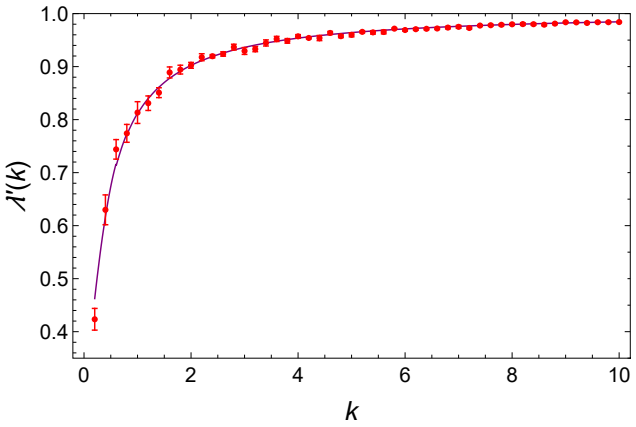

Figure 4.6: *Consistency test for the driven process. Data points: Mean occupation reached by $\hat{X}_t$ in the long-time limit as a function of k, as in Fig. 4.5. The error bars were obtained by calculating the standard error of the occupation for $T = 100$ and $N = 10$ samples. Blue curve: Theoretical occupation corresponding to $\lambda'(k)$.*

4.3 Drifted Brownian motion

We extend in this section the calculation of the rate function of ρ_T for the drifted BM with $\mu \neq 0$. In this case, the tilted generator becomes

$$L_k = \mu \frac{d}{dx} + \frac{\sigma^2}{2}\frac{d^2}{dx^2} + k\mathbb{1}_\Delta(x), \tag{4.3.1}$$

which leads to the eigenvalue equation

$$\frac{\sigma^2}{2}\frac{d^2}{dx^2}r_k(x) + \mu\frac{d}{dx}r_k(x) - \alpha r_k(x) = 0, \tag{4.3.2}$$

where

$$\alpha = \begin{cases} \lambda(k) - k & x \in [a,b] \\ \lambda(k) & \text{otherwise.} \end{cases} \tag{4.3.3}$$

The general solution of this equation is

$$\begin{cases} r_k(x) = e^{-\frac{\mu}{\sigma^2}x}\left(Ae^{\zeta x} + Be^{-\zeta x}\right) & x < a \\ r_k(x) = e^{-\frac{\mu}{\sigma^2}x}\left(C\cos\gamma x + D\sin\gamma x\right) & a \leq x \leq b \\ r_k(x) = e^{-\frac{\mu}{\sigma^2}x}\left(Ee^{-\zeta x} + Fe^{\zeta x}\right) & x > b, \end{cases} \tag{4.3.4}$$

where

$$\zeta^2 = \frac{2}{\sigma^2}\left(\lambda(k) + \frac{\mu^2}{2\sigma^2}\right) \tag{4.3.5}$$

and

$$\gamma^2 = \frac{2}{\sigma^2}\left(k - \lambda(k) - \frac{\mu^2}{2\sigma^2}\right). \tag{4.3.6}$$

We will see next that there are now two solutions or "branches" that give the correct SCGF $\lambda(k)$: one quantum branch related to the case $\mu = 0$ and one non-quantum branch that arises for $\mu \neq 0$. We discuss these separately next and then bring them together after to find the complete $\lambda(k)$. The driven process associated with the occupation fluctuations is also constructed from these two branches.

4.3.1 Quantum branch

The quantum branch of the general solution (4.3.4) is the solution that decays to 0 when $x \to \pm\infty$. There are two ways to approach this solution:

1. We can seek the same quantum solution that was found in the previous section for the part of Eq. (4.3.4) in the parentheses by setting $B = D = F = 0$.

2. We can symmetrize, following Sec. 2.5.3, the non-Hermitian equation (4.3.2) with
$$P_s(x) = ce^{-\frac{2\mu x}{\sigma^2}}, \tag{4.3.7}$$
to obtain
$$H_k\psi_k(x) = \lambda(k)\psi_k(x), \tag{4.3.8}$$
where
$$H_k = \frac{\sigma^2}{2}\frac{d^2}{dx^2} - V_k, \tag{4.3.9}$$
with the potential
$$V_k(x) = \begin{cases} \frac{\mu^2}{2\sigma^2} - k & x \in [a,b] \\ \frac{\mu^2}{2\sigma^2} & \text{otherwise.} \end{cases} \tag{4.3.10}$$
The relation to $r_k(x)$ is then
$$r_k(x) = e^{-\frac{\mu x}{\sigma^2}}\psi_k(x). \tag{4.3.11}$$

These two approaches lead to the same solution shown in Eq. (4.3.4) in which the term $e^{-\frac{\mu}{\sigma^2}x}$ is the symmetrization term and the term in parentheses is the quantum solution $\psi_k(x)$. Moreover, it is clear from both approaches that $\psi_k(x)$ is the same solution as for $\mu = 0$. All that changes is the eigenvalue $\lambda(k)$ which is shifted by $\mu^2/2\sigma^2$ compared to the eigenvalue obtained for $\mu = 0$, as can be seen from Eq. (4.3.5) and Eq. (4.3.6) or Eq. (4.3.10). This is also obvious by looking at Fig. 4.1, which shows that the quantum well is shifted upwards by $\mu^2/2\sigma^2$. As a result, we have that the "quantum" eigenvalue $\lambda_q(k)$ for $\mu \neq 0$ is
$$\lambda_q(k) = \lambda(k)|_{\mu=0} - \frac{\mu^2}{2\sigma}, \tag{4.3.12}$$

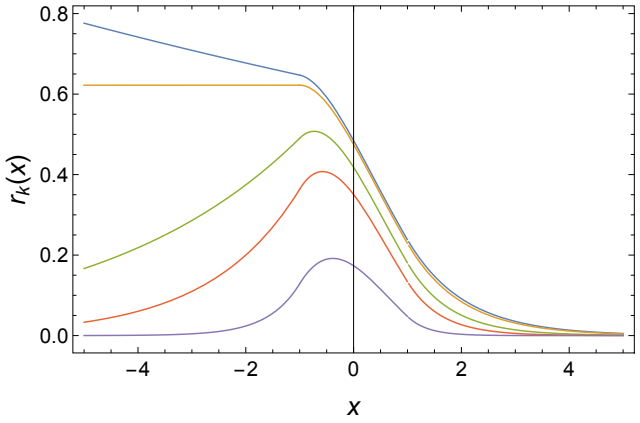

Figure 4.7: *Quantum solution for the eigenfunction* $r_k(x)$ *for* $k \in \{0.3, k_c, 0.6, 1, 3\}$ *(from the blue to the purple curve). When* $\lambda_q(k)$ *becomes negative,* $r_k(x)$ *does not converge to* 0 *anymore for* $x \to -\infty$.

where $\lambda_q|_{\mu=0}$ is the eigenvalue obtained for $\mu = 0$. The corresponding eigenfunction $\psi_k(x)$ is the same again as for $\mu = 0$ and leads to the eigenfunction

$$\begin{cases} r_k(x) = Ae^{(\zeta - \frac{\mu}{\sigma^2})x} & x < a \\ r_k(x) = e^{-\frac{\mu}{\sigma^2}x}\left(C\cos\gamma x + D\sin\gamma x\right) & a \le x \le b \\ r_k(x) = Ee^{-(\zeta + \frac{\mu}{\sigma^2})x} & x > b, \end{cases} \tag{4.3.13}$$

where the coefficients A, C, D, E are found by imposing the continuity conditions. This solution is plotted in Fig. 4.7 for $a = -1$ and $b = 1$. We can see that $r_k(x)$ decays to 0 as $x \to \pm\infty$, as required, as long as $\zeta - \frac{\mu}{\sigma^2} > 0$, that is, according to Eq. (4.3.5), as long as $\lambda(k) > 0$. The eigenfunction is also now non-symmetric with respect to $x = 0$ because of the "symmetrization" shift $e^{-\frac{\mu x}{\sigma^2}}$.

4.3.2 Non-quantum branch

The quantum solution cannot give the complete SCGF for two reasons:

1. The quantum eigenvalue $\lambda_q(k)$ becomes negative below a certain critical value k_c, which leads to $\lambda_q(0) \neq 0$, in contradiction with the definition of the SCGF (see Sec. 2.3).

2. The corresponding eigenfunction $r_k(x)$, given by Eq. (4.3.13) does not become constant as $k \to 0$.

As a result, there must be another solution to Eq. (4.3.2) related to a different eigenfunction. This solution, having the correct limit $r_k(x) \to 1$ as

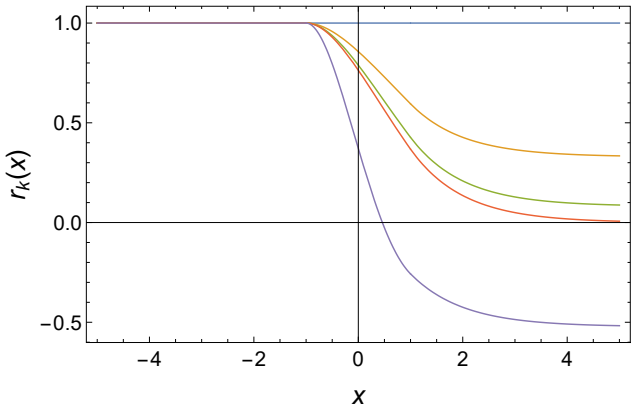

Figure 4.8: *Non-quantum solution of the eigenfunction* $r_k(x)$ *for* $k \in \{0, 0.1, 0.2, k_c, 1\}$ *(from the blue to the purple curve).*

$k \to 0$, is found to be

$$\begin{cases} r_k(x) = 1 & x < a \\ r_k(x) = e^{-\frac{\mu}{\sigma^2}x}\left(C\cos\gamma x + D\sin\gamma x\right) & a \leq x \leq b \\ r_k(x) = Ee^{-\frac{2\mu}{\sigma^2}x} + F & x > b, \end{cases} \tag{4.3.14}$$

where

$$\gamma = \frac{\sqrt{2k\sigma^2 - \mu^2}}{\sigma^2} \tag{4.3.15}$$

and is associated with the non-quantum eigenvalue $\lambda_{nq}(k) = 0$. This can be verified by applying L_k to this solution to obtain $L_k r_k(x) = 0$. This is obvious, for example, for the branches $x < a$ and $x > b$. The coefficients C, D, E and F are fixed as always by imposing the continuity conditions.

This solution for $r_k(x)$ is plotted in Fig. 4.8 for $a = -1$ and $b = 1$, and for different values of k from $k = 0$ to $k = 1$. We can see first that $r_k(x) = 1$ for $k = 0$, which is the correct eigenfunction associated with $L_{k=0} = L$. For $k > 0$, the left branch of $r_k(x)$ is still equal to 1, but the middle and right branches start to decrease, with the right branch of $r_k(x)$ converging to the constant F as $x \to \infty$. Surprisingly, we notice numerically that this constant becomes negative for all $k > k_c$. As a result, this solution for $r_k(x)$ cannot be the dominant eigenfunction for $k > k_c$, since that function must be positive by the Perron-Frobenius Theorem.

4.3.3 Combining the solutions

The full solution for the SCGF $\lambda(k)$ is obtained by combining the two previous branches. For $k \in [0, k_c]$, we have seen that $\lambda_q(k)$ does not converge to 0 for $k \to 0$, so $\lambda(k)$ must be given by the non-quantum branch $\lambda_{nq}(k)$, which has the

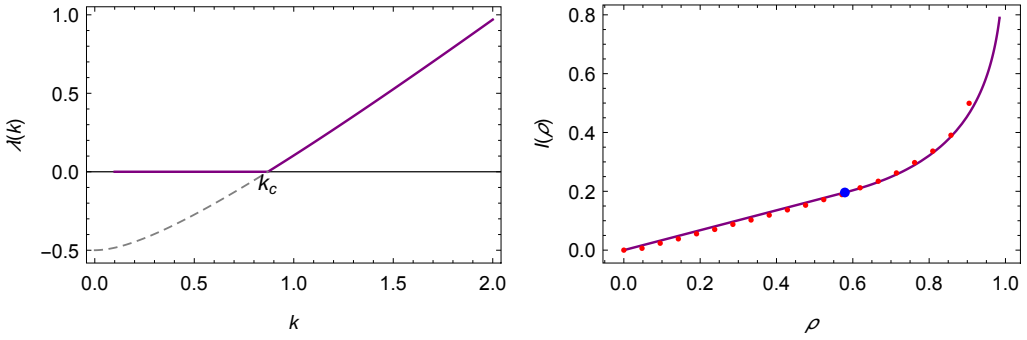

Figure 4.9: *Left: SCGF $\lambda(k)$ for the drifted BM conditioned to stay in the symmetric interval $\Delta = [-1, 1]$ for the values $\mu = 1$ and $\sigma = 1$. Right: Rate function $I(\rho)$ for $\mu = 0.5$ and $\sigma = 1$. The blue disk marks the phase transition point $\lambda'(k_c) = \rho_c$ below which $I(\rho)$ is linear with slope k_c.*

correct eigenfunction $r_k(x)$ that converges to 1 as $k \to 0$. On the other hand, for $k \geq k_c$, the non-quantum branch is no longer valid since $r_k(x)$ becomes negative, so that $\lambda(k)$ is given by the quantum solution. Therefore, we can write

$$\begin{aligned} \lambda(k) &= \begin{cases} \lambda_{nq}(k) & k \in [0, k_c] \\ \lambda_q(k) & k \geq k_c. \end{cases} \\ &= \begin{cases} 0 & k \in [0, k_c] \\ \lambda(k)|_{\mu=0-\frac{\mu^2}{2\sigma^2}} & k \geq k_c. \end{cases} \end{aligned} \tag{4.3.16}$$

Since the crossing point at k_c is where $\lambda_q(k)$ becomes negative, we can also write

$$\lambda(k) = \max\left\{\lambda_{nq}(k), \lambda_q(k)\right\}. \tag{4.3.17}$$

Note that, for $k = k_c$, the quantum solution for $r_k(x)$ is the same as the non-quantum solution. This means that both $\lambda(k)$ and $r_k(x)$ are continuous in k.

The resulting $\lambda(k)$ is shown in the left plot of Fig. 4.9 which clearly shows the crossing point k_c at which the slope of $\lambda(k)$ is discontinuous. The Legendre-Fenchel transform of this function is shown on the right plot and is compared with data (red dots) obtained by direct Monte Carlo simulations of the drifted BM (using 10^7 independent trajectories with $T = 30$ and $\Delta t = 0.05$). The numerical data is in agreement with the Legendre-Fenchel transform and thus shows that, although the Gärtner-Ellis Theorem cannot be applied here, because $\lambda(k)$ is not differentiable, the rate function $I(\rho)$ is correctly given by this transform. In this case, the non-differentiable point of $\lambda(k)$ at $k = k_c$ leads to a linear branch with slope k_c of $I(\rho)$ extending from $\rho = 0 = \lambda'(k_c^-)$ to a critical occupation ρ_c given by $\rho_c = \lambda'(k_c^+)$.

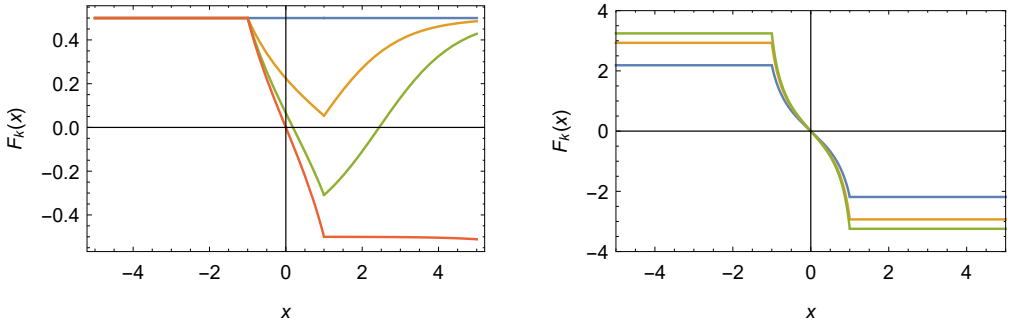

Figure 4.10: *Left: Effective force $F_k(x)$ associated with the non-quantum solution for $k \in \{0, 0.2, k_c, 1\}$ (from the blue to red curve) and $\sigma = 1$. Right: $F_k(x)$ associated with the quantum solution for $k \in \{3, 4, 6\}$ (from the blue to green) and $\sigma = 1$.*

Beyond ρ_c, $I(\rho)$ is simply the rate function obtained for $\mu = 0$ shifted by the constant $\frac{\mu^2}{2\sigma^2}$, since it is the Legendre transform of $\lambda_q(k)$ given by Eq. (4.3.12). In the limit $\mu \to 0$, both ρ_c and this shift go to 0, thus recovering the rate function of pure BM.

4.3.4 Driven process

The effective drift $F_k(x)$ of the driven process obtained from the eigenfunction $r_k(x)$ is

$$F_k(x) = \mu + \sigma^2 \frac{d}{dx} \ln r_k(x). \tag{4.3.18}$$

This is shown in Fig. 4.10 for $\sigma = 1$, $a = -1$ and $b = 1$. The left plot shows this force for $k \in [0, k_c]$, obtained from the non-quantum solution. There we see that

- $F_k(x)$ for $x < a$ is not modified since $r_k(x) = 1$ in this region.
- The derivative of $F_k(x)$ jumps at $x = a$ and $x = b$ since the second derivative of $r_k(x)$ is discontinuous.
- $F_k(x)$ is modified mostly in the region $[a, b]$.
- $F_k(x) \to \mu$ as $x \to \infty$ so the force away from $[a, b]$ is not modified much.
- $F_{k=0}(x) = F(x) = \mu$.

The effective potential $U_k(x)$, defined in Eq. (4.2.23), is plotted in Fig. 4.11 and shows that the effect of conditioning is to create a local minimum of the potential around $[a, b]$ so as to attract the particle in that interval and thus increase ρ_T. The effective potential is not confining since $F_k(x) \to \mu$

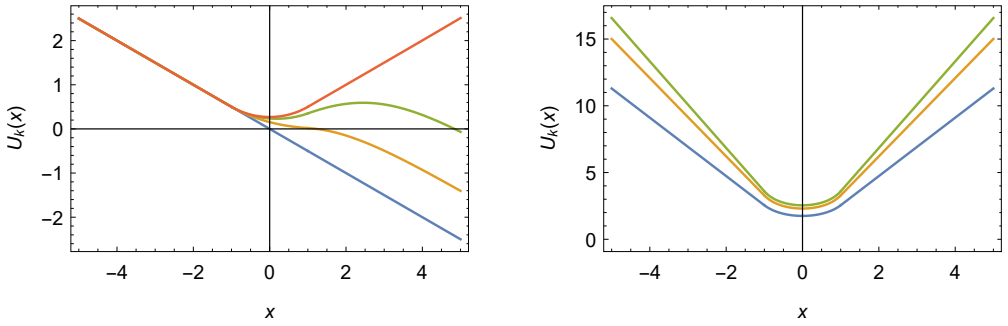

Figure 4.11: *Left: Effective potential $U_k(x)$ for the non-quantum branch solution for $k = \{0, 0.2, k_c, 1\}$ (from the blue to red curve) and $\sigma = 1$. Right: $U_k(x)$ associated with the quantum solution for $k \in \{3, 4, 6\}$ (from blue to green) and $\sigma = 1$.*

as $x \to \infty$, so that the effective process described by $F_k(x)$ or $U_k(x)$ has no stationary distribution, like the drifted BM.

For $k \geq k_c$, the effective force $F_k(x)$, shown in the right plot of Fig. 4.10, is the same as the effective force that we found for $\mu = 0$, since the $e^{-\mu x/\sigma^2}$ term in front of the quantum solution in Eq. (4.3.11) exactly cancels the μ in the expression of $F_k(x)$. In this case, we have that $F_k(x)$ is also constant for $x < a$ and $x > b$ and has the form of a tangent for $x \in [a, b]$, as found in Eq. (4.2.21). This means that the effective potential for $k \geq k_c$ is symmetric around $x = 0$ (for $a = -1$, and $b = 1$), with linear tails for $x < a$ and $x > b$ and a cosine potential in $[a, b]$. As k grows from k_c, the linear branches of the effective potential in $[a, b]$ become steep, so that the driven process spends more time in the occupation interval $[a, b]$. Compared with the case $k < k_c$, the driven process now has a stationary distribution because $U_k(x)$ is steep. Moreover, as $k \to \infty$, that distribution becomes all contained in $[a, b]$, so that $\rho_T \to 1$. These results for $F_k(x)$ and $U_k(x)$ are confirmed in Fig. 4.12, which shows the typical or mean occupation fraction ρ_T reached by the driven process with $F_k(x)$ for different values of k. As in the previous section, the mean fraction approaches $\lambda'(k)$, which is equal to 0 for $k \in [0, k_c]$ and $\lambda'(k)|_{\mu=0}$ for $k \geq k_c$. The fluctuations in the data shown on the plot are due to the finite number of samples used in the simulations. Moreover, the fact that $F_k(x)$ is the same as $F_k(x)|_{\mu=0}$ for $k > k_c$ can be understood from Eq. (4.3.12), which shows that

$$\lambda'(k) = \lambda'(k)|_{\mu=0}, \tag{4.3.19}$$

for $k > k_c$. Thus, the mean occupation of the effective process for $k > k_c$ is the same whether $\mu = 0$ or $\mu \neq 0$.

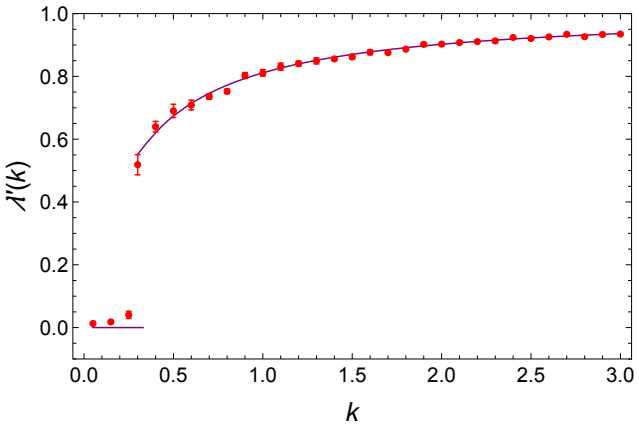

Figure 4.12: *Consistency test for the effective process. Data points: Mean occupation reached by $\hat{X}_t$ in the long-time limit by $\hat{X}_t$ as a function of k. The error bars were obtained by calculating the standard error of the occupation after $T = 200$ for $N = 10$ samples. Blue curve: Theoretical expectation corresponding to $\lambda'(k)$.*

4.4 Dynamical phase transition

The jump in the derivative of the SCGF $\lambda(k)$, seen in Fig. 4.12 for $\mu \neq 0$, corresponds to what is called a first-order dynamical phase transition, in analogy with equilibrium first-order phase transitions which appear when the derivative of the free energy jumps. The difference with equilibrium phase transitions is that the transition seen in $\lambda(k)$ is not for an equilibrium or typical state, but for the dynamical fluctuations, which are different depending on whether we consider $k < k_c$ or $k > k_c$.

As observed before, for $k < k_c$ the driven process varies in k but leads to $\rho_T \to 0$ because $U_k(x)$ is not confining, so the process escapes to infinity like the drifted BM. For $k > k_c$, on the other hand, the driven process leads to $\rho_T \to \lambda'(k) > 0$ (see Fig. 4.12) and so describes non-trivial fluctuations that are effectively created by a process that is more and more confined or localized around the occupation interval $[a, b]$. We thus see that the phase transition in the fluctuations is between a non-localized phase and a localized phase of the effective process. As also mentioned, the jump in $\lambda'(k)$ leads for the rate function $I(\rho)$ to a linear part which describes essentially a coexistence between the delocalized and localized phases. This is similar to coexisting phases observed in equilibrium first-order phase transitions.

For $\mu = 0$, there is no dynamical phase transition. The SCGF $\lambda(k)$ in this case is analytic, as already mentioned, since the ground state energy of the finite well is known to be an analytic function of the depth of the well.

Finally, it is interesting to note that the dynamical phase transition that we

see for $\mu \neq 0$ arises only in the long-time limit, $T \to \infty$. In all stochastic models that have been studied before, a dynamical phase transition is seen in a double limit: either the limit where both the number N of particles and the time T go to infinity [18, 49–52, 59–71] or the limit where the noise power goes to zero while the time T goes to infinity [40, 41, 53–55, 72–76]. The current of the ring model studied in the previous chapter is an example of the latter double limit. This shows that a dynamical phase transition can arise in a homogeneous Markov process with only the long-time limit. A non-homogeneous Markov model showing a dynamical phase was described previously in [77].

4.5 Application for the geometric BM

To close this chapter we present an application of the calculations of the previous sections to the geometric Brownian motion (gBM) defined by

$$dS_t = \tilde{\mu} S_t dt + \sigma S_t dW_t, \tag{4.5.1}$$

where $\tilde{\mu}$ and σ are constants and W_t, is, as before, the Wiener process. This SDE is often used as a model describing the stochastic evolution of stock prices [3, 4, 78]. Following this application, it can be interesting to study the probability that S_t stays in some interval $[\alpha, \beta]$ for a fraction of time.

As before, we could answer this question by finding the dominant eigenvalue of the tilted generator L_k associated with this problem. However, we can note that the gBM is only a transformation of the drifted BM. Indeed, the solution of the SDE (4.5.1) is

$$S_t = S_0 e^{(\tilde{\mu} - \frac{\sigma^2}{2})t + \sigma W_t}, \tag{4.5.2}$$

where $S_0 > 0$ is the initial condition of gBM. As a result S_t is the exponential of a drifted BM with

$$\mu = \tilde{\mu} - \frac{\sigma^2}{2} \tag{4.5.3}$$

and the same noise parameter σ.

With this transformation between S_t and X_t, we see that the occupation problem for $S_t \in [\alpha, \beta]$ is equivalent to the occupation problem for $X_t \in [a, b]$ with

$$\begin{aligned} a &= \ln \frac{\alpha}{S_0} \\ b &= \ln \frac{\beta}{S_0}. \end{aligned} \tag{4.5.4}$$

The large deviation functions $\lambda(k)$ and $I(\rho)$ are therefore the same for both processes, provided that the intervals $[\alpha, \beta]$ and $[a, b]$ are related as above, and

$\tilde{\mu}$ and μ are related as in Eq. (4.5.3). This means that the effective process $\hat{S}_t$ that describes how fluctuations of the occupation of S_t arise is given by

$$\hat{S}_t = S_0 e^{\hat{X}_t}, \tag{4.5.5}$$

where $\hat{X}_t$ is the effective process describing the fluctuations of X_t in $[a, b]$. Using Itô's calculus, this is equivalent to

$$d\hat{S}_t = \hat{S}_t \left(F_k(\hat{X}_t) + \frac{\sigma^2}{2} \right) dt + \hat{S}_t \sigma dW_t. \tag{4.5.6}$$

As an example, consider the simulation of the effective process shown in Fig. (4.12) which corresponds to the drifted BM with $\mu = 1/2$, $S_0 = 1$, $\sigma = 1$, $a = -1$, and $b = 1$. By transforming these parameters as above, this effective process then describes the same occupation fluctuations of gBM with $\tilde{\mu} = 1$, $\sigma = 1$, $\alpha = e^{-1}$ and $\beta = e$. Other applications of the conditioning of gBM can be constructed in the same way.

4.6 Conclusions

We have studied in this chapter the BM conditioned on staying for a fraction of time in an interval. We have first derived the large deviation functions for the occupation ρ_T for both pure and drifted BM and have then derived for these results the large deviations of the occupation of gBM. From there several conclusions can be given:

- We have seen that for the pure BM, the SCGF $\lambda(k)$ is an analytic function in k for all $k \geq 0$ and that the rate function is also analytic for all $\rho \in [0, 1]$. Therefore there is no dynamical phase transition in the fluctuations of ρ_T in the long-time limit.
- For the drifted BM, the fluctuations of ρ_T undergo a first-order phase transition at k_c. This transition is found by considering a quantum and non-quantum branches for the full solution of the dominant eigenfunction $r_k(x)$.
- The linear branch observed in the rate function $I(\rho)$ for drifted BM corresponds for the SCGF to a crossing of two eigenvalues and implies in our context that the fluctuations of ρ_T are exponential for $\rho \in [0, \rho_c]$.
- The effective dynamics shows that there is no occupation below k_c. However, for every values of $k > k_c$, we can find any corresponding occupation values $\rho_T > \rho_c$.

These results have been reported in a paper published in Europhysics Letters [79].

Chapter 5

Future problems

The two models studied in the previous chapters give clear and simple illustrations of the driven process, how this process is obtained, and how it helps us to understand the origin of fluctuations in Markov processes. To conclude this thesis, we propose a number of open problems related to these two models and more general systems.

- For the ring model, we have seen that we can obtain the large deviation functions and the driven process exactly for $\gamma \neq 0$ and $V_0 = 0$. Can we obtain these functions and the driven process for $V_0 \neq 0$ by linear perturbation theory from the exact solution at $V_0 = 0$?
- Similarly, can we apply linear perturbation theory to obtain the rate functions and driven process from the trivial solution at $k = 0$, for which $\lambda(0) = 0$ and $r_{k=0}(x) = 1$?
- For $\gamma = 0$, the ring model with the cosine potential resembles the Sine-Gordon model [80]. Can we use this connection to solve the ring model exactly in this case?
- Can we use path integrals to study the current large deviations of the ring model, in particular, in the low-noise $\sigma \to 0$ limit?

For the pure and drifted Brownian motion there are also a number of interesting problems. For example:

- We have argued that the solution of the SCGF $\lambda(k)$ for the drifted Brownian motion is the crossing of two spectral solutions that we have called the quantum and non-quantum solutions. This is also supported by numerical calculations. Can we prove that there are no other spectral solutions?

- We have seen that the drifted Brownian motion shows a surprising dynamical phase transition in the occupation fluctuations. Can we understand the physical origin of this transition? We know that the Ornstein-Uhlenbeck process does not show such a transition [23]. Moreover we think that any stationary and confined processes, like the Ornstein-Uhlenbeck process, should not show any dynamical phase transition. Can we prove this?

- As a way to answer the previous question, it would be interesting to study the drifted Brownian motion by confining it to an interval with reflecting boundary condition or on the ring with periodic boundary conditions. Do we still have a dynamical phase transition in these cases? Do we recover that transition in the limit where the box or the ring become infinite?

- Can we apply the calculation of the occupation fluctuations of the geometric Brownian motion to a real problem in finance involving the conditioning of stock prices?

Finally, it would be interesting to apply the driven process to more complicated processes, in particular, processes evolving in higher dimensions or involving many particles. For example, we could study the underdamped Langevin equation or the noisy Van der Pol oscillator as a 2D generalization of the ring model. For the case of many particles, we could study systems such as the Kuramoto model of synchronization [81] or interacting particle models such as the zero-range process or the exclusion process. Some studies have already obtained the driven process for the current fluctuations [15]. Other observables such as the density could be studied.

Appendices

Appendix A

SCGF for Markov chains

We show in this appendix that the SCGF $\lambda(k)$ for Markov chains is given as in Eq. (2.4.5) by the largest eigenvalue of the tilted matrix shown in Eq. (2.4.6). The moment generating function of the general observable (2.4.4) for a Markov chain with transition matrix $\Pi(y|x)$ is written as

$$\left\langle e^{nkS_n} \right\rangle = \sum_{x_1,\ldots,x_n} P(x_1) e^{kf(x_1)} \Pi(x_2|x_1) e^{k(f(x_2)+g(x_1,x_2))} \cdots \Pi(x_n|x_{n-1}) e^{k(f(x_n)+g(x_{n-1},x_n))}. \tag{A.0.1}$$

By defining

$$P_k(x_1) = P(x_1) e^{kf(x_1)} \tag{A.0.2}$$

and the matrix

$$\Pi_k(y|x) = \Pi(y|x) e^{k(f(y)+g(x,y))}, \tag{A.0.3}$$

Eq. (A.0.1) can be rewritten as

$$\left\langle e^{nkS_n} \right\rangle = \sum_{x_n} \sum_{x_{n-1}} \Pi_k(x_n|x_{n-1}) \sum_{x_2} \cdots \sum_{x_1} \Pi_k(x_2|x_1) P_k(x_1). \tag{A.0.4}$$

We recognize in this expression a sequence of $n-1$ products involving the matrix Π_k, to which we can apply the Perron-Frobenius Theorem since Π_k is positive. To this end, let ζ_i denote the eigenvalues of Π_k and ν_i denote the eigenvectors obeying

$$\Pi_k \nu_i = \zeta_i \nu_i. \tag{A.0.5}$$

The Perron-Frobenius Theorem implies that the dominant eigenvalue $\zeta_{\max}$ is real and that

$$\Pi_k^{n-1} P_k \approx \text{const} \cdot \zeta_{\max}^n \nu_{\max} \tag{A.0.6}$$

as $n \to \infty$, where $\nu_{\max}$ is the positive eigenvector associated with $\zeta_{\max}$. Taking the large deviation limit then yields

$$\lambda(k) = \lim_{n\to\infty} \frac{1}{n} \ln \langle e^{nkS_n} \rangle = \ln \zeta_{max}, \tag{A.0.7}$$

as expressed in Eq. (2.4.5).

Appendix B

Feynman-Kac formula

The Feynman-Kac formula is an evolution equation for the generating function of additive observables of continuous-time diffusions [82]. It is essentially the continuous-time generalization of Eq. (A.0.4) giving the evolution of the generating function of S_n in discrete time.

To derive this formula, consider a diffusion X_t giving by the general SDE (2.5.1) and the general observable S_T as given by Eq. (2.5.12). The moment generating function of this observable started at the position $X_0 = x$ and at time $t + dt$ is written as

$$G(x, t + dt) = \left\langle e^{\int_0^{t+dt} f(X_s)ds + \int_0^{t+dt} g(X_s)\circ dX_s} \right\rangle_x . \tag{B.0.1}$$

Propagating the time from 0 to dt and then from dt to $t + dt$ gives

$$G(x, t + dt) = \left\langle e^{\int_0^{dt} f(X_s)ds + \int_{dt}^{t+dt} f(X_s)ds + \int_0^{dt} g(X_s)\circ dX_s + \int_t^{t+dt} g(X_s)\circ dX_s} \right\rangle_x , \tag{B.0.2}$$

where $e^{\int_0^{dt} f(X_s)ds}$ is a Riemann integral, which yields by choosing the lower left Riemann sum

$$e^{\int_0^{dt} f(X_s)ds} = e^{f(X_0)dt} = e^{f(x)dt}. \tag{B.0.3}$$

Since we have the initial point $X_0 = x$. Similarly,

$$e^{\int_0^{dt} g(X_s)\circ dX_s} = e^{g(\frac{x+X_{dt}}{2})(X_{dt}-x)} \tag{B.0.4}$$

for the Stratonovich integral. Substituting this into Eq. (B.0.2) yields

$$\begin{aligned} G(x, t + dt) &= \left\langle e^{f(x)dt} e^{g(\frac{x+X_{dt}}{2})(X_{dt}-x)} e^{\int_{dt}^{t+dt} f(X_s)ds + \int_{dt}^{t+dt} g(X_s)\circ dX_s} \right\rangle_x \\ &= e^{f(x)dt} \left\langle e^{g(\frac{x+X_{dt}}{2})(X_{dt}-x)} e^{\int_0^{t} f(X_s)ds + \int_0^{t} g(X_s)\circ dX_s} \right\rangle_x . \end{aligned}$$

The expectation depends on X_{dt} and the starting point at $X_0 = x$, so we need to shift the starting point from $X_0 = x$ to X_{dt}. To this end, we first propagate

the process from X_0 to X_{dt} as

$$\begin{aligned} G(x,t+dt) &= e^{f(x)dt}\int dy \left\langle e^{g(\frac{x+X_{dt}}{2})(X_{dt}-x)} \right. \\ &\quad \left. e^{\int_0^t f(X_s)ds \int_0^t g(X_s)\circ dX_s} \middle| X_{dt}=y \right\rangle P(X_{dt}=y|X_0=x). \end{aligned} \tag{B.0.5}$$

We know from the Langevin equation that X_{t+dt} can be found from X_t as

$$X_{t+dt} = X_t + F(X_t)dt + \sigma dW_t, \tag{B.0.6}$$

which can be rewritten as

$$X_{dt} = x + \zeta, \tag{B.0.7}$$

where

$$\zeta = F(x)dt + \sigma dW_t. \tag{B.0.8}$$

Replacing these expressions into Eq. (B.0.5), we then obtain

$$\begin{aligned} G(x,t+dt) &= e^{f(x)dt}\int d\zeta p(\zeta)\left\langle e^{g(x+\frac{\zeta}{2})\zeta} e^{\int_0^t f(X_s)ds+\int_0^t g(X_s)\circ dX_s}\right\rangle_{x+\zeta} \\ &= e^{f(x)dt}\int d\zeta p(\zeta) e^{g(x+\frac{\zeta}{2})\zeta}\left\langle e^{\int_0^t f(X_s)ds+\int_0^t g(X_s)\circ dX_s}\right\rangle_{x+\zeta} \\ &= e^{f(x)dt}\int d\zeta p(\zeta) e^{g(x+\frac{\zeta}{2})\zeta} G(x+\zeta,t), \end{aligned} \tag{B.0.9}$$

where

$$G(x+\zeta,t) = \left\langle e^{\int_0^t f(X_s)ds+\int_0^t g(X_s)dX_s}\right\rangle_{x+\zeta} \tag{B.0.10}$$

is now the generating function started at $x+\zeta$. Because ζ is small we can expand $g(x+\frac{\zeta}{2})$ and $G(x+\zeta,t)$ up to the second order in ζ as

$$G(x,t+dt) = e^{f(x)dt}\int d\zeta\, p(\zeta) e^{\left(g(x)+\frac{\zeta}{2}g'(x)\right)\zeta}\left(G(x,t)+\zeta\frac{\partial}{\partial x}G(x,t)+\frac{\zeta^2}{2}\frac{\partial^2}{\partial x^2}G(x,t)\right). \tag{B.0.11}$$

Taking the development of the exponential function up to the second order yields

$$\begin{aligned} G(x,t+dt) &= (1+f(x)dt)\int d\zeta\, p(\zeta)\left(1+\zeta g(x)+\frac{\zeta^2}{2}g(x)^2\right) \\ &\quad \left(1+\frac{\zeta^2}{2}g'(x)\right)\left(G(x,t)+\zeta\frac{\partial}{\partial x}G(x,t)+\frac{\zeta^2}{2}\frac{\partial^2}{\partial x^2}G(x,t)\right). \end{aligned} \tag{B.0.12}$$

Expanding the previous equation gives

$$\begin{aligned} G(x,t+dt) &= (1+f(x)dt)\int d\zeta\, p(\zeta)\Big[G(x,t)+\zeta G(x,t)\left(g(x)+\frac{\partial}{\partial x}\right) \\ &\quad +\frac{\zeta^2}{2}G(x,t)\left(\frac{\partial^2}{\partial x^2}+2g(x)\frac{\partial}{\partial x}+g(x)^2+g'(x)\right)\Big]. \end{aligned} \tag{B.0.13}$$

Noting that the first and the second moments are

$$\int d\zeta \zeta p(\zeta) = F(x)dt, \tag{B.0.14}$$

$$\int d\zeta \frac{\zeta^2}{2} p(\zeta) = \frac{\sigma^2}{2} dt, \tag{B.0.15}$$

we can rewrite Eq. (B.0.13) as

$$\begin{aligned} G(x,t+dt) &= G(x,t) + F(x)dt\left(g(x) + \frac{\partial}{\partial x}G(x,t)\right)G(x,t) \\ &\quad + \frac{\sigma^2}{2}dt\left(\frac{\partial^2}{\partial x^2} + 2g(x)\frac{\partial}{\partial x} + g(x)^2 + g'(x)\right)G(x,t) \\ &\quad + f(x)G(x,t)dt, \end{aligned} \tag{B.0.16}$$

which can be rewritten as

$$\begin{aligned} \frac{G(x,t+dt) - G(x,t)}{dt} &= \left(F(x)\left(\frac{\partial}{\partial x} + g(x)\right) + \frac{\sigma^2}{2}\left(\frac{\partial}{\partial x} + g(x)\right)\left(\frac{\partial}{\partial x} + g(x)\right)\right. \\ &\quad \left. + f(x)\right)G(x,t). \end{aligned} \tag{B.0.17}$$

This previous equation yields the evolution equation written as consequently,

$$\frac{\partial G(x,t)}{\partial t} = L_k G(x,t), \tag{B.0.18}$$

where

$$L_k = F(x)\left(\frac{\partial}{\partial x} + g(x)\right) + \frac{\sigma^2}{2}\left(\frac{\partial}{\partial x} + g(x)\right)\left(\frac{\partial}{\partial x} + g(x)\right) + f(x). \tag{B.0.19}$$

Appendix C

Angular velocity

The mean current of the ring model without noise is given by

$$\langle \dot{\theta}_t \rangle = \frac{2\pi}{T}, \tag{C.0.1}$$

where T is the period of oscillation which represents the time needed for the particle on the ring to complete one cycle. This can be found as

$$T = \int_0^T dt = \int_{-\pi}^{\pi} \frac{dt}{d\theta} d\theta = \int_{-\pi}^{\pi} \frac{1}{\gamma + V_0 \sin\theta} d\theta. \tag{C.0.2}$$

To solve this integral, we use the change of variables $u = \tan\frac{\theta}{2}$, which leads to

$$T = \frac{2}{\gamma} \int_{-\infty}^{+\infty} \frac{du}{u^2 + \frac{2V_0}{\gamma}u + 1} = \frac{2}{\gamma} \int_{-\infty}^{+\infty} \frac{du}{(u + \frac{V_0}{\gamma})^2 - (\frac{V_0}{\gamma})^2 + 1}. \tag{C.0.3}$$

By using $x = u + \frac{V_0}{\gamma}$ and $v = \frac{\sqrt{\gamma^2 - V_0^2}}{\gamma}$, this integral then becomes

$$T = \frac{2}{\gamma} \int_{-\infty}^{+\infty} \frac{dx}{v^2(1 + (\frac{x}{v})^2)}, \tag{C.0.4}$$

which leads to

$$T = \frac{2}{\gamma v} \int_{-\infty}^{+\infty} \frac{dy}{1 + y^2} = \frac{2\pi}{\sqrt{\gamma^2 - V_0^2}} \tag{C.0.5}$$

by choosing $y = \frac{x}{v}$. Inserting this equation into Eq. (C.0.1) then gives

$$\langle \dot{\theta}_t \rangle = \sqrt{\gamma^2 - V_0^2}. \tag{C.0.6}$$

Appendix D

Application: Josephson junctions

We explain in this appendix one application of the ring model for Josephson junctions. The explanation follows the discussions found in [10, 30, 31].

D.1 Josephson junction relations

A Josephson junction is a junction between two superconductors which is weak enough to allow only a slight overlap of the electron pair wavefunctions $\psi_1 e^{i\chi_1}$ and $\psi_2 e^{i\chi_2}$ of the two superconductors. Under this condition, electron pairs can pass from one superconductor to the other even with no applied voltage and, in doing so, create a supercurrent equal to

$$I_s = I_c \sin\phi, \tag{D.1.1}$$

where I_c is the critical current and $\phi = \chi_2 - \chi_1$ is the phase difference between the two wavefunctions. This current produces a charge imbalance which creates a potential across the junction. This voltage induces in turn a variation of the phase difference according to

$$\frac{d\phi}{dt} = \frac{4\pi eV}{h}, \tag{D.1.2}$$

where h is Planck's constant and e is the electron charge. By analogy with the ring, the measurable quantity that we have called the current is represented in a Josephson junction by the average voltage. From the previous equation we get

$$\langle V \rangle = \frac{h}{4\pi e}\langle \dot{\phi} \rangle. \tag{D.1.3}$$

We can classify Josephson junctions in two regimes according to whether the phase difference is constant or varies in time:

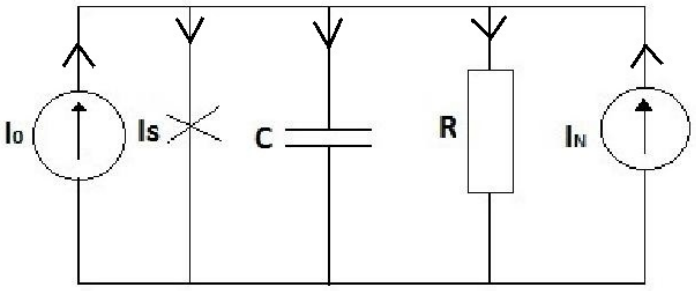

Figure D.1: *Circuit diagram for the Josephson junction.*

- Assuming $V = 0$, the phase difference ϕ becomes from Eq. (D.1.2) constant but not necessarily zero, so that from Eq. (D.1.1) a finite current with a maximum value I_c can flow through the barrier with zero voltage across the junction. This is called the DC Josephson effect, first observed by Anderson and Rowell in 1963 [10].

- If we apply a constant voltage $V \neq 0$, it follows by integrating Eq. (D.1.2) that the phase ϕ varies in time according to

$$\phi_t = \phi_0 + \frac{4\pi eV}{h}t. \tag{D.1.4}$$

  In this case, there appears an alternating current, corresponding to the AC Josephson effect.

D.2 Josephson circuit and ring analogy

A Josephson junction is usually controlled according to the circuit shown in Fig. D.1. Kirchhoff's law applied to this circuit leads to

$$I_C + I_R + I_s = I_0 + I_N, \tag{D.2.1}$$

where I_s is the current flowing in the Josephson junction, given by Eq. (D.1.1), $I_R = \frac{V}{R}$ is the current through the resistor, $I_C = C\dot{V}$ is the current through the capacitor, I_0 is an externally applied current and I_N represents a noise current (essentially the Nyquist thermal noise). Replacing these expressions into the previous relation yields

$$C\dot{V} + \frac{V}{R} + I_c \sin\phi = I_0 + I_N \tag{D.2.2}$$

Inserting relation (D.1.2) into this equation gives rise to

$$\frac{hC}{4\pi e}\ddot{\phi} + \frac{h}{4\pi eR}\dot{\phi} + I_c \sin\phi = I_0 + I_N. \tag{D.2.3}$$

Let us define the dimensionless time as

$$\tau = \frac{4\pi eR}{h}t. \tag{D.2.4}$$

Using this time τ, Eq. (D.2.3) becomes

$$\beta\phi'' + \phi' + I_c \sin\phi = I_0 + I_N, \tag{D.2.5}$$

where $\phi' = \frac{d\phi}{d\tau}$ and $\beta = \frac{4\pi eR^2C}{h}$. In the overdamped limit, we drop the term $\beta\phi''$ in the previous equation and we get

$$\phi' + I_c \sin\phi = I_0 + I_N, \tag{D.2.6}$$

which can can be rewritten as

$$\phi' = -U'(\phi) + I_0 + I_N. \tag{D.2.7}$$

This is equivalent to Eq. (3.1.1) for the particle motion on the ring with the correspondences $\theta_t = \phi_t$, $I_0 = \gamma$, $I_c = V_0$, $I_N = \frac{dW}{dt}$.

Let us evaluate the average angular velocity $\langle\dot{\phi}\rangle$ for the Josephson junction and the average value of the voltage given by Eq. (D.1.2). According to the dimensionless time, given by the expressions (D.2.4), the angular velocity becomes

$$\langle\dot{\phi}\rangle = \left\langle\frac{d\phi}{dt}\right\rangle = \left\langle\frac{d\phi}{d\tau}\frac{d\tau}{dt}\right\rangle = \frac{4\pi eR}{h}\langle\phi'\rangle. \tag{D.2.8}$$

Subtituting this result into Eq. (D.1.3) yields

$$\langle V\rangle = R\langle\phi'\rangle. \tag{D.2.9}$$

The analysis made in Sec. 3.1.1 can also be applied to Josephson junctions. At low noise, if $I_0 < I_c$, the particle remains in one of the wells and it is impossible for the particle to turn around the ring. The solution of Eq. (D.2.7) without noise current approaches the fixed point $\phi^\star = \sin^{-1}(\frac{-I_0}{I_c})$ where $-\pi \leq \phi^\star \leq \pi$. Thus the average angular velocity is zero ($\langle\phi'\rangle = 0$) and from there $\langle V\rangle = 0$. This confirms what we have argued before concerning the DC Josephson effect.

When $I_0 > I_c$, all solutions of noiseless Eq. (D.2.7) are periodic with the period given by Eq. (C.0.5), which confirms the AC Josephson effect described before. By analogy with the ring model, this corresponds to the case where the particle rolls freely down the entire potential depending on the driving force. This represents a junction switching from superconducting state to the normal conducting $V \neq 0$ state with a maximum observed critical current. We will observe this by analysing the voltage-current characteristic curve.

D.3 Voltage-current characteristics

Replacing Eq. (C.0.6) into Eq. (D.2.9), we find the voltage as

$$\langle V \rangle = R\sqrt{I_0^2 - I_c^2}, \tag{D.3.1}$$

with $\langle V \rangle / R$ representing the mean current in the Josephson junction, which is the electrical analogue of the mean current on the ring given by Eq. (3.1.23). This shows that Fig. 3.4 is also the analogue of the voltage-current characteristics given in the previous relation where the x-axis represents the current I_0 and the y-axis represents the mean voltage $\langle V \rangle$.

List of References

[1] N. G. Van Kampen. *Stochastic Processes in Physics and Chemistry*. Elsevier Science & Technology books, 3rd edition, 2007.

[2] C. W. Gardiner. *Handbook of Stochastic Methods for Physics, Chemistry and the Natural Sciences*, volume 13 of *Springer Series in Synergetics*. Springer, New York, 2nd edition, 1985.

[3] K. Jacobs. *Stochastic Process for Physicists*. Cambridge University Press, Cambridge, 2010.

[4] G. Grimmett and D. Stirzaker. *Probability and Random Processes*. Oxford University Press, Oxford, 1982.

[5] M. Doi and S. F. Edwards. *The Theory of Polymer Dynamics*. Oxford University Press, Oxford, 1986.

[6] K. Mallick T. Chou and R. K. P. Zia. Non-equilibrium statistical mechanics from a paradigmatic model to biological transport. *Rep. Prog. Phys*, 74:116601, 2011.

[7] U. Seifert. Stochastic thermodynamics: Principles and perspectives. *Eur. Phys. J. B*, 64:423–431, 2008.

[8] P. Reimann, C. Van den Broeck, H. Linke, P. Hänggi, J. M. Rubi, and A. Pérez-Madrid. Diffusion in tilted periodic potentials: Enhancement, universality, and scaling. *Phys. Rev. E*, 65:031104, 2002.

[9] K. Sekimoto. *Stochastic Energetics*. Springer, New York, 2010.

[10] H. Risken. *The Fokker-Planck Equation: Methods of Solution and Applications*. Springer, Berlin, 3rd edition, 1996.

[11] R. J. Harris and H. Touchette. Large deviation approach to nonequilibrium systems. In R. Klages, W. Just, and C. Jarzynski, editors, *Nonequilibrium Statistical Physics of Small Systems: Fluctuation Relations and Beyond*, volume 6 of *Reviews of Nonlinear Dynamics and Complexity*, pages 335–360, Weinheim, 2013. Wiley-VCH.

[12] R. Chetrite and H. Touchette. Nonequilibrium Markov processes conditioned on large deviations. *Ann. Inst. Poincaré A*, 16(9):2005–2057, 2015.

[13] H. Touchette. The large deviation approach to statistical mechanics. *Phys. Rep.*, 478(1-3):1–69, 2009.

[14] A. Dembo and O. Zeitouni. *Large Deviations Techniques and Applications.* Springer, New York, 2nd edition, 1998.

[15] B. Derrida. Non-equilibrium steady states: Fluctuations and large deviations of the density and of the current. *J. Stat. Mech.*, 2007(07):P07023, 2007.

[16] Y. Oono. Large deviation and statistical physics. *Prog. Theoret. Phys. Suppl.*, 99:165–205, 1989.

[17] L. Bertini, A. De Sole, D. Gabrielli, G. Jona-Lasinio, and C. Landim. Lagrangian phase transitions in nonequilibrium thermodynamic systems. *J. Stat. Mech.*, 2010(11):L11001, 2010.

[18] C. P. Espigares, P. L. Garrido, and P. I. Hurtado. Dynamical phase transition for current statistics in a simple driven diffusive system. *Phys. Rev. E*, 87:032115, 2013.

[19] R. J. Harris and Schütz G. M. Fluctuation theorems for stochastic dynamics. *J. Stat. Mech*, 2007(07):P07020, 2007.

[20] J. L. Lebowitz and H. Spohn. A Gallavotti-Cohen-type symmetry in the large deviation functional for stochastic dynamics. *J. Stat. Phys.*, 95(1-2):333–365, 1999.

[21] R. Chetrite and H. Touchette. Nonequilibrium microcanonical and canonical ensembles and their equivalence. *Phys. Rev. Lett.*, 111:120601, 2013.

[22] R. Chetrite and H. Touchette. Variational and optimal control representations of conditioned and driven processes. *J. Stat. Mech.*, 2015(12):P12001, 2015.

[23] F. Angeletti and H. Touchette. Diffusions conditioned on occupation measures. *J. Math. Phys.*, 53:023303, 2016.

[24] H. Touchette. A basic introduction to large deviations: Theory, applications, simulations. In R. Leidl and A. K. Hartmann, editors, *Modern Computational Science 11: Lecture Notes from the 3rd International Oldenburg Summer School.* BIS-Verlag der Carl von Ossietzky Universität Oldenburg, 2011.

[25] F. den Hollander. *Large Deviations.* Fields Institute Monograph. AMS, Providence, 2000.

[26] R. L. Jack and P. Sollich. Effective interactions and large deviations in stochastic processes. *Eur. Phys. J. Spec. Top.*, 224:2351–2367, 2015.

[27] P. Reimann, C. Van den Broeck, H. Linke, P. Hänggi, J. M. Rubi, and A. Pérez-Madrid. Giant acceleration of free diffusion by use of tilted periodic potentials. *Phys. Rev. Lett.*, 87:010602, 2001.

[28] V. Blickle, T. Speck, C. Lutz, U. Seifert, and C. Bechinger. Einstein relation generalized to nonequilibrium. *Phys. Rev. Lett.*, 98:210601, 2007.

[29] U. Seifert and T. Speck. Fluctuation-dissipation theorem in nonequilibrium steady states. *Europhys. Lett.*, 89(1):10007, 2010.

[30] R. L. Kautz. Noise, chaos, and the Josephson voltage standard. *Rep. Prog. Phys.*, 59:935–992, 1996.

[31] R. L. Kautz. Thermally induced escape: The principle of minimum available noise energy. *Phys. Rev. A*, 38(4):2066–2080, 1988.

[32] P. Reimann. Brownian motors: Noisy transport far from equilibrium. *Phys. Rep.*, 361:57–265, 2002.

[33] J. R. Gomez-Solano, A. Petrosyan, S. Ciliberto, R. Chetrite, and K. Gawedzki. Experimental verification of a modified fluctuation-dissipation relation for a micron-sized particle in a nonequilibrium steady state. *Phys. Rev. Lett.*, 103:040601, 2009.

[34] S. Ciliberto, S. Joubaud, and A. Petrosyan. Fluctuations in out-of-equilibrium systems: From theory to experiment. *J. Stat. Mech.*, 2010(12):P12003, 2010.

[35] J. R. Gomez-Solano, A. Petrosyan, S. Ciliberto, and C. Maes. Fluctuations and response in a non-equilibrium micron-sized system. *J. Stat. Mech.*, 2011(01):P01008, 2011.

[36] S. H. Strogatz. *Nonlinear Dynamics and Chaos.* Addison-Wesley, Reading, Mass., 1994.

[37] T. Nemoto and S.-I. Sasa. Thermodynamic formula for the cumulant generating function of time-averaged current. *Phys. Rev. E*, 84:061113, 2011.

[38] T. Nemoto and S.-I. Sasa. Variational formula for experimental determination of high-order correlations of current fluctuations in driven systems. *Phys. Rev. E*, 83:030105, 2011.

[39] T. Speck, V. Blickle, C. Bechinger, and U. Seifert. Distribution of entropy production for a colloidal particle in a nonequilibrium steady state. *Europhys. Lett.*, 79(3):30002, 2007.

[40] J. Mehl, T. Speck, and U. Seifert. Large deviation function for entropy production in driven one-dimensional systems. *Phys. Rev. E*, 78:011123, 2008.

[41] T. Speck, A. Engel, and U. Seifert. The large deviation function for entropy production: The optimal trajectory and the role of fluctuations. *J. Stat. Mech.*, 2012(12):P12001, 2012.

[42] F. J. Alexander and G. L. Eyink. Rayleigh-Ritz calculation of effective potential far from equilibrium. *Phys. Rev. Lett.*, 78(1):1–4, 1997.

[43] G. Gallavotti and E. G. D. Cohen. Dynamical ensembles in nonequilibrium statistical mechanics. *Phys. Rev. Lett.*, 74(14):2694–2697, 1995.

[44] G. Gallavotti and E. G. D. Cohen. Dynamical ensembles in stationary states. *J. Stat. Phys.*, 80(5):931–970, 1995.

[45] J. Kurchan. Fluctuation theorem for stochastic dynamics. *J. Phys. A: Math. Gen.*, 31:3719–3729, 1998.

[46] T. R. Gingrich, J. M. Horowitz, N. Perunov, and J. L. England. Dissipation bounds all steady-state current fluctuations. *Phys. Rev. Lett.*, 116:120601, 2016.

[47] P. Pietzonka, A. C. Barato, and U. Seifert. Universal bounds on current fluctuations. *Phys. Rev. E*, 93:052145, 2016.

[48] A. Dickson, S. M. Ali Tabei, and A. R. Dinner. Entrainment of a driven oscillator as a dynamical phase transition. *Phys. Rev. E*, 84:061134, 2011.

[49] J. P. Garrahan, R. L. Jack, V. Lecomte, E. Pitard, K. van Duijvendijk, and F. van Wijland. First-order dynamical phase transition in models of glasses: An approach based on ensembles of histories. *J. Phys. A: Math. Theor.*, 42:075007, 2009.

[50] J. P. Garrahan, R. L. Jack, V. Lecomte, E. Pitard, K. van Duijvendijk, and F. van Wijland. Dynamical first-order phase transition in kinetically constrained models of glasses. *Phys. Rev. Lett.*, 98(19):195702, 2007.

[51] L. O. Hedges, R. L. Jack, J. P. Garrahan, and D. Chandler. Dynamic order-disorder in atomistic models of structural glass formers. *Science*, 323:1309–1313, 2009.

[52] J. Hooyberghs and C. Vanderzande. Thermodynamics of histories for the one-dimensional contact process. *J. Stat. Mech.*, 2010(02):P02017, 2010.

[53] P. Tsobgni Nyawo and H. Touchette. Large deviations of the current for driven periodic diffusions. *Phys. Rev. E*, 94:032101, 2016.

[54] M. I. Freidlin and A. D. Wentzell. *Random Perturbations of Dynamical Systems*, volume 260 of *Grundlehren der Mathematischen Wissenschaften*. Springer, New York, 1984.

[55] R. Graham. Macroscopic potentials, bifurcations and noise in dissipative systems. In F. Moss and P. V. E. McClintock, editors, *Noise in Nonlinear Dynamical Systems*, volume 1, pages 225–278, Cambridge, 1989. Cambridge University Press.

[56] A. Ashkin. Optical trapping and manipulation of neutral particles using lasers. *Proc. Nat. Acad. Sci. (USA)*, 94(10):4853–4860, 1997.

[57] A. E. Cohen and W. E. Moerner. Method for trapping and manipulating nanoscale objects in solution. *App. Phys. Lett.*, 86(9):093109, 2005.

[58] R. van Zon, S. Ciliberto, and E. G. D. Cohen. Power and heat fluctuation theorems for electric circuits. *Phys. Rev. Lett.*, 92(13):130601, 2004.

[59] R. L. Jack and J. P. Garrahan. Metastable states and space-time phase transitions in a spin-glass model. *Phys. Rev. E*, 81(1):011111, 2010.

[60] D. Chandler and J. P. Garrahan. Dynamics on the way to forming glass: Bubbles in space-time. *Ann. Rev. Chem. Phys.*, 61(1):191–217, 2010.

[61] J. P. Garrahan, A. D. Armour, and I. Lesanovsky. Quantum trajectory phase transitions in the micromaser. *Phys. Rev. E*, 84:021115, 2011.

[62] S. Genway, J. P. Garrahan, I. Lesanovsky, and A. D. Armour. Phase transitions in trajectories of a superconducting single-electron transistor coupled to a resonator. *Phys. Rev. E*, 85:051122, 2012.

[63] C. Ates, B. Olmos, J. P. Garrahan, and I. Lesanovsky. Dynamical phases and intermittency of the dissipative quantum Ising model. *Phys. Rev. A*, 85:043620, 2012.

[64] J. M. Hickey, C. Flindt, and J. P. Garrahan. Intermittency and dynamical Lee-Yang zeros of open quantum systems. *Phys. Rev. E*, 90:062128, 2014.

[65] R. L. Jack and P. Sollich. Large deviations of the dynamical activity in the East model: Analysing structure in biased trajectories. *J. Phys. A: Math. Theor.*, 47(1):015003, 2014.

[66] A. Rákos and R. J. Harris. On the range of validity of the fluctuation theorem for stochastic Markovian dynamics. *J. Stat. Mech.*, 2008(05):P05005, 2008.

[67] M. Gorissen, J. Hooyberghs, and C. Vanderzande. Density-matrix renormalization-group study of current and activity fluctuations near nonequilibrium phase transitions. *Phys. Rev. E*, 79:020101, 2009.

[68] M. Gorissen and C. Vanderzande. Finite size scaling of current fluctuations in the totally asymmetric exclusion process. *J. Phys. A: Math. Theor.*, 44(11):115005, 2011.

[69] M. Gorissen, A. Lazarescu, K. Mallick, and C. Vanderzande. Exact current statistics of the asymmetric simple exclusion process with open boundaries. *Phys. Rev. Lett.*, 109:170601, 2012.

[70] P. I. Hurtado and P. L. Garrido. Spontaneous symmetry breaking at the fluctuating level. *Phys. Rev. Lett.*, 107:180601, 2011.

[71] T. R. Gingrich, S. Vaikuntanathan, and P. L. Geissler. Heterogeneity-induced large deviations in activity and (in some cases) entropy production. *Phys. Rev. E*, 90:042123, 2014.

[72] R. Graham and T. Tél. On the weak-noise limit of Fokker-Planck models. *J. Stat. Phys.*, 35(5):729–748, 1984.

[73] R. Graham and T. Tél. Weak-noise limit of Fokker-Planck models and nondifferentiable potentials for dissipative dynamical systems. *Phys. Rev. A*, 31(2):1109–1122, 1985.

[74] R. Graham. Fluctuations in the steady state. In J. J. Brey, J. Marro, J. M. Rubí, and M. San Miguel, editors, *25 Years of Non-Equilibrium Statistical Mechanics*, pages 125–134, New York, 1995. Springer.

[75] F. Bouchet, K. Gawedzki, and C. Nardini. Perturbative calculation of quasi-potential in non-equilibrium diffusions: A mean-field example. *J. Stat. Phys.*, 163(5):1157–1210, 2016.

[76] C. Beck and F. Schlögl. *Thermodynamics of Chaotic Systems: An Introduction.* Cambridge University Press, Cambridge, 1993.

[77] R. J. Harris and H. Touchette. Phase transitions in large deviations of reset processes. *J. Phys. A: Math. Theor.*, 50:10LT01, 2017.

[78] J. P. Bouchaud and M. Potters. *Therory of Financial Risk and Derivative Pricing.* Cambridge University Press, Cambridge, 2000.

[79] P. Tsobgni Nyawo and H. Touchette. A minimal model of dynamical phase transition. *Europhys. Lett.*, 116(5):50009, 2016.

[80] T. Dauxois and M. Peyrard. *Physics of solitons.* Cambridge University Press, Cambridge, 2006.

[81] A. Campa and S. Gupta. Dynamics of coupled oscillator systems in presence of a local potential. *Europhys. Lett.*, 116:30003, 2016.

[82] S. N. Majumdar. Brownian functionals in physics and computer science. *Curr. Sci.*, 89(12):2076–2092, 2005.